Master of Science Thesis

CONFIDENTIAL

Development of an in-panel attachment method for fiber-placed composite lattice and grid-stiffened structures

Design, analysis, manufacturing and testing

Bart J. R. Smeets

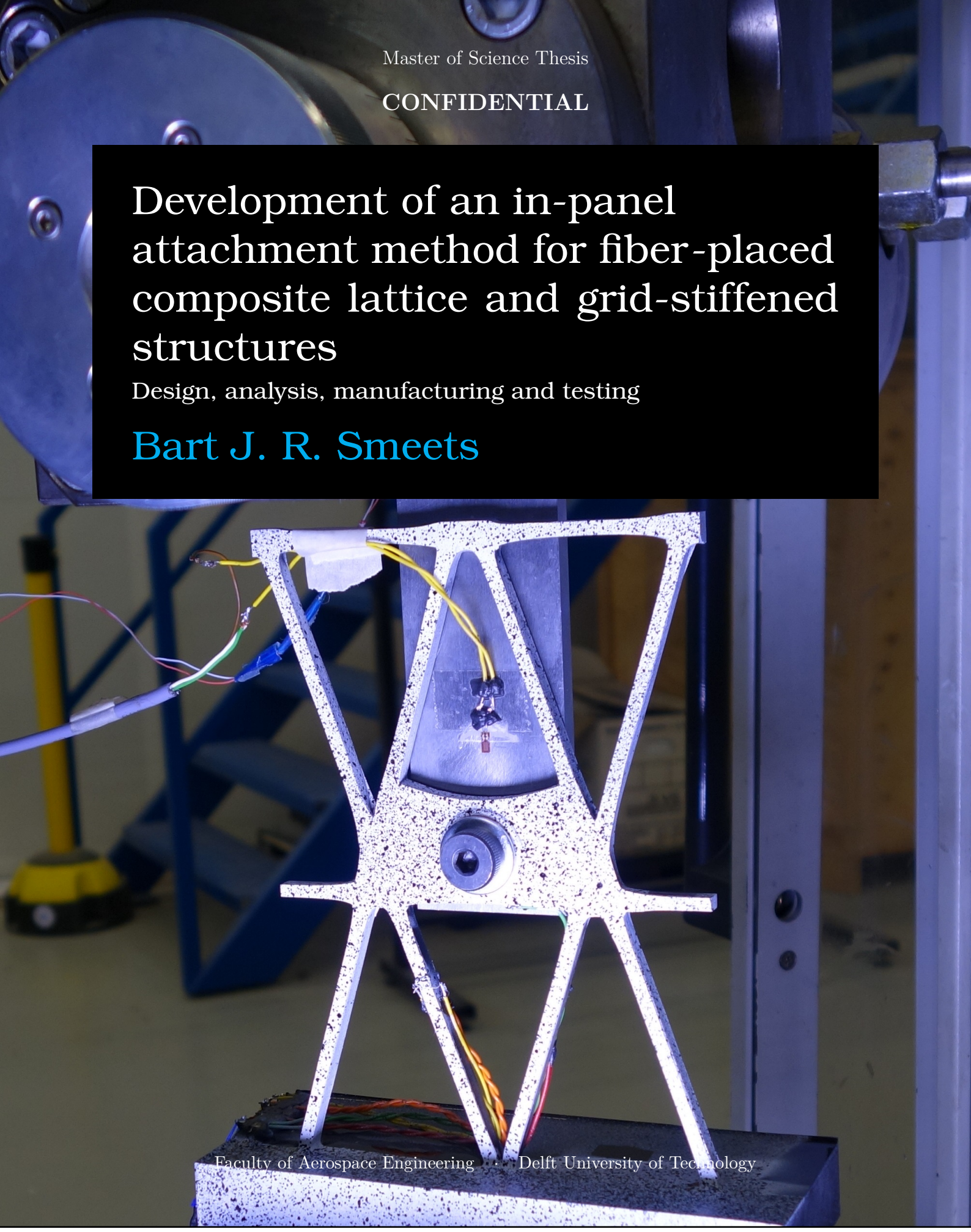

Faculty of Aerospace Engineering · Delft University of Technology

TU Delft Delft University of Technology

CONFIDENTIAL

Development of an in-panel attachment method for fiber-placed composite lattice and grid-stiffened structures

Design, analysis, manufacturing and testing

Master of Science Thesis

For obtaining the degree of Master of Science in Aerospace Engineering
at Delft University of Technology

Bart J. R. Smeets

July 8th, 2016

Faculty of Aerospace Engineering · Delft University of Technology

The work presented in this thesis was completed with significant support from ATG Europe. Their cooperation is gratefully acknowledged.

Delft University of Technology
Faculty of Aerospace Engineering
Department of Aerospace Structures and Materials

GRADUATION COMMITTEE

Dated: July 8th, 2016

Chair holder:

dr. C. Kassapoglou

Committee members:

dr. ir. S. Shroff

dr. C. D. Rans

ir. L. Pavlov

Abstract

Composite grid-stiffened and lattice structures have been the focus of an increasing amount of research over the past decades, mainly because of their excellent structural performance. Most of the previous and current research focuses on analysis, manufacturing, and optimization of the base structure. Although more and more is becoming known about grid structures, methods for introducing loads mid-panel are scarce. With some applications requiring hundreds of attachment points, the potential impact of the attachment points is significant. Therefore, development of an efficient attachment method can allow grid structures to be used in an increasing number of applications.

Recognizing the state of the art, a new concept for in-panel attachments is developed, which adds a laminate patch between the ribs of the structure to allow traditional fastening methods to be used. To analyze this concept, a rapid analysis method is constructed which makes use of several analytical methods and a fully parametrized finite element model to predict the strength of the attachment point. The feasibility of the concept and the used analysis method are validated by destructive testing of multiple test samples, and correlating the obtained data to the model. Resulting from the observations, several improvements are made to the model. Although some issues in the base structure are identified in the process, the feasibility of the novel attachment method is shown.

Table of Contents

List of Figures

List of Tables

List of Symbols

Abbreviations

AFP	Automated Fiber Placement
AFRL/VS	Air Force Research Laboratory Space Vehicles Directorate
CFRP	Carbon Fiber Reinforced Polymer
CNC	Computer Numerical Control
CRISM	Central Research Institute of Special Machinery
CTE	Coefficient of Thermal Expansion
DIC	Digital Image Correlation
FBD	Free Body Diagram
FE	Finite Element
FEM	Finite Element Method
FI	Failure Index
GSS	Grid-Stiffened Structure
ILSS	Inter-Laminar Shear Strength
LVDT	Linear Variable Differential Transformer
QI	Quasi-Isotropic
SCT	Satellite Central Tube
Tg	Glass transition temperature

Symbols

$A_{s,nom}$	Nominal stress area of bolt
d_b	Bolt diameter
d_h	Bolt head diameter
e	Edge distance
F_b	Bearing load
F_{pt}	Pull-through load
F_s	Shear load
F_{so}	Shear-out load
F_t	Tension load
k	Knockdown factor
t	Laminate thickness
σ_b	Allowable bearing stress
σ_{vm}	Von Mises stress
τ	Allowable stress value for shear-out

Acknowledgments

The research project presented in this thesis would have been impossible to achieve without support from other people, so some thanks are in order.

First of all I would like to thank ATG Europe for letting me work on this project, and for providing such a great working environment. Special thanks go to Leonid Pavlov for being my daily supervisor at ATG, providing a lot of support during the project, and putting up with my sense of poor humor.

Similarly, I want to thank Christos Kassapoglou for being my supervisor at the Delft University of Technology. By being genuinely interested in the research and always asking questions, you have motivated me to do more than I thought was possible.

A large part of the duration of this research was spent manufacturing and testing samples, there were multiple people who helped make this possible. The staff of the Delft Aerospace Structures and Materials Laboratory have always kindly provided support in operating all the manufacturing and testing equipment, preventing and resolving a lot of difficulties there. On the manufacturing side, I'd also like to thank Thijs Papenhuijzen for helping with the machining of the test samples, sacrificing a saturday evening in the process.

Thanks also go to Calvin Rans and Sonell Shroff, for taking the time to read this thesis and for being part of the assessing committee.

During any project, there is always the need to balance work and free time. This was pointed out to me by my friends on multiple occasions, especially in the final months of the project. My friends, by reminding me to do something other than work every now and then, you have prevented me from turning into a machine.

Last but definitely not the least, big thanks go to my parents. Not only for their continued support during this thesis project, but also for the support in all the years that came before. I wouldn't have made it this far without it.

Delft, University of Technology — Bart J. R. Smeets
July 8th, 2016

"The ability to improve a design occurs primarily at the interfaces.
This is also the prime location for screwing it up."

— *Akin's law of spacecraft design #15*

Chapter 1

Introduction

Grid structures, as the name implies, consist of a grid of load-bearing ribs. These ribs run in multiple directions, and usually form a repetitive pattern. A structure consisting of only these load-bearing ribs is known as a lattice structure. When the lattice is complemented with a skin, this is known as a grid-stiffened structure (GSS). Examples of both types of structure are shown in Figure 1.1.

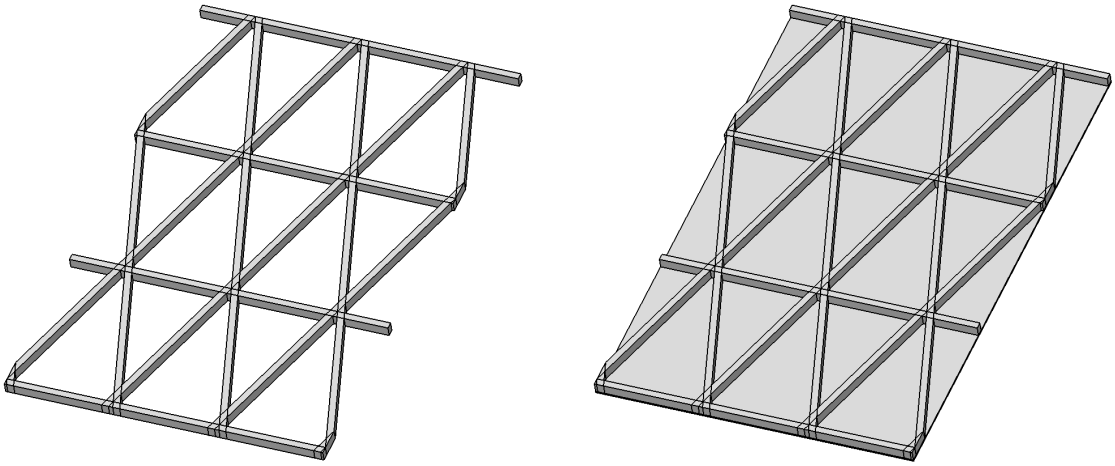

(a) Lattice structure (b) Grid-stiffened structure

Figure 1.1: Two different types of grid structures, with a triangular grid.

When made from fiber-reinforced polymer composites with the fibers in the rib direction, these structures make good use of the high specific strength and stiffness that this material provides. Use of these structures has been shown to result in mass reductions of up to 61% over conventional aluminum designs. [4]

Despite the fact that these structures offer such significant advantages in terms of mass, strength and stiffness, only a few applications are seen to date. This can be partly attributed to the lack of commonly accepted analysis methods for this type of structure. [5,6] Recent advances in finite element (FE) analysis methods and the widespread availability of the

required processing power have opened new possibilities for analyzing these structures though. Additionally, there is inertia in the industry to accept grid structures. More traditional methods such as skin/stiffener or sandwich structures are often preferred over grid structures, despite the advantages the latter can offer. Another factor limiting the use of these structures is the lack of methods to attach the structure to other structures and parts.

Recognizing the potential of grid structures, ATG Europe has been working on several developments of fiber-placed lattice and GSS. First steps in this research were establishing manufacturing, analysis and optimization methods for the far-field structure.[7] The subsequent development of attachment methods was split into two fields. The first being the end-panel load introduction zones, for which a method has recently been developed.[8] The second part is the development of a method for in-panel attachments, which is the topic of the presented work.

The goal of the presented research can be summarized as:

Develop a universal in-panel attachment concept for fiber-placed grid structures, with a rapid analysis method for initial design.

In this goal, a *universal concept* implies that the concept is applicable to both lattice and GSS, is not limited to a single location in a grid, and can be used for both high and low loads. The *rapid analysis method* serves to make the analysis method more applicable to any real design procedure, where a rapid method is desired. Without it, the iterative design of many attachment points on a single structure would take too much time.

To achieve this goal, the following subtasks are identified:

- Identify a suitable concept.
- Develop a (rapid) analysis method for the selected concept.
- Manufacture and test representative samples to validate the model and prove the feasibility of the concept.
- Correlate the test data to the model, to validate the modeling approach.
- Improve the analysis method if necessary.

The research and its results are presented by first providing some additional context in chapter 2. The selected in-panel attachment concept is then presented in chapter 3, after which chapter 4 presents the analysis methods that are used to assess the attachment point. chapter 5 contains several trend studies, investigating the effects of several design parameters. Both a more detailed modeling of the interface with the base structure, and several design guidelines are also presented in this chapter. The approach taken for the verification of the modeling method is explained in chapter 6, also elaborating on the test samples and test setups that were used. In chapter 7 the manufacturing methods used to make the test samples is shown, and the quality of the manufactured parts is discussed. chapter 8 then discusses the test results, and elaborates on the changes made to the models after comparing to the test results. Finally, the conclusions and recommendations are presented in chapter 9.

Chapter 2

Context of presented research

To clarify the context in which the presented research is performed, this chapter presents the actual use and research of lattice and GSS. This also allows identification of current in-panel attachments methods, which are briefly discussed. Furthermore, the reference case that is provided by ATG Europe is presented.

2.1 Typical use of composite lattice and grid-stiffened structures

The majority of composite grid-stiffened and lattice structures that are being used today are developed and manufactured at the Central Research Institute of Special Machinery (CRISM) in Russia. Both lattice structures and GSS are made there, with filament winding used as the manufacturing method. [1]

Types of open lattice structures manufactured at CRISM are conical payload adapters and satellite central tubes (SCTs), examples of which are shown in Figure 2.1.

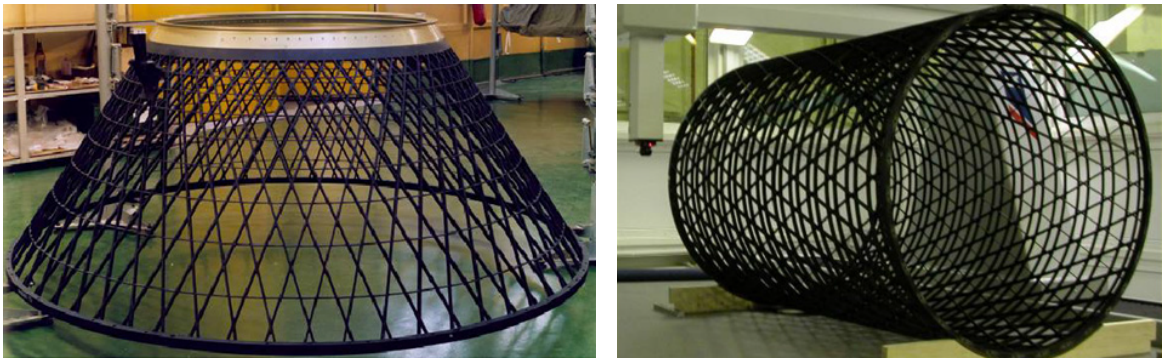

(a) Payload adapter [9]

(b) Satellite central tube [1]

Figure 2.1: Open lattice composite structures made at CRISM.

A type of GSS made at CRISM is the interstage for the Proton-M rocket, a recent version of which is shown in Figure 2.2. The first version of this structure was flown in 1988, and the design has gone through many improvements since. [10]

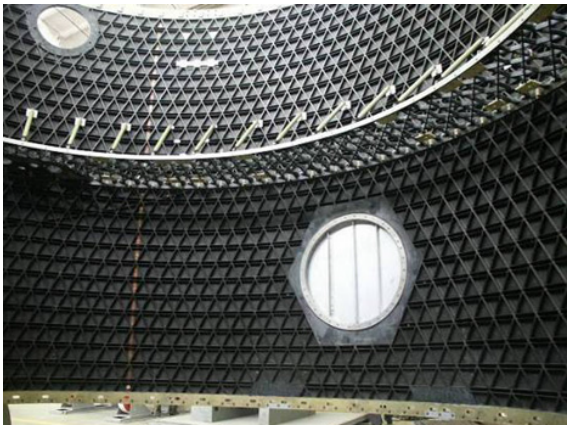

(a) Interior view

(b) Exterior view

Figure 2.2: Grid-stiffened composite interstage for the Proton-M rocket.[1]

Another party that has developed and manufactured GSS for actual use is the United States Air Force Research Laboratory Space Vehicles Directorate (AFRL/VS). Research there has been focused on payload fairings for military applications. The two known applications are shown in Figure 2.3. The conical fairing shown on the left is manufactured using filament winding followed by an autoclave cure[4], whereas the Minotaur fairing is made using automated fiber placement (AFP).[11]

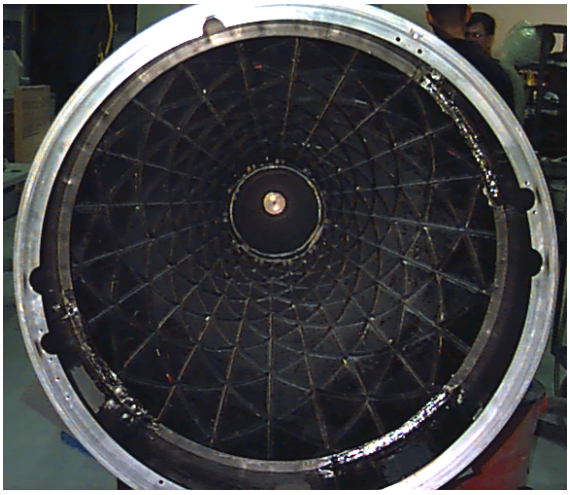

(a) For the Ballistic Missile Defense Organization's Combined Experiments Program.[11]

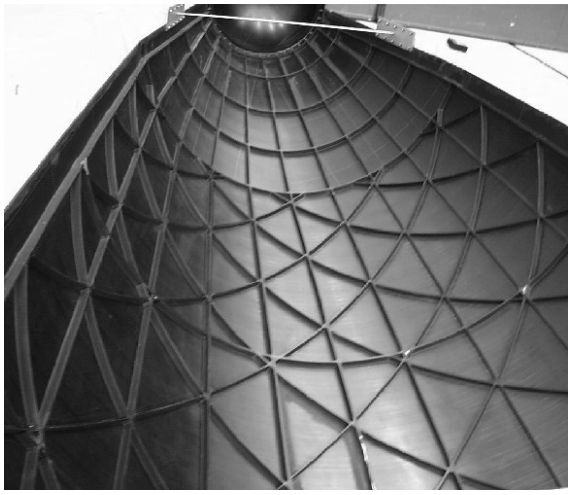

(b) For the Minotaur launch vehicle (joint development with Boeing Phantom Works).[12]

Figure 2.3: Grid-stiffened payload fairings developed at AFRL/VS.

All the aforementioned applications are in spacecraft or launch vehicles. While there has been some research on aircraft applications[2,5], these have not yet lead to actual use.

2.2 Typical research fields

Multiple aspects of composite grid-stiffened and lattice structures have been researched. General fields of research are:

- *Analysis* of the overall structure, including but not limited to: smeared stiffness approaches, local and global (semi-)analytical buckling analyses, noise transmission, and post-buckling analyses using finite element methods (FEM).[12–20]
- *Optimization*, both using combined analytical and numerical methods[21,22] or FEM.[23,24]
- *Manufacturing* of the structure. This is not limited to the aforementioned methods of wet filament winding and AFP. Other researched methods include resin transfer molding, which has been used to manufacture a relatively large cylindrical structure.[25] The feasibility of manufacturing both flat and curved panels from thermoplastic material has also been demonstrated.[26] Other manufacturing-related research concerns the tooling as well, showing the aforementioned methods can be used with various types of tooling between the ribs, including flexible rubber tooling in various shapes, foam, composite, metal, no tooling at all (free-standing layup and cure), or a combination of aforementioned methods.[6,10,25,27–29]

Research performed at ATG Europe partly falls in the aforementioned categories, with research on optimization of several types of GSS and lattice structures, as well as manufacturing methods.[7,30–32] Additionally, other research was focused on the development of end-panel load introduction zones.[8]

2.3 State of the art of in-panel attachment methods

Although there are no publications specifically on the development of in-panel attachments, active use of some types of structures indicates that a solution must exist.

2.3.1 Known in-panel attachment methods

Of the structures identified in section 2.1, some of the Russian-made structures make use of in-panel attachments. There are many papers concerning these structures,[1,2,6,9,10,33] and it is in these publications that some indirect information on the used solution(s) can be found.

The structure that makes most use of in-panel attachments is the SCT, since numerous shear webs and other structural and equipment parts need to be mounted onto the structure. One paper includes photos of several SCTs with attachment points[1], one of which is shown in Figure 2.4. It shows a lattice cylinder with three large rings and a multitude of smaller attachment points. The additional parts appear to be made of metal. Of the three metal rings, the one on the lower end of the satellite is used to connect to the launcher, it therefore will likely contain the required geometry to interface with the payload separation system. The other two rings are used to connect to other structural parts of the satellite, which will usually be either an exterior panel or an equipment deck. Long rows of attachment points along the length of the structure can also be seen, these are likely used to attach the shear webs, as can also be seen in Figure 2.5.

A more detailed view of the attachment points can not be found in literature. Fortunately, several high-resolution images of lattice structures in satellites can be found outside of literature. With sufficiently high resolutions, parts of these images can be enlarged to show

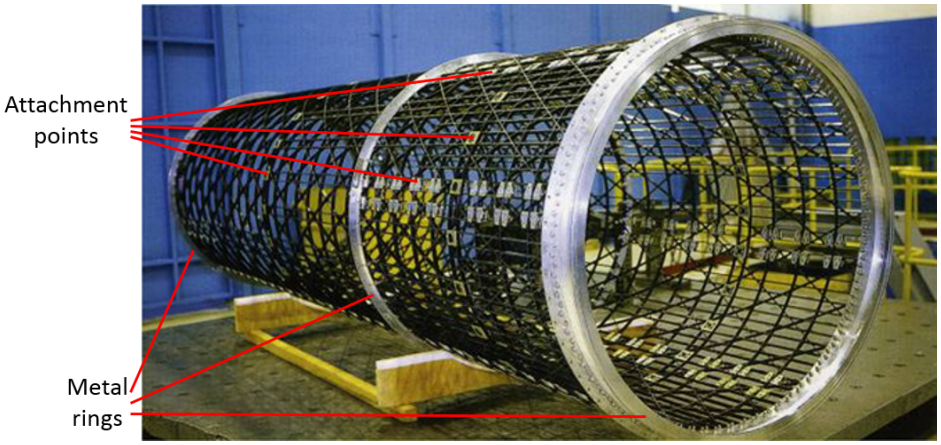

Figure 2.4: Lattice satellite central tube, with the location of end rings and some attachment points indicated. [1]

more detailed views of the in-panel attachments. Two such enlargements are shown in Figure 2.5. It can be seen that the metal parts are placed in small cells surrounded by ribs, covering almost the entire cell. The parts are placed on both the inside and the outside of the cylinder, partly covering the surrounding ribs. Whether or not the parts are bonded or only mechanically fastened can not be determined from the available information, but both are considered possibilities.

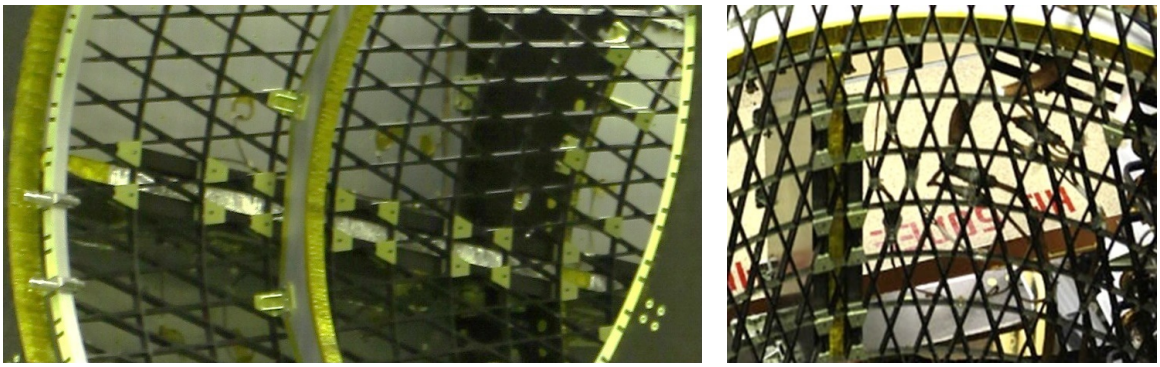

(a) KazSat-3 [34] (b) Lybid satellite [35]

Figure 2.5: Attachment points on lattice central tubes as seen on details of photos.

Considering that these structures are made using filament winding, the metal parts are most likely added after curing of the structure since this would otherwise disturb the manufacturing process. The fibers that make up the lattice structure are wound into grooves in silicone rubber tooling. [1] While this tooling might be adapted to accommodate some of the metal parts, the ones that have parts that lie on the outer surface of the cylinder would make it impossible to wind the fibers into the grooves in the tooling.

As can be seen in Figure 2.2, the Proton-M interstage appears to utilize similar methods. This is further supported by a paper where it is stated that the lattice ring inside the Proton-M interstage is mechanically joined to the shell. [33] However, the presence of a skin dictates a slightly different approach. The used solution still includes metal parts on both sides of the cylinder, although their shape is different from what is observed on the SCTs.

At the time these interstages were first made, development of a grid-stiffened composite aircraft fuselage was also ongoing at CRISM. As can be seen in Figure 2.6 this structure has some attachment points as well.

Figure 2.6: Grid-stiffened composite fuselage for Ilyushin IL-114. [2]

The shown fuselage was made in 1986. [10] Considering that this structure was developed and made around the same time as the interstage mentioned earlier, the used attachment methods are probably similar. However, adding metal parts on the outside of the cylinder would have aerodynamic disadvantages, so it is likely that the solution is modified such that it does not have any parts on the external surface.

In more recent developments of this fuselage, similar methods are presented for use in a repair method of locally damaged ribs. Metal parts are embedded in the structure and then a repair patch is mechanically fastened to them. [36] While not intended as an attachment method, it is a method of introducing loads locally.

The other applications shown in section 2.1 do not make use of in-panel attachments, and no other in-panel attachment methods are currently known.

2.3.2 Discussion of current method

All of the currently used attachments are made by adding metal parts. This might be due to metal parts being more easily made and machined into complex shapes, thus giving more design freedom. As an additional benefit a thread can be made integral with the metal parts, removing the need to add a bolt or nut later on. However, the different material properties can give rise to some issues.

Any mismatch in coefficient of thermal expansion (CTE) of the used components results in the development of stresses under thermal loading. Metals usually have a positive CTE, while carbon fiber reinforced polymer (CFRP) usually has a negative CTE in the fiber direction. Combined with the high thermal loads often encountered in space applications this can result in high stresses. Especially aluminum, which has a relatively high CTE, has the potential of creating large stresses when combined with CFRP.

Different materials, when in contact, can also develop galvanic corrosion. In space the lack of atmosphere prevents this, but storage between manufacturing, testing, integration and launch gives an opportunity for corrosion to occur. This might compromise the strength of the part. Not all material combinations suffer from this effect, for instance the combination of CFRP and titanium is safe, whereas CFRP with aluminum is known to result in galvanic corrosion. Apart from changing the materials there are other ways to prevent galvanic corrosion. A corrosion-inhibiting coating can be applied to the metal part, or a non-corrosive layer of fiberglass or adhesive can be added between the materials.

From the actual use of metal parts in attachment points it is evident that the aforementioned issues are overcome.

Conclusive arguments about mass efficiency are difficult to make, since there is no data available on the mass of the attachment points. The cost associated with launching a certain mass into orbit is very high, up to several tens of thousands US$/kg.[37] The assembled structure must be relatively lightweight, since the launch cost would otherwise become prohibitive. There are usually several hundreds of attachment points in an SCT, so the potential impact on the total mass is high. This does not necessarily mean that the attachments are the pinnacle of lightweight design though, since knowing that bare lattice and GSS have shown mass decreases of up to 61% over more conventional designs[1,6], there is some room for mass inefficiency in the attachments.

Considering the large variety in manufacturing methods that can be used to manufacture the basic structure, it is unlikely that a single concept is optimal for all these processes. Since the only known solution is for filament wound structures, a new method developed specifically for fiber-placed structures has a significant chance it will be more optimal than the current solution.

2.4 Reference case

A reference case is provided by ATG Europe. The case gives realistic loads and dimensions of the base grid structure that can be used for the analyses. While the goal is to obtain a general solution for in-panel attachments in grid structures, use of a reference case ensures that the developed method is applicable to current and foreseen uses of lattice and GSS.

The provided reference case is a fiber-placed lattice SCT, a cylindrical structure of several meters tall and over a meter in diameter, with several hundred attachment points. This structure is somewhat similar to the ones shown in Figure 2.4 and Figure 2.5. The overall optimization of this structure is one of the ongoing developments at ATG Europe. Figure 2.7 shows the shape of the triangular cells and the parameters that determine the shape and size. The corresponding dimensions are listed in Table 2.1.

Table 2.1: Base structure dimensions of the reference SCT

Dimension	Value
Helical rib spacing	70 mm
Helical rib angle	18°
Rib width	4.4 mm
Rib height	6.6 mm

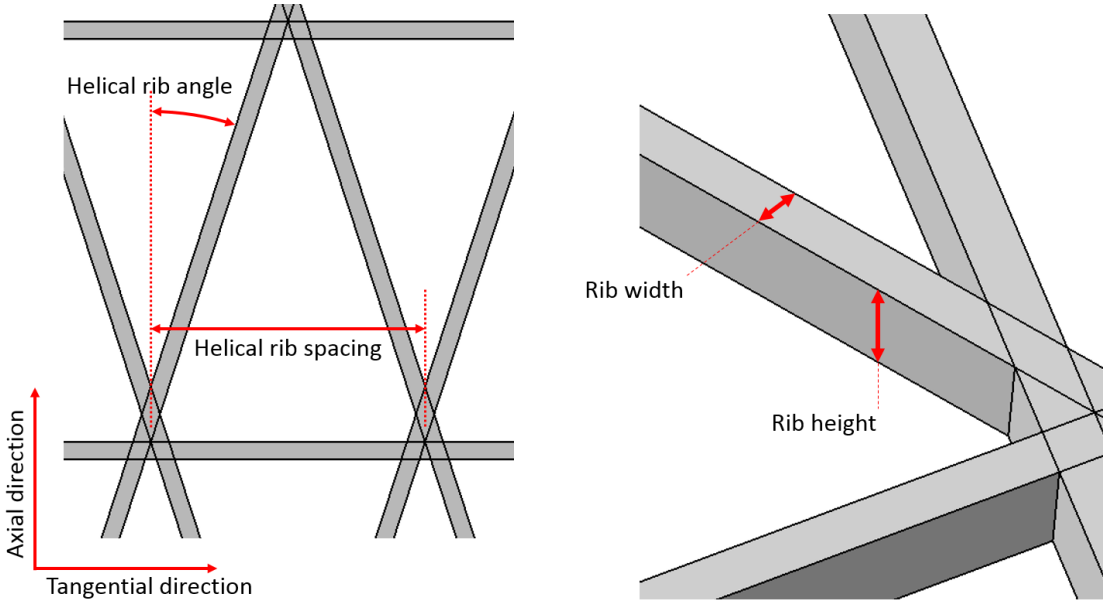

(a) Grid dimensions (b) Rib dimensions

Figure 2.7: Triangular grid layout, and design parameters.

Furthermore a set of loads as acting on the SCT attachments is provided. It contains 40 quasi-static load cases for each of the several hundred attachment points. All required factors of safety are included in the loads, so no additional factors need to be taken into account. This load set is the same as is used for the optimization of the SCT itself.

Additionally, general requirements and guidelines for space applications can be considered since this is the typical field of application. Some relevant examples of such requirements and guidelines are:

- The design must be safe-life.
- Fatigue and damage tolerance are not critical.
- Attached equipment must be mountable and dismountable multiple times, without degrading structural performance of the attachment.
- The structure must perform as designed after multiple years of storage, integration and testing.

Chapter 3

Concept

The used concept is one of multiple identified possible methods, of which a mixed quantitative and qualitative comparison showed it outperformed other concepts. Main advantages are the flexibility, high strength, large interface area, low mass, and good compatibility with the manufacturing method for the SCT. More information on the selection process and the other concepts that were considered can be found in Appendix A.

The selected concept is the 'laminate patch'. Essentially this consists of a small area of laminate that is added in between the ribs of the base structure. The shape and thickness of this patch are variable, dependent on the design. This laminate can then be used for a bolted attachment. Key elements of the concept are shown in Figure 3.1.

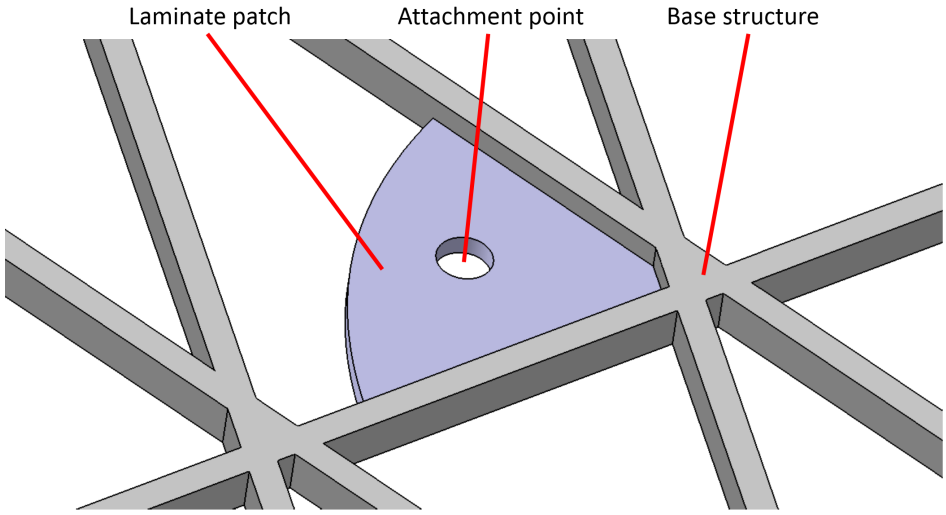

Figure 3.1: An example laminate patch in a triangular grid.

3.1 Manufacturing of the laminate patch

The patch consists of a laminate made from multiple plies of composite material. These are placed during the same layup phase as the main structure. Some plies are placed between the ribs, and some extend into the ribs.

The ability to extend plies of the patch into the ribs without interrupting the rib plies results from the way the ribs are formed. The plies used to make the ribs are continuous through the nodes, so this results in a faster build-up of material in these areas. The rib plies then bridge the space between the nodes, thus leaving some room in between the plies. This is resolved by the silicone rubber tooling which is placed between the cells during curing. As temperature increases the tooling expands and applies compaction to the side of the rib. This forces the rib plies into a narrower volume, and since the cross-sectional area must remain more or less constant this results in the plies forming a single rib if enough compaction is applied. A drawing of a rib cross-section before and after curing is shown in Figure 3.2a.

It is in the space between the plies of the rib before compaction that some plies of the patch can be extended. The distance by which these extend can be varied depending on the design, but the rubber tooling needs to be adjusted accordingly, since the local changes may require more or less compaction to be applied to the rib. When assuming equal compaction from both sides of the rib, extending plies halfway into the rib allows the other side of the rib to compact as usual, thus allowing unmodified rubber tooling to be used in adjacent cells. Then only the cell in which the patch is placed requires different tooling. Given the reduction in complexity this is the desired choice, unless the design requires a different extension into the ribs. Schematic cross-section of such extensions before and after cure are shown in Figure 3.2b and c, for both partial and full-thickness patches.

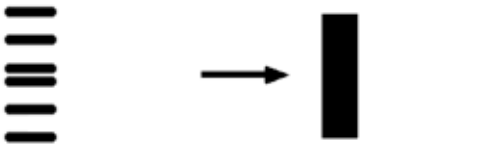

(a) Regular rib, without patch.

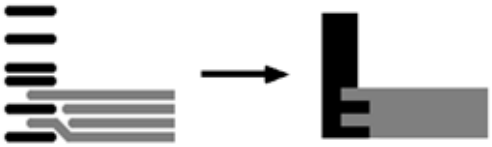

(b) Rib with a partial thickness patch.

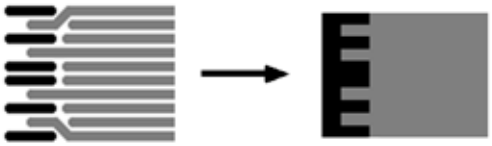

(c) Rib with a full thickness patch.

Figure 3.2: Schematic representation of compaction of the rib-patch interface, showing the cross-section of plies in the rib and patch before cure, and of the resulting part after cure. Black: rib plies, gray: patch plies.

To confirm that this manufacturing approach works as desired, a small sample containing both a full-thickness and partial thickness patch was manufactured. A detail of this part is

shown in Figure 3.3, indicating some features.

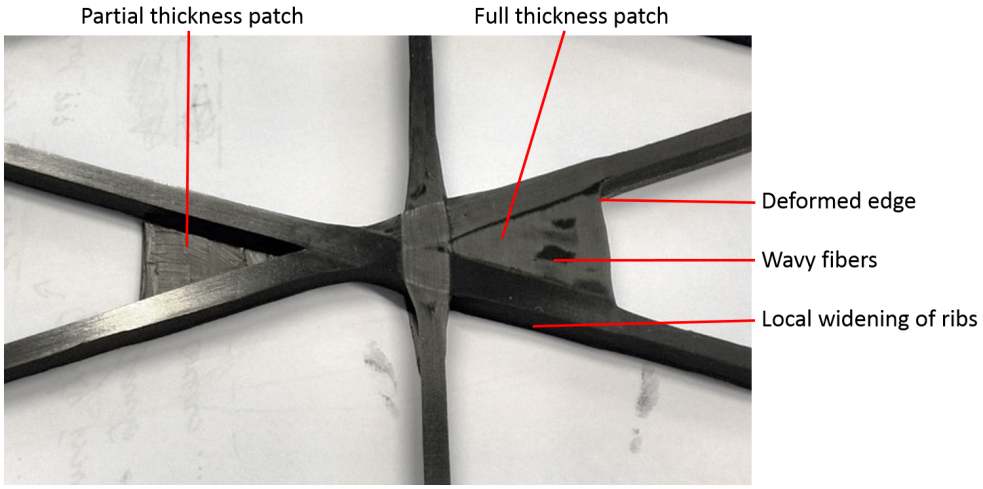

Figure 3.3: Manufacturing trial part, with two laminate patches.

From this manufactured part, the following observations were made:

- Both a full-thickness and partial thickness part can be manufactured.
- This part was made before determining that the patch plies are best extended halfway into the ribs, so it was made with some patch plies extending to the far side of the rib. This resulted in a local widening of the ribs at the interface.
- The compaction applied to the patches was somewhat irregular, resulting in deformed edges and some waviness in the patch plies. It was expected that this could be avoided by improved design of the tooling.

3.2 Attaching to the laminate

The addition of a laminate allows for conventional methods to be used to connect to this laminate. A typical requirement for space applications is that the entire structure can be assembled and disassembled multiple times for the different tests and final integration. This makes bolts the most suitable fastener type since these can be easily removed and replaced. Since making a thread directly in the composite laminate usually results in low strength and unfavorable stresses in the laminate, the bolt is best extended through the laminate, and a nut is used.

While bolting directly to the laminate is possible, using bonded inserts can improve the strength of the attachment. Additionally, these improve the surface quality of the interface, and reduce the risk of damaging the composite when placing the bolt. In the current research two types of insert are considered: a ring of the same thickness as the laminate, and 'hat' inserts with a flange on the surface of the laminate. Examples of these inserts are shown in Figure 3.4. These inserts are chosen since they have shown to increase the in-plane strength when compared to holes without inserts.[38–41] Practical applicability is not limited to these types of inserts though, other types might be used if they better suit the application.

(a) Ring insert (b) Hat insert

Figure 3.4: The two insert types that are considered.

3.3 Load transfer into grid

In this concept two interfaces can be recognized: the bolt in the laminate, and the rib-patch interface.

3.3.1 From bolt into laminate

The transfer of loads from a bolt to the laminate is relatively straightforward, the free body diagrams (FBDs) given in Figure 3.5 show the different distributions of load on the laminate, depending on the load type.

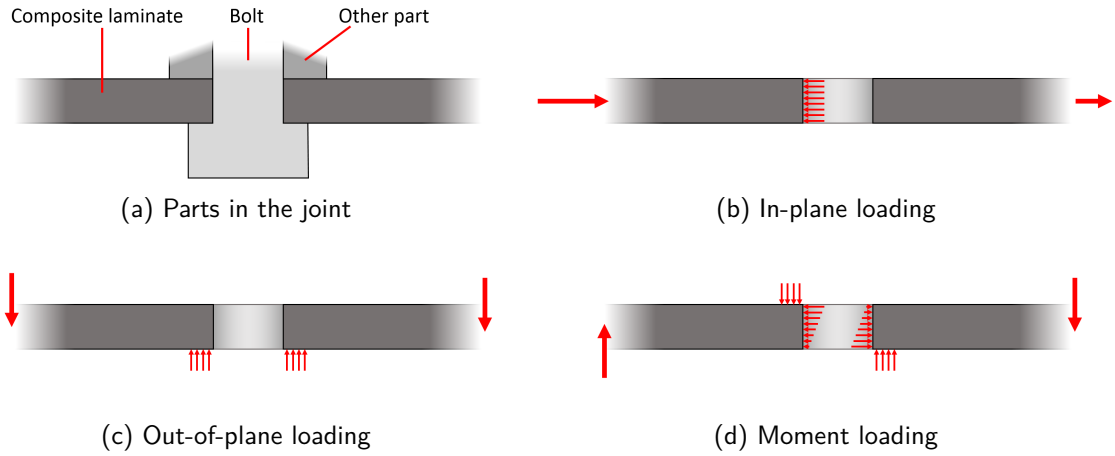

(a) Parts in the joint (b) In-plane loading

(c) Out-of-plane loading (d) Moment loading

Figure 3.5: FBDs of reaction forces in the laminate patch, resulting from a bolt load.

An in-plane load results in a bearing load, and out-of plane loads are introduced on the contact surface with the bolt head. A bending load introduced by the bolt is spread over multiple contact surfaces.

The presented FBDs do not include the effects of a bolt preload. In case such a bolt preload is applied there will be an additional clamping load on the contact surfaces, and a part of the in-plane load will be taken up by friction.

These types of loads may result in the following types of failure:

- *Bearing.* A progressive failure mode with a significant load-carrying ability after initial failure. This is therefore a desirable failure mode. [42]
- *Shear-out.* An undesirable failure mode since the failure is abrupt, and the load-carrying ability is greatly reduced after failure, and the damage to the base structure is significant. [42]

- *Pull through.* A relatively desirable failure mode, since failure is progressive, and the load-carrying ability after the onset of failure is high. [43]
- *Laminate failure* at a distance from the bolt. This is usually also a progressive failure mode, with some load-carrying ability between first ply failure and last ply failure. The damage is not necessarily concentrated around the bolt though, which is undesirable for attachment points since damage to the base structure is to be avoided.
- *Bolt failure.* This type of failure results in a complete loss of strength, and is therefore very undesirable.

3.3.2 From laminate into grid

Figure 3.6 shows the detailed cross-section of a typical rib-patch interface. Only a fraction (usually 30-50%) of the plies extend into the rib to transfer the load to the ribs. This means that the load locally has to be transferred by only a part of the laminate plies. This is not a problem since the loads are introduced locally by the bolt, and are then spread out over a larger interface. The only part of the laminate that is highly loaded is the area close to the bolt, the local stress concentrations present there even out at a distance from the bolt.

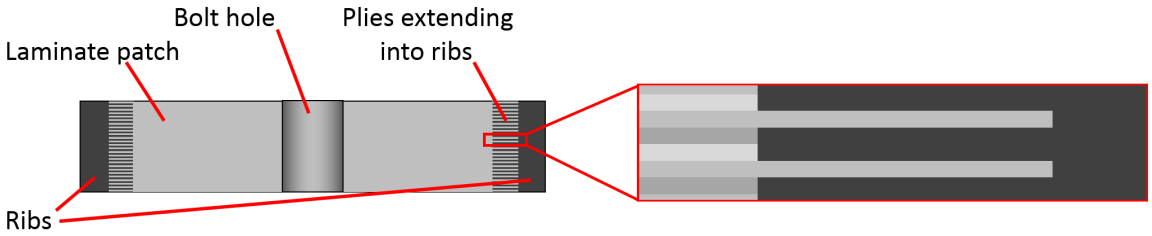

Figure 3.6: Schematic drawing of a laminate patch between two ribs, with a detail of the rib-patch interface.

Looking back at Figure 3.5, it is recognized that the applied loads result in either an in-plane or an out-of-plane load on the rib-patch interface. For an in-plane load, the FBD of the loads acting on a part of the laminate in the interface is shown in Figure 3.7.

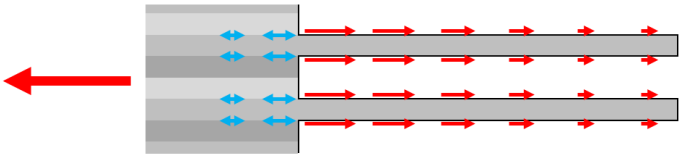

Figure 3.7: FBD of forces in the laminate patch at the interface. Red: applied load or load on interface. Blue: interlaminar stresses in the laminate.

Of the load on the plies that do not continue into the rib, only a small fraction can be transferred directly into the ribs through the matrix material. The majority of the load has to go through the plies that do extend. This results in interlaminar stresses in the laminate near the interface.

The out-of-plane behavior is dominated by the matrix properties, so the out-of-plane load simply results in an overall shear load through the interface. Any overall bending load in the laminate results in local in-plane loads, compressive on one side of the laminate, and tensile on the other. Locally this is then similar to the situation shown in Figure 3.7.

Chapter 4

Analysis

This chapter presents the analysis method used for the concept presented in the previous chapter. The analysis method comprises a mix of analytical and numerical methods implemented in a parametrized and scripted analysis method.

4.1 Analysis of failure modes

Several different failure modes of the attachment are identified:

- Bolt failure
- Bearing
- Shear-out
- Pull-through
- Failure in the structure surrounding the attachment

The methods used to analyze these failure modes are discussed separately hereafter.

In determining the analysis methods, the typical loads that act on the SCT attachments are taken into consideration. Since these loads are mostly in-plane, the analysis focuses on those failure modes.

4.1.1 Bolt failure

Failure of the bolt under combined loading is calculated analytically.

The plane in which a bolt fails depends on the type of load that is applied. When a bolt is loaded in shear it fails in the shear plane, which is usually in an unthreaded part of the bolt. A bolt loaded in pure tension usually fails in the threaded part of the bolt, since the cross-sectional area there is smaller. FBDs of loaded bolts, also indicating the two failure planes, are shown in Figure 4.1. Here A indicates the failure plane for a shear load, and plane B indicates the failure plane for a tensile load.

Under combined loading, failure can occur in either of the two planes, depending on the ratio between the tensile and shear loads. To simplify the calculations, the cross-sectional area of

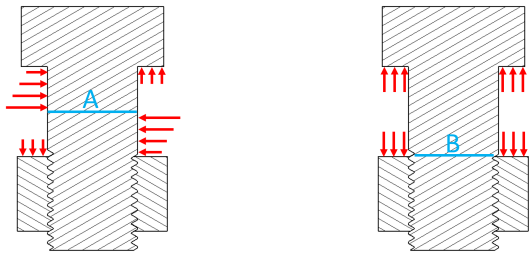

(a) In-plane (shear) load (b) Out-of-plane (tension) load

Figure 4.1: FBDs of a bolt under loading, also indicating the failure plane (blue).

the tension failure plane (B) is used for all combinations of loads. Use of the smaller of the two failure planes introduces some conservatism into the model.

Since the diameter of the effective cross-section in the threaded section is smaller than the nominal diameter due to the presence of threads, this is first corrected for. The ISO 898-1 standard gives this nominal stress area of bolts, with a method to calculate it. This is a rather straightforward method using several other standardized dimensions of bolts. One of the variables that is used in the calculation of the nominal stress area is the depth of the threads, which is determined by the thread pitch. The pitch is not a continuous variable, and can not be calculated directly from the nominal diameter thus complicating flexible implementation in a script. However, a linear trend is observed between the nominal stress area and the unthreaded cross-sectional area, this is shown in Figure 4.2.

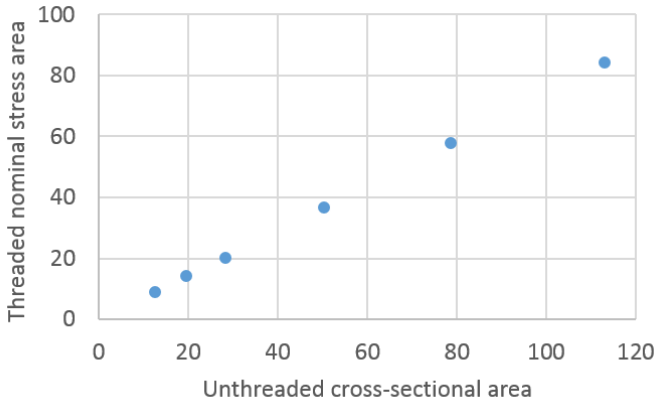

Figure 4.2: Nominal stress area and unthreaded cross-sectional area for bolts, sizes M4 to M12.

The nominal stress area is therefore approximated by multiplying the unthreaded cross-sectional area by a constant, using 0.72 for coarse thread and 0.78 for fine threaded bolts. The comparison of this approach with the values from the ISO standard is shown in Table 4.1 for bolt sizes from M4 to M12, which covers the range of sizes typically used in an SCT.

For coarse thread bolts the approximation is within 3.5%, with errors both positive and negative in various magnitudes. The error is a lot more constant for fine threads, with the exception of the 5 mm diameter bolt for which the stressed area is underpredicted.

The shear and tensile loads applied to the bolt are then used to calculate the von Mises stress

Table 4.1: Nominal stress areas of metric thread bolts, from ISO 898-1 [3] and a linear approximation.

	Coarse thread				Fine thread			
Bolt dia. mm	Pitch mm	ISO 898-1 mm^2	Approxim. mm^2	Error	Pitch mm	ISO 898-1 mm^2	Approxim. mm^2	Error
4	0.70	8.8	9.0	3.1%	0.5	9.8	9.8	0.1%
5	0.80	14.2	14.1	-0.3%	0.5	16.1	15.3	-5.0%
6	1	20.1	20.4	1.2%	0.75	22.0	22.1	0.1%
8	1.25	36.6	36.2	-1.1%	1	39.2	39.2	0.1%
10	1.5	58.0	56.5	-2.5%	1.25	61.2	61.3	0.1%
12	1.75	84.3	81.4	-3.4%	1.5	88.1	88.2	0.1%

in the cross-section. For the applied loads, the equations reduce to:

$$\sigma_{vm} = \frac{\sqrt{{F_t}^2 + 3 * {F_s}^2}}{A_{s,nom}} \tag{4.1}$$

With F_t and F_s the tensile and shear loads on the bolt, and $A_{s,nom}$ the nominal stress area discussed earlier. This is then divided by the allowable stress to get the failure index (FI). The bolt preload is not taken into account here, since it was shown that the preload does not affect the load-carrying capability of the bolt. [44]

Different values can be used as allowable stress in the bolt, depending on the requirements. Usually, one uses either the yield strength or the proof strength. The yield strength is the stress level at which the fastener as a whole starts yielding. The proof strength is the load the bolt must support without evidence of any permanent deformation. This load is usually around 90% of the yield strength. For the presented research, the proof strength is used.

The approximations introduce a slight inaccuracy in the calculated strengths, but the bolt should not be limiting in most designs. If analysis shows that the bolt is limiting the strength, more accurate methods can be used, but this is not required for most designs since one usually wants other 'softer' failure modes to occur first.

This method is only usable if there is no separation in the joint, since that will allow bending loads to develop in the bolt shaft, leading to failure at a lower load.

An additional calculation is made to check if the applied preload can be taken by the bolt without causing a tension failure.

4.1.2 Bearing

Figure 4.3 shows a simplified geometry loaded by an in-plane load. The area on which bearing damage occurs is indicated as well.

The bearing strength is calculated using analytical methods. While several studies have shown that FE methods can also give acceptable results [42,45,46] these methods are complex and will not result in a rapid analysis method.

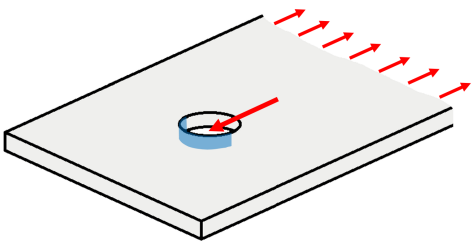

Figure 4.3: FBD showing bearing failure area (blue).

The used method starts with a basic calculation of the bearing load F_b:[47]

$$F_b = d_b * t * \sigma_b \tag{4.2}$$

Where d_b is the bolt diameter, t is the laminate thickness, and σ_b the allowable bearing stress, which is best obtained from bearing tests or other relevant test data. This base value is then multiplied with several factors to take some of the design parameters into account. These factors are listed in Table 4.2, and discussed separately afterwards.

Table 4.2: Multiplication factors for the bearing strength that are used in the analysis.

Effect of	Factor	Note
Inserts	×1.2	Only if insert is present
Bolt preload	×1.0	Postpones only final failure, not initial
Load offset	×0.5	Arbitrary factor*
Layup	-	Not implemented, but guidelines apply
Hole oversize	-	Not implemented, but guidelines apply
Out-of-round hole	-	Not implemented, but guidelines apply

* Adjusted to ×0.67 after test results correlation

Effect of inserts

In general, the use of a bonded ring insert in the laminate reduces the peak stress on the interface.[38–40] Without an insert all bearing loads act on the hole surface in the loaded direction, but a bonded insert spreads this load over the entire hole surface. Care has to be taken though with the selection of the insert material, since a stiff material like steel transfers more load, causing higher tensile stresses in the adhesive layer. This causes the adhesive to fail at a lower load than with aluminum inserts, leading to a lower strength.[40]

Reported values of strength increase due to the use of both circular or 'hat' shaped aluminum inserts are between 20% and 55%.[38,41] To remain on the safe side of the reported values, an increase of 20% is used, which corresponds to a factor 1.2.

Effect of bolt preload

Multiple studies have been performed of the effect a bolt preload has on the bearing strength. These studies all report that strength increases with an applied preload.[45,48,49] This is however the ultimate bearing strength, not the initial. Since any damage in the structure is undesirable the initial failure is used for design purposes. Both the initial nonlinearity and the initial load drop are as good as unaffected by the clamp-up load.[50,51] The reduced loss of stiffness and the postponed final failure is due to the initial damage in the laminate accumulating in the area that is clamped by the bolt, which restrains transverse expansion.[48]

Since preload does not have an effect on the onset of bearing failure, it does not result in an increase of the design strength. But because the application of a preload has the advantage of reducing the stiffness loss after initial failure, and postponing final failure, it is still preferred to apply a preload to the bolt.

Effect of load offset

With an in-plane load offset from the neutral plane of the laminate, the bearing stress through the thickness of the laminate varies, it is higher on the side where the load is applied. In metals this effect is usually negated by plasticity, which redistributes the loads. Composites however are brittle, showing no plasticity before failure, so this unequal stress distribution has to be accounted for in the design. This is typically done by reducing the strength by an arbitrary factor of 1.5 to 2 until test data is available.[52]

For the analysis a conservative reduction factor of 2 is selected, resulting in a multiplication factor of 0.5.

Effect of layup

The effect layup has on the bearing strength can be significant, the differences between reported minimum and maximum values are around a factor 2.[47,51]

Both in 0/90° and ±45/90° laminates the highest bearing strength is achieved with 25% of 90° plies, and when exceeding 50% the strength drops significantly.[47] Not only the ratio between the ply orientations has an effect on bearing strength, but the stacking sequence is of influence as well.[51,53]

Implementing all these effects requires either an enormous amount of test data or a thorough understanding of the underlying behavior. Since neither of these is available the effects of layup are not implemented.

This does not mean that any layup can make a good design though. To keep the bearing strength at a high level laminates with a large portion of the plies in one direction need to be avoided. More specifically, for a laminate with 0°, 90° and ±45° plies the following guidelines can be given:

- Don't use more than 50% 90° plies, if exceeded this results in a significant reduction in strength.[47]
- Use at least 25% of ±45° plies to improve the resistance to splitting.[47]
- Don't group plies of the same orientation, since this reduces the bearing strength.[51]

Effect of hole oversize

A hole with a larger diameter than the bolt has been shown to have an effect on the onset of bearing damage, although the effect on final bearing strength is very small. A bigger clearance results in a lower initial failure load.[54]

With the high degree of process control typically seen in space engineering, machining the hole in the laminate with a high accuracy is considered possible. In case it proves to be too difficult to machine the hole in the composite laminate to within the required tolerance, the use of an insert can provide a solution, since those are definitely machinable to the required tolerance. The inaccuracy of the hole diameter in the laminate can then be taken up by the bondline thickness, for which the tolerances are less strict than for the hole size. The required tolerances are dependent on the design, if bearing is not critical, the required tolerances can be less strict.

The effect of hole oversize is therefore not included, but care has to be taken. If the hole in the laminate can not be made to the required tolerance, the use of an insert may be required to achieve a high strength.

Effect of out of round holes

The effect of out-of-round holes on the final bearing strength was shown to be less than 5%.[51] For the effect on the onset of bearing failure one could see out of round holes as holes with a variable clearance over the circumference. In that case the same argumentation as for the effects of hole oversize applies. Therefore, no multiplication factor is included for the effect of out of round holes.

4.1.3 Shear-out

A simplified geometry loaded by an in-plane load is shown in Figure 4.4. The area on which shear-out failure occurs is shown as well.

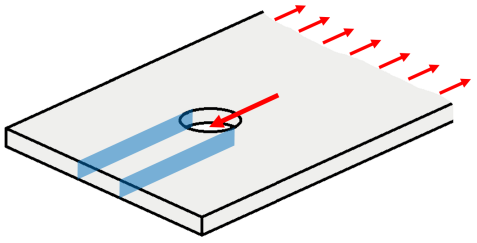

Figure 4.4: FBD showing shear-out failure area (blue).

Again analytical methods are used for the analysis, for similar reasons as for the calculation of bearing strength. The used method is the same as the method used to calculate shear-out strength for isotropic materials, so the shear-out load F_{so} is found using:[49,53]

$$F_{so} = 2 * \tau * e * t \tag{4.3}$$

With e the distance of the hole center to the edge, and t the thickness of the laminate. τ is the allowable stress value. Ideally this value is again determined from test data.

It is observed that the allowable stress value decreases slightly for increasing edge distances.[49] This indicates that some local effects near the hole influence the failure somehow. The reduction in allowable stress is very small, especially for laminates that also perform well in bearing and shear-out, for which the said reduction is no more than 5%.

Several other effects influence the strength in similar ways as they did for bearing. Although there is not enough data available to implement them, these are discussed briefly.

A higher bolt preload results in a slight increase of the shear-out strength, although the effect is less apparent than for bearing. It is believed that this is due to friction between the washers and the laminate.[48]

Similar to bearing, different layups result in different strengths, again showing differences between the minimum and maximum of a factor 2.[49] Just like bearing, this is not implemented due to lack of the required data but the same design guidelines still apply.

Additionally, an effect due to the inserts is expected since these distribute the loads over the interface. There is however no data available to confirm this.

4.1.4 Pull-through

A simplified representation of an out-of-plane loaded plate is shown in Figure 4.5. The cylindrical area on which pull-through failure occurs is shown as well. In the figure the bolt is not shown, but the diameter of the failure area is equal to the bolt head diameter.

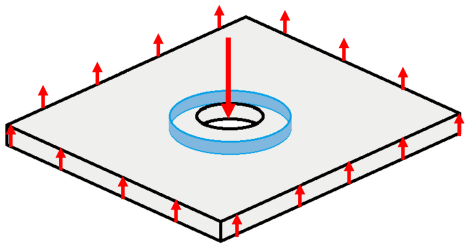

Figure 4.5: FBD showing pull-through failure area (blue), bolt omitted for clarity.

Even though the out-of-plane loads that act on the SCT are relatively small and unlikely to cause pull-through failure, a simple check is included in the model.

Similar to bearing and shear-out failure, modeling this failure type with FEM has shown to require complicated modeling methods and results in less than optimal correlation with reality.[43,55,56] Experimental analysis showed that the initial damage is in through the thickness and interlaminar shear under the bolt head edge.[57]

Considering the typical failure mode, the following equation to estimate the pull-through load F_{pt} is proposed:

$$F_{pt} = \pi * d_h * t * ILSS * k \tag{4.4}$$

Where d_h is the bolt head diameter, t the thickness of the laminate and $ILSS$ is the interlaminar shear strength of the material. k is a knockdown factor used to account for the uneven distribution of the stress through the thickness.

A comparison of this method with experimentally obtained initial failure loads is shown in Table 4.3.

Table 4.3: Comparison of estimation method to experimental values.

Experimental data[57]			Estimation, k=0.7	
t [mm]	D [mm]	F_{pt} [kN]	F_{pt} [kN]	% of actual
3.50	8.0	6.9	5.3	77%
3.50	7.2	6.5	4.8	74%
3.50	9.9	8.3	6.6	79%
3.50	8.3	7.2	5.5	77%
0.87	8.0	1.3	1.3	99%
1.75	8.0	2.8	2.6	96%
5.24	8.0	11.0	7.9	72%
3.50	8.0	6.5	5.3	81%
2.40	8.0	4.4	3.6	83%

It can be seen that using k=0.7 gives accurate to conservative results for this dataset.

For the analysis the estimation method described above is used with k=0.5. While this is more conservative than required according to the shown data comparison, some extra margin is taken to allow for unexpected effects. The use of washers or a flanged insert may further increase the strength. On the contrary, when a bending load is also applied, the pull-through load will concentrate on one side of the bolt, reducing the pull-through strength. Since these effects are difficult to quantify, and pull-through is not an expected failure mode, these effects

are not taken into account. In case pull-through does become an issue, further investigation into this failure mode is recommended.

4.1.5 First ply failure

Calculation of the stresses and strains in the surrounding structure and in the patch is done using FEM since no analytical methods are available for local effects in this complex geometry. The approach taken is explained in the following section.

4.2 Finite element analysis

The FE model is used to determine the stiffness response of the attachment, and to determine the strains in the laminate surrounding the bolt.

The attachment is modeled as if in a flat base structure. While the base structure is often cylindrical, the part of the structure that contains the attachment is only a small part of the circumference of the cylinder. The local curvature is therefore small with respect to the size of the model, so approximating it as a flat structure does not result in a large error, while making the construction and parametrization of the model much simpler.

To representatively model the sequence in which loads act on a typical structure, the preload is applied first, and all other loads are applied in a subsequent step. This is analogous to the installation of all parts before the structure is used and experiences the actual load.

The performed analysis is linear, since only low deflections are expected due to the high stiffness of the material that is used. The composite material behaves linearly up to failure, showing a brittle failure with no plasticity. Use of a linear analysis also limits the required analysis time.

Some aspects of the model are elaborated on hereafter.

4.2.1 Element selection

Considering that local and through the thickness effects are of interest, solid elements are the preferred choice. In the ribs, insert, and other areas where a single solid material is defined reduced-integration hex (C3D8R) elements are used. Additionally, areas of complex geometry contain some wedge elements (C3D6) to facilitate meshing. Full-integration hex (C3D8) elements are used where a composite layup is specified, since the use of reduced-integration elements led to mild hourglassing in these laminates.

A mesh convergence study was performed, which is shown in section B.1.

4.2.2 Material assignment

To facilitate further explanations, the zones that are used in the FE model are shown in Figure 4.6.

The aluminum inserts are assigned isotropic elastic properties. No plasticity is included since it is not expected to significantly influence the results of the analyses, while it would increase the computational time significantly.

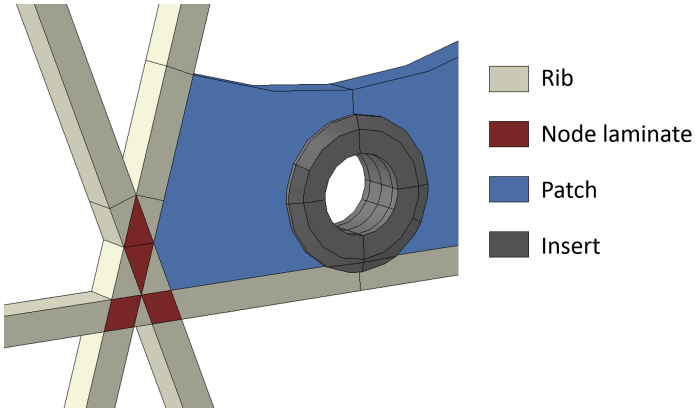

Figure 4.6: Different zones in the FE model.

The elastic properties of the composite material are input as 'engineering constants', which allows different properties to be assigned in all principal directions. The used properties are listed in section B.6 A solid section of this material is applied to the ribs, and a laminate consisting of plies of this material is used for the patch. In this patch, care is taken to minimize the error that results from how Abaqus calculates laminate properties in solid elements, as explained in section B.2. A laminate is also specified in the node laminates, ply properties there are corrected as explained in section B.3. The modeling approach for the rib is not changed in the rib-patch interface, although some patch plies extend into the rib, this is not modeled as such. section 5.2 shows a comparison of this method with more detailed models, showing that the taken approach gives conservative results.

4.2.3 Boundary conditions and load introduction

In the initial and bolt preload steps the edges of the model are pinned. In the loading step there is the possibility of specifying a far-field compressive or tensile displacement in the plane of the structure. The magnitude can be defined separately for the horizontal and vertical directions. This allows a simplified version of the far-field loads to be included in the analysis. An example of such boundary conditions is shown in Figure 4.7.

The bolt loads are introduced by coupling the load to several surfaces. Details of this method and a comparison to several other methods are shown in section B.4.

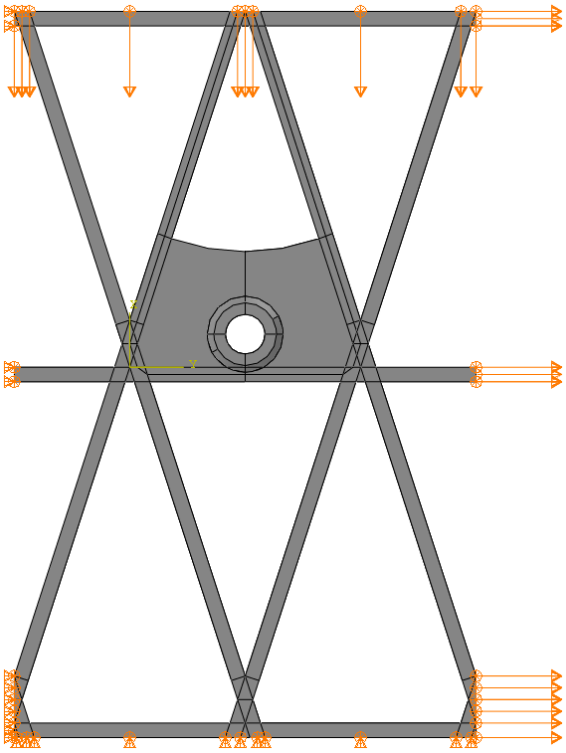

Figure 4.7: Boundary conditions in the loading step with vertical compression and horizontal tension applied.

4.2.4 Failure analysis

To determine failure in the composite the maximum strain criterion is used. While this may not be the best criterion available, using more complex criteria is a refinement which would be necessary only with a more accurate modeling approach.

The area directly surrounding the bolt is excluded from the analysis, since failure there is in one of the failure modes determined analytically. The region on the boundary of the model is also excluded since it is not the region of interest, and the local effects caused by the attachment will have a reduced impact there.

The used modeling method occasionally resulted in singular points on the rib-patch interface, due to the sharp geometry and stiffness changes there. Care must be taken to keep this behavior in mind when evaluating the results. More information on the singular behavior can be found in section B.5.

4.3 Parametric scripted implementation

The described analysis method is implemented in a script, with the entire attachment design determined by several parameters. A flowchart highlighting the tasks performed and controlled by this script is shown in Figure 4.8.

The first steps are checking the design rules that are outlined in section 5.3 and calculating the failure indexes for the failure modes that do not require additional steps.

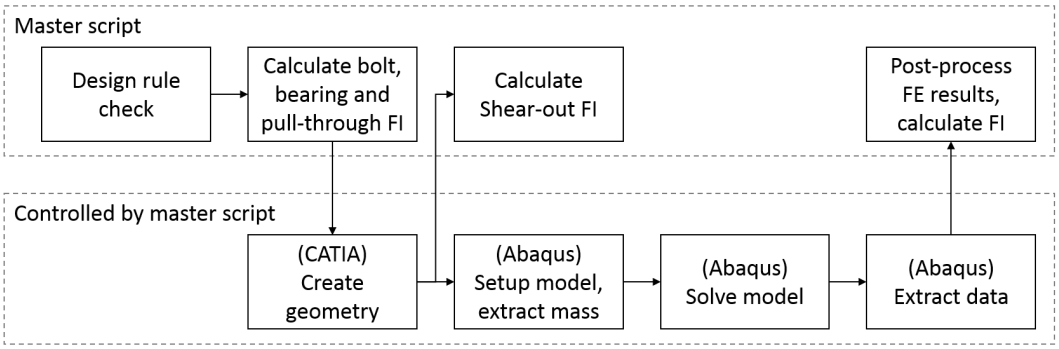

Figure 4.8: Flowchart of the scripted implementation.

In the taken approach the patch design is fully parametric, with three parameters determining the shape of the patch around the attachment point. How these control the patch shape is shown in Figure 4.9. Several other parameters control the patch thickness, bolt size, insert dimensions and other details.

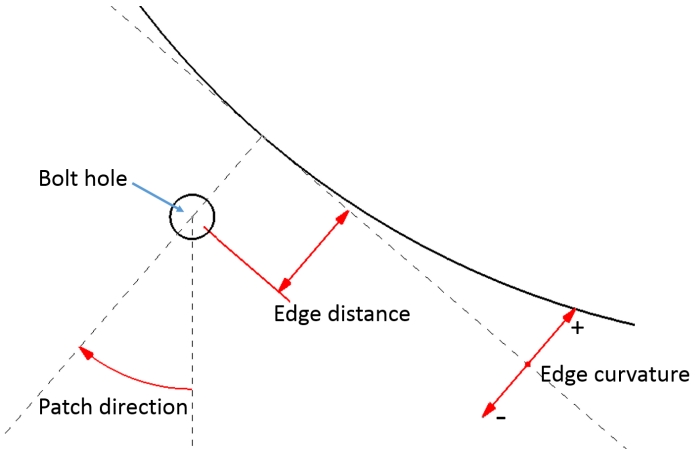

Figure 4.9: Parameters controlling the patch shape.

Several examples of patch shapes that can be made using this method are shown in Figure 4.10.

The CATIA model that is used to generate the geometry is fully parametric, a macro is used to change the parameters and then export the generated geometry as a step file.

The edge distance for the shear-out calculations is measured in CATIA as well, since it depends on too many variables to allow it to be directly calculated from the design parameters. The edge distance is measured by drawing two lines from the hole edge to the edge of the structure, in the direction of the in-plane load. This is illustrated in Figure 4.11. Of the two lengths, the shortest is then used in the shear-out calculations.

In Abaqus, a script is used to import the geometry, generate the mesh, and apply the material properties, loads, boundary conditions and other required inputs as described in section 4.2. The mass of the attachment is extracted in this step as well, since this is the first time that the geometry and the material properties are both in one model. After construction of the model, input files are written and the model is solved. Stresses and strains are extracted from the output files and written to text files. This data is then processed externally. By

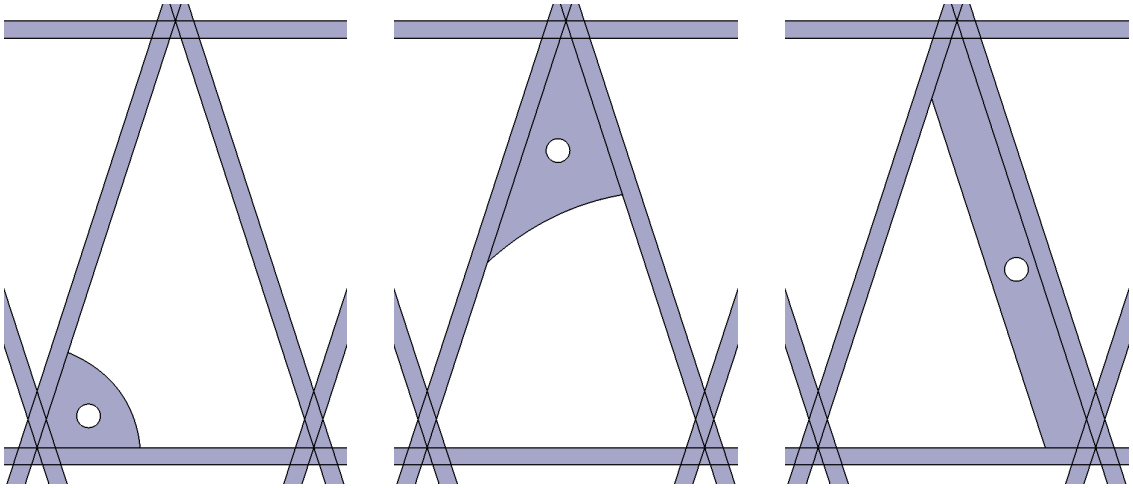

(a) Parameters: 55/10/-5 (b) Parameters: 160/15/2 (c) Parameters: 252/7/0

Figure 4.10: Examples of some possible patch shapes for different attachment locations. With parameters: patch direction/edge distance/edge curvature.

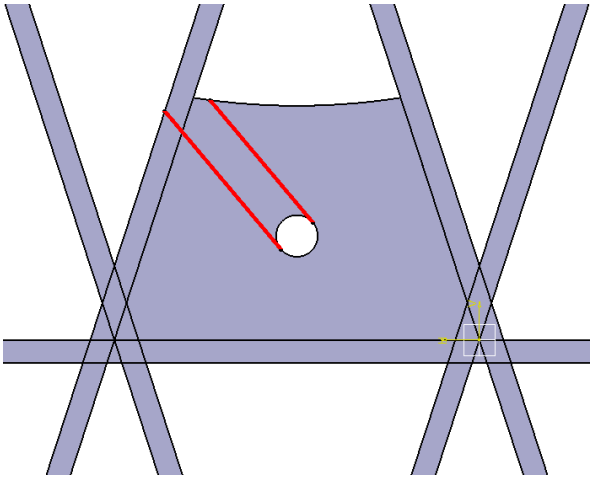

Figure 4.11: Measurement of the edge distance for shear-out in CATIA.

doing so, a significant reduction in computation time is achieved, compared to doing all the post-processing in Abaqus.

If failure of the attachment is found in one of the steps before the FE analysis the script is stopped since further analysis of a failed design is unnecessary.

Due to the full parametrization of the design and automated analysis it is possible to couple the analysis to an optimization algorithm, but this is outside of the scope of the current research.

With the presented approach, the runtime of the entire analysis is around 5 to 10 minutes on a stand-alone computer that is equipped with an Intel Xeon E3-1270 CPU, and 16 GB of memory.

4.4 Design method for rapid initial design

With the numerous variables determining the design of the attachment, finding a proper starting design can become a lengthy iterative process. To accelerate this, the relations between several parameters can be assembled in a single design graph.

Considering the typical loads acting on a SCT are mostly in-plane, this is likely to be driving the design. The design graph therefore focuses on bearing, shear-out and bolt shear failure, which are the three in-plane failure modes that are calculated analytically. Although it would also be desirable to include failure in the composite surrounding the attachment, the lack of a clear dependence on the input parameters disallows this.

The design graph presents a method to determine good combinations of initial values for the bolt size, edge distance and patch thickness, based on a given load. An example is shown in Figure 4.12, how it is constructed and used is discussed afterwards.

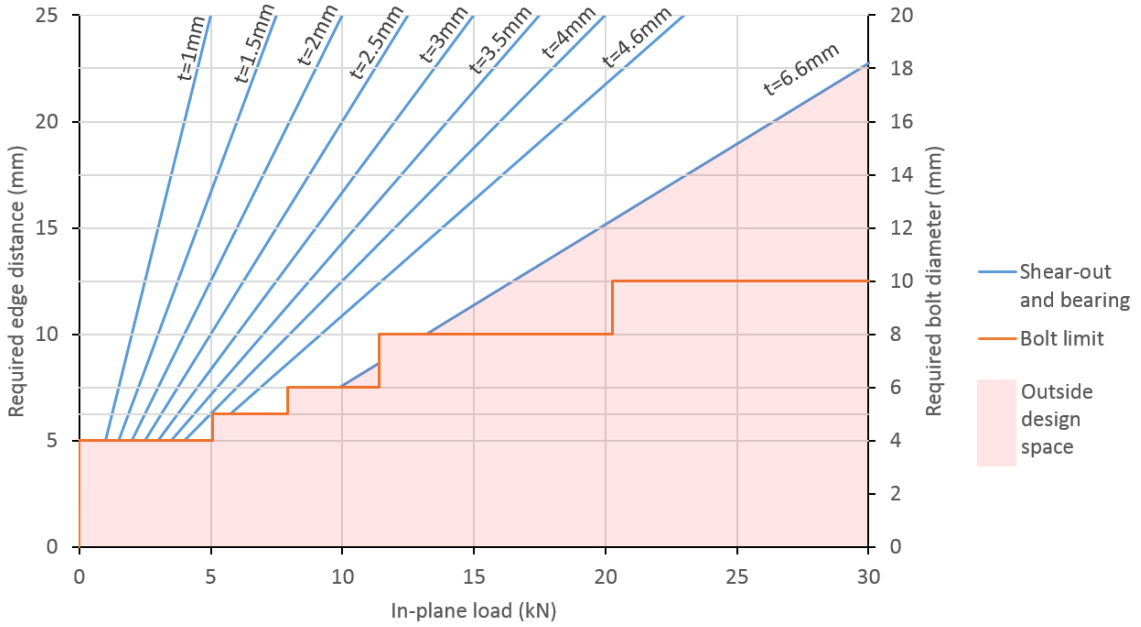

Figure 4.12: Example of an initial design graph.

4.4.1 Construction

For a fixed laminate thickness, the graphs shown in Figure 4.13 can be drawn. These show two relations: between the edge distance and the shear-out strength, and between the bolt diameter and the bearing strength. The latter is intentionally plotted on the secondary vertical axis.

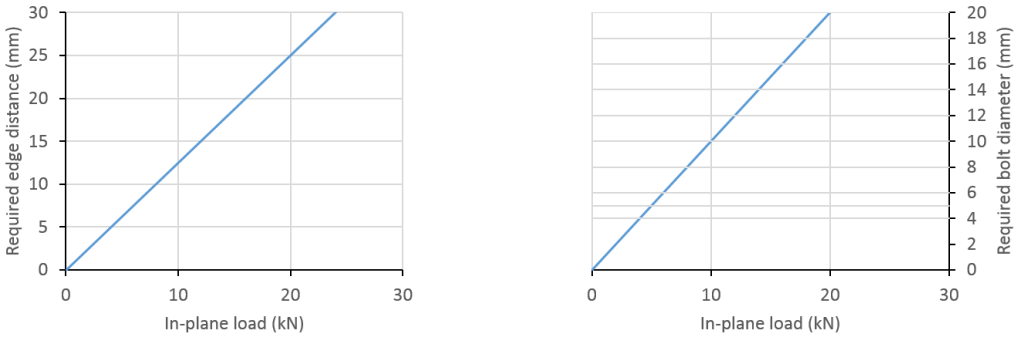

(a) Edge distance for shear-out strength.

(b) Bolt diameter for bearing strength.

Figure 4.13: Relation between the in-plane load and the required edge distance and bolt diameter, for a laminate of 4 mm thickness.

Both relations are linear and have the in-plane load on the horizontal axis. When the range of both horizontal axes is identical, the vertical axes can be scaled such that the edge distance and bolt diameter plots for a given thickness coincide when the graphs are overlaid on top of each other.

Recalling the equations used for calculating the shear-out and bearing loads:

$$F_b = d_b * t * \sigma_b \tag{4.2}$$

$$F_{so} = 2 * \tau * e * t \tag{4.3}$$

And setting these equal to each other:

$$d_b * t * \sigma_b = 2 * \tau * e * t \tag{4.5}$$

Since the thickness is equal for both, it cancels out, and after some rearranging this gives:

$$d_b = e * \frac{2 * \tau}{\sigma_b} \tag{4.6}$$

Now $\frac{2*\tau}{\sigma_b}$ is the ratio between the two vertical axes that is required to have the two lines coincide. This is a ratio of the allowable shear-out and bearing stresses, and these allowables should include all the applicable multiplication and knockdown factors.

The two graphs can now be merged, and more lines can be added for other patch thicknesses. Then, the lower limit on bolt dimensions can be plotted on the secondary vertical axis. This limit depends on the shear strength of the bolts, as well as on the minimum bolt diameter. The bolt limit is a stepwise function, since only standard bolt sizes are considered. The earlier plotted lines for shear-out and bearing are truncated below this line.

Now also recognizing the maximum patch thickness, the area outside of the design space can be identified. This completes the graph.

The example graph shown in Figure 4.12 is constructed using allowables for Hexcel 8552/IM7 CFRP, grade 12.9 steel bolts with regular thread, and no inserts. Constructing these curves for different combinations of materials is rather simple, and has the potential of saving significant amounts of time if multiple attachment points need to be designed on the same structure, with the same materials. Looking at the reference SCT with several hundred attachment points, this is definitely the case.

4.4.2 Use

To illustrate the use of the design graph, an example is given based on the attachment point location shown in Figure 4.14, loaded with 11 kN in-plane. The combination of this location and load direction makes the edge distance directly dependent on the design.

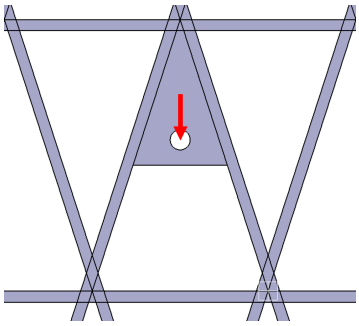

Figure 4.14: Location and load direction used for the example.

To find good combinations of initial parameters one starts with finding the applied load on the horizontal axis. From this point go upwards up to the first possible bolt size inside of the design space at that load. At this point lies the first design, the values for the edge distance and bolt size can be read from their respective axes, and the patch thickness seen from the location between the lines in the graph. Other designs lie in a vertical line upwards from the initial point. This is graphically shown in Figure 4.15.

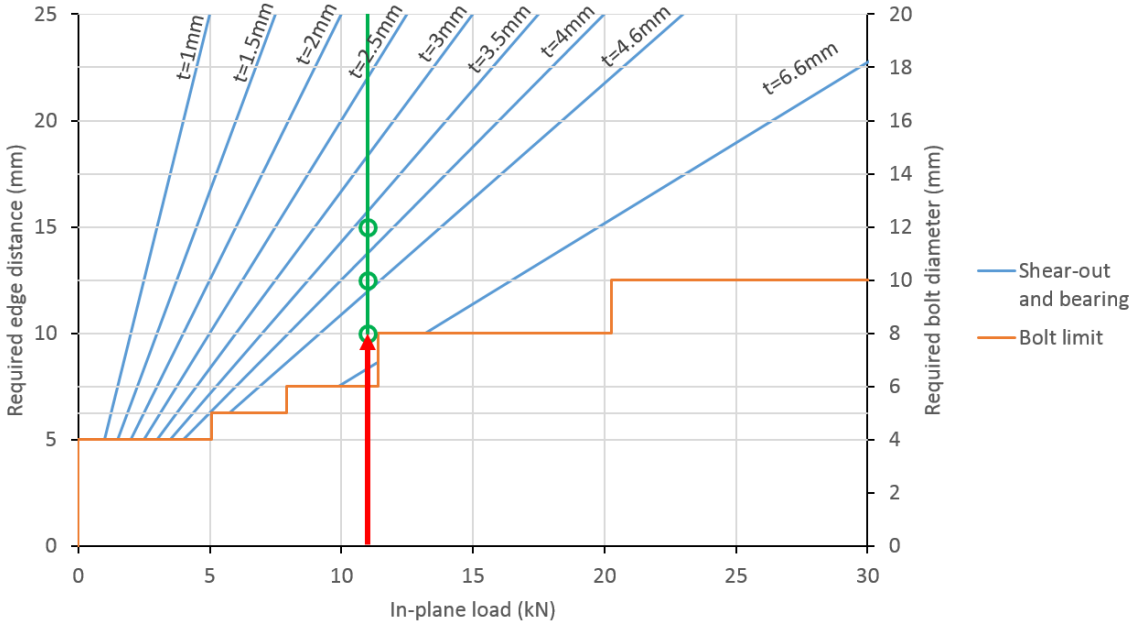

Figure 4.15: Example of use of the design graph, for an 11 kN load.

The first three designs are encircled, the resulting parameters shown in Table 4.4. An estimation of the bolt, nut and patch masses are made, based on a 20 mm long bolt and typical density of the considered materials.

The lowest total mass is obtained using a thick patch, and the smallest bolt diameter. One

Table 4.4: Parameters of the first three designs found using the design graph.

Bolt diameter	Patch thickness	Edge distance	Bolt+nut mass	Patch mass	Total mass
8 mm	6.6 mm *	10.0 mm	19.2 g	10.6 g	29.8 g
10 mm	4.4 mm	12.5 mm	38.5 g	7.6 g	46.1 g
12 mm	3.7 mm	15.0 mm	56.2 g	6.7 g	62.9 g

* Increased to 6.6 due to manufacturing constraints

could argue that the use of heavy steel bolts in this example is distorting the conclusions drawn from it. However, assuming that the bolt strength does not change, the bolt density would have to be decreased by more than 84% before a design with a larger diameter bolt achieves a lower mass. Such a reduction is unrealistic. Therefore it can be concluded that the lightest initial design is usually the one with the smallest possible bolt diameter.

In some designs, additional constraints like a maximum edge distance may apply, for instance for an attachment close to a rib. These can be taken into account by simply setting an upper limit on that parameter, which limits the amount of available designs.

Chapter 5

Behavior and design guidelines

Using the analysis methods presented in chapter 4, several studies are performed to increase the understanding of the structure's behavior, and response to changes in design. This gives valuable information that is later used for a rapid design of the attachment test samples. To make sure that these samples can actually be made, the manufacturing constraints and other design limits are elaborated upon.

5.1 Trend study

To get an understanding of the influence of several of the design parameters, a trend study is performed. This is done by slightly varying one of the parameters of a reference model, while keeping the others unchanged. The results are then compared to the reference model.

For this study, the reference model is that of an attachment point next to the hoop rib, with the in-plane load applied in the direction of that rib. The in-plane load is offset from the neutral plane of the structure, so also results in a bending moment. The attachment point location and load type are very similar to one of the locations chosen for testing, making the results of the trend study more applicable to the design of the test samples. The geometry of the reference model and the load direction are shown in Figure 5.1.

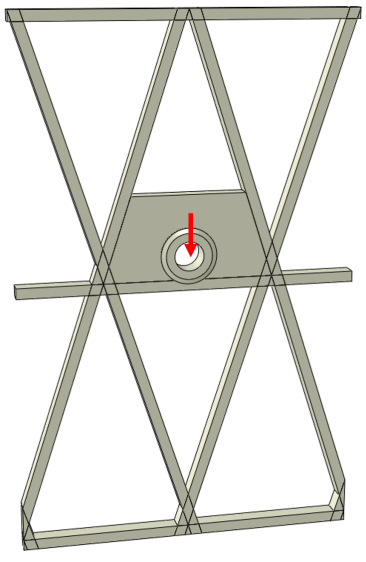

Figure 5.1: Reference model and in-plane load direction.

Three parameters are varied, which control the size, shape and layup of the laminate patch. The results are shown using the strains in a part of the laminate, where all the relevant differences can be seen.

5.1.1 Patch size

To see the effects of the patch size it is changed by 10 mm, making it both smaller and larger. As might be expected the smaller patch shows higher strains overall, and the larger patch has lower strains. The effect is clearly seen in the strain in the fiber direction, a comparison of which is shown in Figure 5.2. Both the strain transverse to the fiber and the shear strain show similar differences.

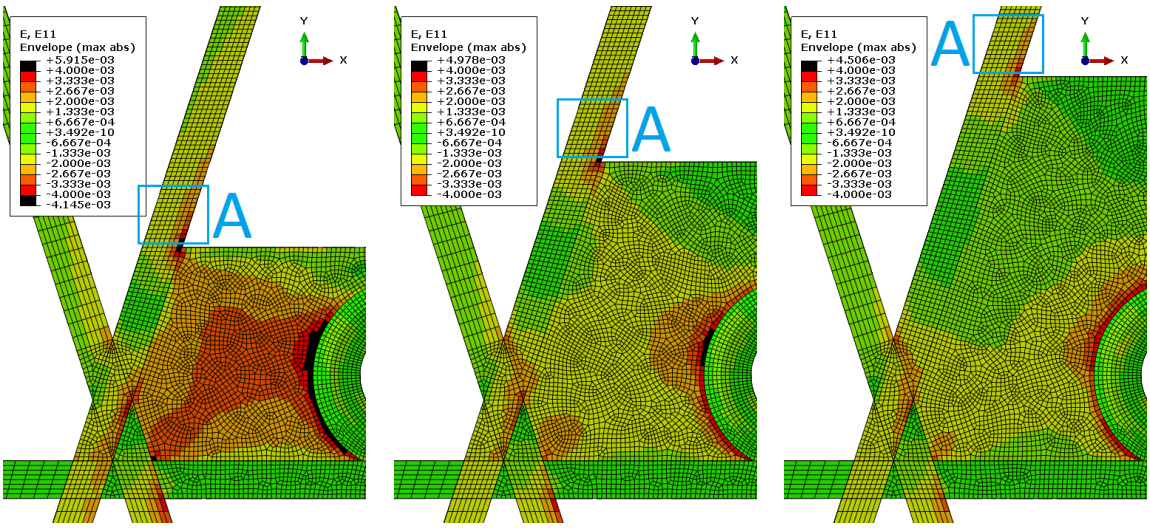

(a) Smaller patch (b) Reference model (c) Larger patch

Figure 5.2: Strain along the fiber in patches with different sizes.

With a reduced patch size, the strains in the patch at a distance from the bolt are relatively high compared to the larger patches. In the larger patches, the strains at a distance from the the insert are noticeably lower than the strains near the insert.

An overview of the patch masses and the highest absolute strains in the laminates is given in Table 5.1. The elements at singular points are excluded from this comparison, and in line with the analysis method presented in chapter 4, the area directly surrounding the bolt is also excluded. The relative mass and strain changes with respect to the smallest patch are also given.

Table 5.1: Mass and maximum strain in the patch for different patch sizes.

Patch size	Patch mass	Max strain (abs)	Mass change	Strain change
Smaller	17.4 g	$3.94{*}10^{-3}$	0%	0%
Reference	22.6 g	$3.21{*}10^{-3}$	+30%	-19%
Larger	27.2 g	$2.90{*}10^{-3}$	+56%	-26%

The reduction in strain going from the smallest to the medium-sized patch is quite significant. By making the patch even larger only little further reduction of strain is achieved, while this does increase the mass further. This indicates diminishing returns when increasing the patch size to reduce the strains in the laminate.

Also noticeable is that the size of the patch has very little effect on the strain in the rib just outside of the patch (the region marked A in Figure 5.2).

5.1.2 Layup of the laminate patch

The effect of changing the layup is studied by removing one ply orientation from the quasi-isotropic (QI) layup that is used for the reference model. Given the symmetry of the model, removing one of the ±45° plies does not make sense, so the comparison is made with layups where either the 0° or the 90° plies are removed. The resulting strain in the fiber direction is shown in Figure 5.3.

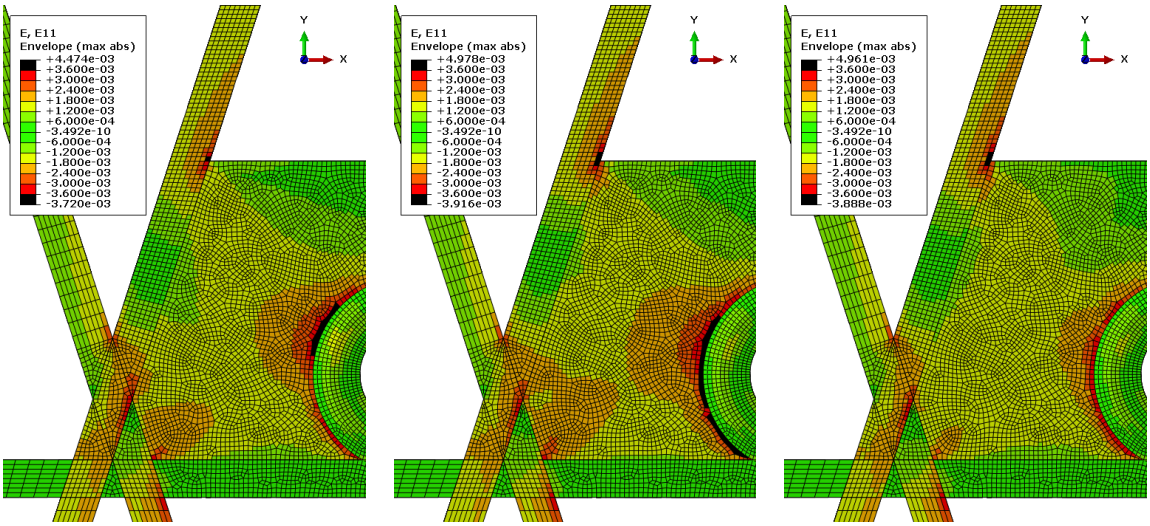

(a) No 90° plies (b) Reference model, QI (c) No 0° plies

Figure 5.3: Strain along the fiber in patches with varying layup.

Overall, an improvement is made by removing the 0° plies, whereas the removal of the 90° plies offers almost no advantage. These differences are very similar for the strain transverse to the fiber. For the shear strain this is different though, here both the changes result in a lower overall strain. This can be attributed to the higher fraction of ±45° plies, which dominate the shear behavior. By removing a ply orientation, the fraction of ±45° plies increases from 50% to 67%.

Furthermore, a comparison was made with laminates that had a 0/90 or ±45 layup. Since these have only two fiber directions in the laminate and showed very high shear strains as a result, these are not considered suitable for any design.

Similar to the changes in patch size, changing the layup has little effect on the strains in the ribs just outside of the patch.

5.1.3 Curvature of laminate edge

The third and final parameter changed in the trend study is the curvature of the edge of the patch. Both a negative curvature, which creates a sharper corner with the rib, and a positive curvature giving a less sharp corner are compared. The differences in strain along the fiber and perpendicular to it are very small, but as can be seen in Figure 5.4 the shear strains do show some differences.

A positive curvature results in the shear strain on the rib-patch interface near the patch edge being more evenly spread, and lower in magnitude. A negative curvature results in the opposite, it increases the shear strain and gives a less desirable distribution.

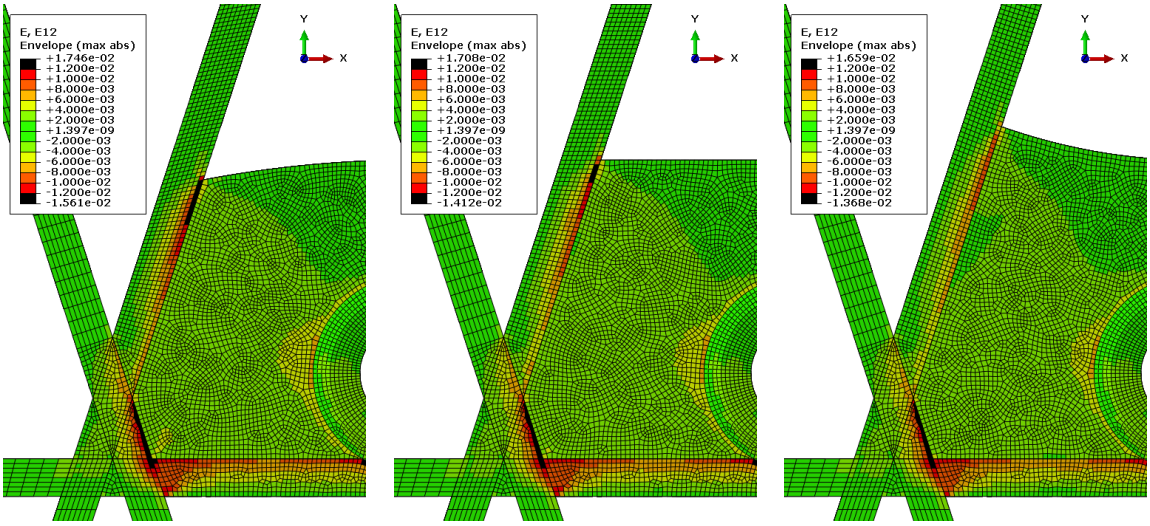

(a) Negative curvature (b) Reference model (c) Positive curvature

Figure 5.4: Shear strain in patches with varying curvature.

The differences on the lower side of the patch are almost non-existent, indicating that the curvature only affects the strain locally.

5.2 Detailed rib-patch interface modeling

In the parametric model all ribs are modeled using the same method, including the ones that are adjacent to the patch. This means that the plies of the patch that extend into the ribs are not modeled as such.

To investigate the impact of this simplification, and to improve the understanding of the behavior of the interface, a model is manually adjusted to include these plies. This is done by modeling the overlapping area as a laminate, with both rib and patch plies.

In the ribs adjacent to the patch the plies are extended halfway into the rib, so the compaction of the ribs from the other side is not affected, thus making sure that the same rubber tooling blocks can be used. In the small section of the node where there are no overlapping rib plies, the patch plies are extended to the center of the node since there is no compaction from the other side. Furthermore, as a result of the observations made from the model with the patch plies extending halfway into the ribs, a third model was made with the additional modification to extend the outermost patch plies to the far side of the rib. The different regions used in these models are visualized in Figure 5.5.

The more complex layout of the interface zone required multiple section cuts to be made so the regions could be assigned different material properties and layups. Some additional cuts were necessary in order to be able to mesh the part. Especially the nodal area presented difficulties in meshing.

The largest differences in the results of the three models can be seen in the in-plane shear strain on the rib interface. These strains are shown in Figure 5.6. By modeling the plies into the ribs a significant reduction of shear strain is observed over the entire interface. Further

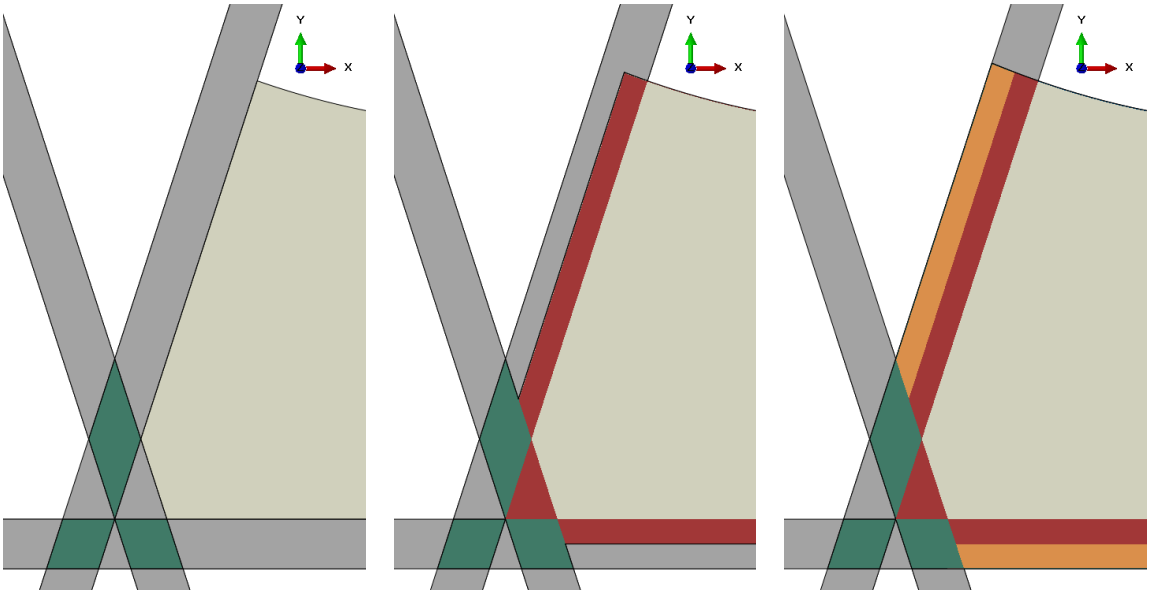

(a) No plies into ribs modeled. (b) Plies modeled halfway into rib. (c) Additional ply to far side of rib.

Figure 5.5: Regions used for the various rib-patch interface models.

extending the outer plies to the far side of the ribs slightly reduces the strain in the hoop rib, but it does not further decrease the maximum shear strain, which is present in the node.

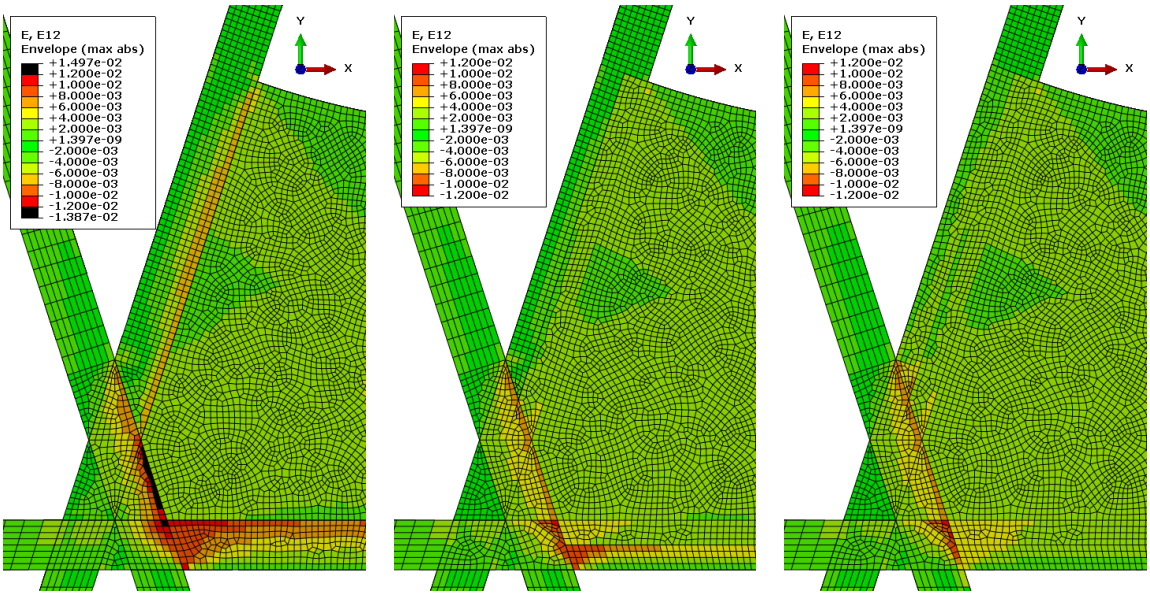

(a) No plies into ribs modeled. (b) Plies modeled halfway into rib. (c) Additional ply to far side of rib.

Figure 5.6: Shear strain for various rib-patch interface models.

Figure 5.7 shows that this is different for the strain transverse to the fiber, which does benefit from the further extension of the top and bottom plies. Extending the plies halfway into the rib already gives a reduction in strains around the node, but near the top of the node a small area with higher strain remains. The higher strains are most pronounced on the surface, and have much lower values in the interior of the rib. Extending the top and bottom patch plies

into this area results in a further reduction of the strain.

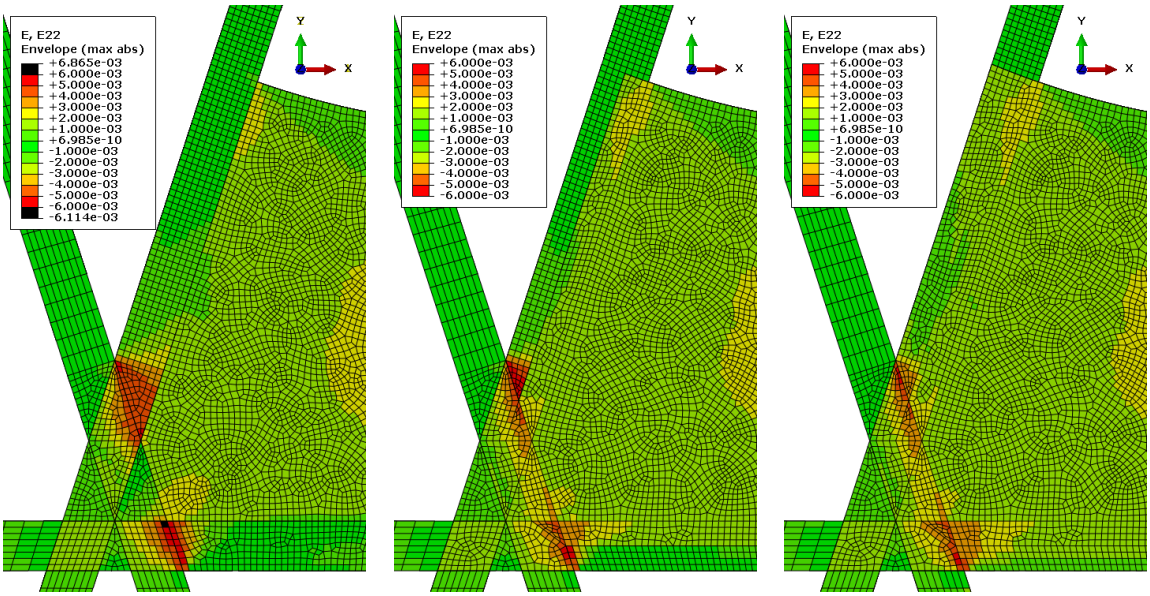

(a) No plies into ribs modeled. (b) Plies modeled halfway into rib. (c) Additional ply to far side of rib.

Figure 5.7: Strain transverse to the fiber for various rib-patch interface models.

By more accurately modeling the interface, the strains do not always decrease. Extending plies to the far side of the rib results in a relatively high strain along the fiber in these plies, as can be seen in Figure 5.8. Still, these strains are low relative to both the allowable values and the strains in other directions. It is therefore chosen to extend the top and bottom plies to the far side of the rib in the test samples as well.

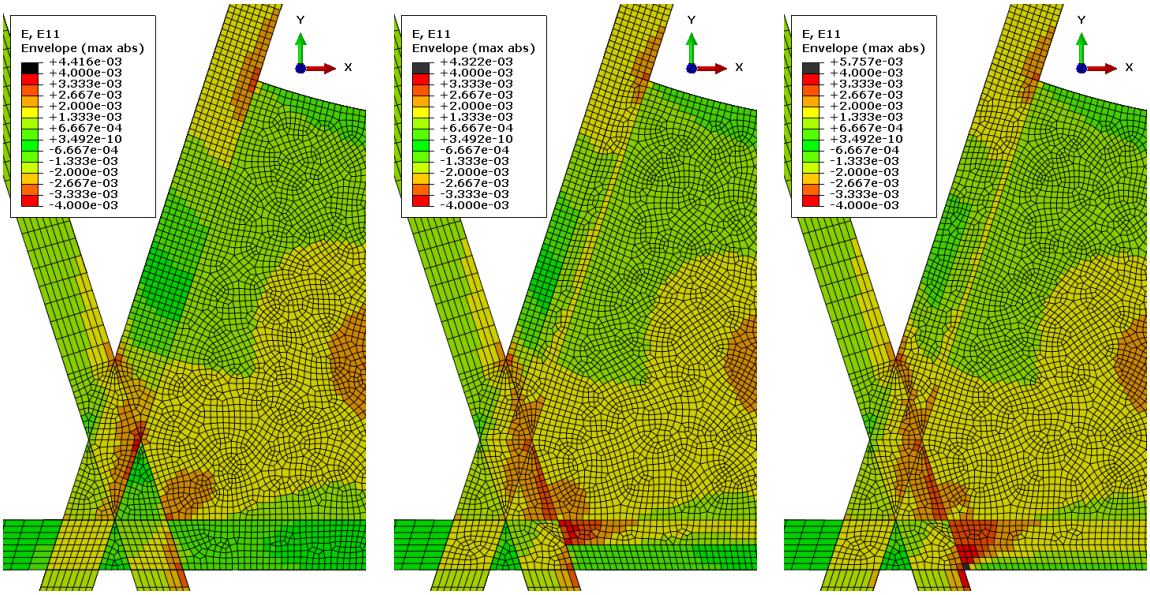

(a) No plies into ribs modeled. (b) Plies modeled halfway into rib. (c) Additional ply to far side of rib.

Figure 5.8: Strain along the fiber for various rib-patch interface models.

The out-of-plane and interlaminar shears do not show any noteworthy changes.

Overall, by more accurately modeling the interface a reduction of the shear and transverse strains is observed. And while the strains along the fiber slightly increase in the interface area, their failure index is still lower than it is for the other strains. Considering the strains in all directions, the maximum failure index decreases by 15%. Therefore it can be concluded that more accurate modeling leads to a lower failure index, so the simplified approach as used in the scripted model is conservative.

5.3 Design limits

The complexity of the manufacturing method for grid-stiffened and lattice structures imposes some limits on the design of the attachment. Especially the compatibility with the expansion tooling is limiting. Furthermore some design rules apply.

5.3.1 Manufacturing constraints

The limits imposed by the manufacturing method can be split into two groups. The first set applies to the base grid structure. These limits should also be taken into account when designing the main structure, which is usually done before designing the attachments. The second set applies specifically to the attachment point.

These limits are based on the current experience with the manufacturing process, and might be refined as the understanding of the process increases.

Base structure

Limits here are determined by the necessary compaction during cure. Since the plies of the rib overlap at the nodes, the height of the layup before cure can be larger than the final rib height, as can be seen in Figure 7.3 for instance. The nodes are compacted before and during the cure cycle. There are limits to this compaction, experience shows that a pre-cure height of between 1 and 1.5 times the desired rib height gives good results. When all ribs are of equal width, this corresponds to a cured rib width between 0.5 and 0.75 times the tow width.

This approach requires the ribs to be compacted laterally, it is required to check if the unexpanded rubber tooling fits between the ribs after layup. If the tooling interferes with the rib tows this disallows placement after layup.

These constraints require the width and thickness of the tows to be known. The width is usually quite clear, and for the thickness the nominal cured ply thickness can be used. If there is a large difference in the widths of the ribs, this complicates the calculations noticeably. In typical structures all ribs have similar dimensions, so this is not usually a problem.

Attachment point

Limits on the design of the attachment point are both due to manufacturability of the laminate patch, and of the insert placed in it.

A minimum patch thickness is imposed by the minimum amount of plies that is necessary. This depends on the specified ply orientations, the ratio between these, and the ply thickness.

For most symmetrical layups consisting of three or four ply orientations, this results in a minimum thickness around 1 mm.

The maximum patch thickness is equal to the rib height. At patch thicknesses just below the rib height an additional difficulty occurs. The rubber tooling then becomes very thin, possibly resulting in difficulties during cure. Based on the current experience with the process, a conservative assumption is made to limit the rubber tooling to be no thinner than 2 mm. Preferably this limit is further refined by manufacturing trials to find the actual limit. Possible patch thicknesses are therefore either between the minimum and 2 mm less than the rib height, or equal to the rib height.

Another constraint is imposed by the expansion of the rubber tooling in the cell. With a patch, the required rubber tooling must still fit in the cell after layup. If the patch is too large or in an unfavorable location, this may no longer be the case, thus making the design unmanufacturable. Since this depends on too many variables to be able to give a direct guideline, this will have to be judged on a case by case basis.

To keep the inserts machinable and handleable, the minimum wall thickness is set at 1 mm. This also ensures that the inserts can transfer enough load to justify the increase in bearing strength they provide in the analysis.

5.3.2 Design rules

Aside from the manufacturability limitations, some design rules apply. These are the minimum requirements a design must fulfill in order to be considered suitable. Some of these were already indicated in chapter 4.

To reduce the shear strains in the laminate, at least three ply orientations must be used, with at least 30° difference in orientation between them. In case more than three ply orientations are used, some of these may be within 30° of other, but the layup must contain three ply orientations that differ by at least 30°. Additionally, no more than 50% of the plies may be oriented in the same direction. Not only do these limits reduce the overall shear strain, this also ensures that the bearing and shear-out strength of the laminate are of a sufficiently high level.

To make sure that the bolt and insert are properly seated within the patch, the distance from the bolt center to the laminate edge must be more than the bolt diameter and the insert thickness combined. This ensures that there is always a minimal part of laminate surrounding the bolt and insert. It must be noted that this is the absolute minimum, most designs will have a larger edge distance to provide more strength.

The diameter of the bolt in millimeters is required to be an integer value, and a minimum bolt diameter is set at 4 mm. While non-integer sizes of bolts can be machined if necessary, requirements often dictate that standard sizes are used.

5.3.3 Implementation into model

All constraints and limits can be checked from the input parameters, with the exception of the patch compatibility with the rubber tooling. This check is therefore performed as the first step at the beginning of the analysis.

Since it is recognized that the given limits are conservative in some cases, exceeding of a limit only results in a warning, not a termination of the analysis.

Chapter 6

Verification approach

The developed model is of no use unless it is shown that it actually represents the behavior of the structure. To test if this is the case, test samples are designed and analyzed. Later, these samples are manufactured and tested to obtain the data required to see if the developed model actually represents reality.

The main goal is to show that the stiffness can be modeled properly, and while it would be desirable, accurate modeling of the failure load is not set as a primary goal. This lies mostly in the fact that failure in composites is hard to predict accurately even for simpler structures. Several different failure modes in the fiber and matrix materials contribute to the overall failure, complicating identification of the initial failure mode. [58] Additionally, damage evolution between first and last ply failure complicates analysis. However, knowing that there is some conservatism in the methods used to calculate the failure loads, failure should not occur at a lower load than predicted. It would be advantageous to predict the correct type of failure as well.

To ensure the results correspond to the actual use of lattice and GSS, the provided load cases are investigated, and a representative load type for testing is determined. The different boundary conditions of the tests demand that some changes to the model are made specifically for the tests. These are discussed along with the expected failure loads and the required instrumentation.

6.1 Selected load cases

The SCT used as a reference case has approximately 380 in-panel attachments, for each of which a total of 40 quasi-static load cases are defined. This results in a total of around 15200 load sets of combined in-plane, out-of-plane and moment loads. To reduce the amount of total load sets, the most critical ones are found for each of the attachment points. Since it is not known in advance which of the load components is most critical, three load cases are kept per attachment point: The ones resulting in the highest in-plane, out-of-plane, or moment load. This reduces the amount of load sets to 1140, which are assembled in a graph, shown in Figure 6.1. The provided loads already include the necessary safety factors and model factors, so no further corrections are necessary.

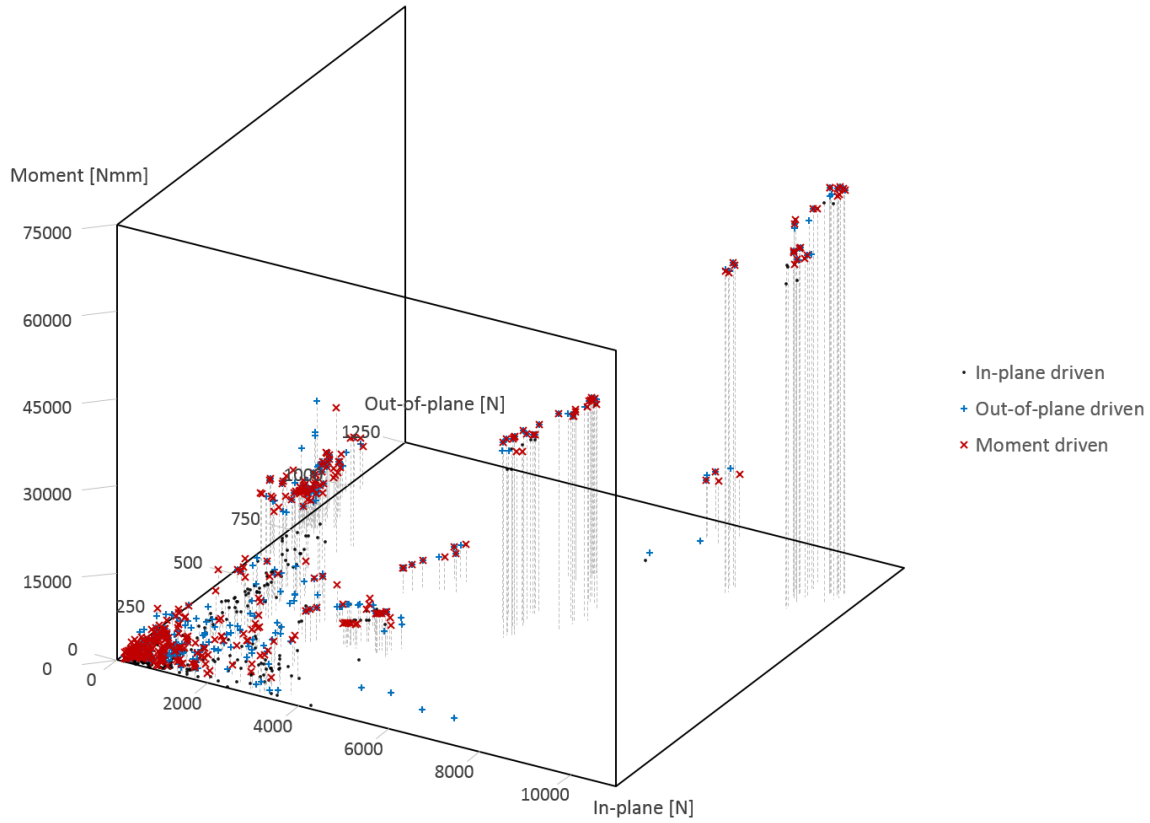

Figure 6.1: Highest load cases for all attachment points.

There are multiple things to note in this graph:

- While there are some small differences, the load component that was used to determine the most critical load case has little influence on the resulting range of loads. It is not uncommon for the load case with the highest in-plane load to be the same as the one with the highest out-of-plane or moment load.
- The majority of the points are relatively low-loaded, and the highly loaded points are grouped somewhat.
- In general, the in-plane loads are an order of magnitude higher than the out-of-plane loads. This is not surprising considering that the plane of the structure is in the vertical direction. Accelerations during launch of the satellite are mostly oriented in this direction, thus resulting in high in-plane loads.

For proving the feasibility of the concept, it is desired to show that the highest loads can be carried by an attachment. Considering the low magnitude of the out-of-plane loads, the main focus becomes the in-plane and moment load. These are plotted in Figure 6.2.

It can be seen clearly that there are two groups of highly loaded points, around 6 kN and 10 kN in-plane load. These coincide with the highest moment loads, and the relation between the magnitudes of the in-plane and moment loads is more or less linear. Considering this relation, and recognizing that a piece of equipment is attached to only one side of the structure (either the inside or the outside of the cylinder), it is likely that the moment is caused by the offset of the in-plane load from the neutral plane of the structure. For the two groups of highly loaded points, the apparent offset of the load is around 6.5 mm. For lower loads

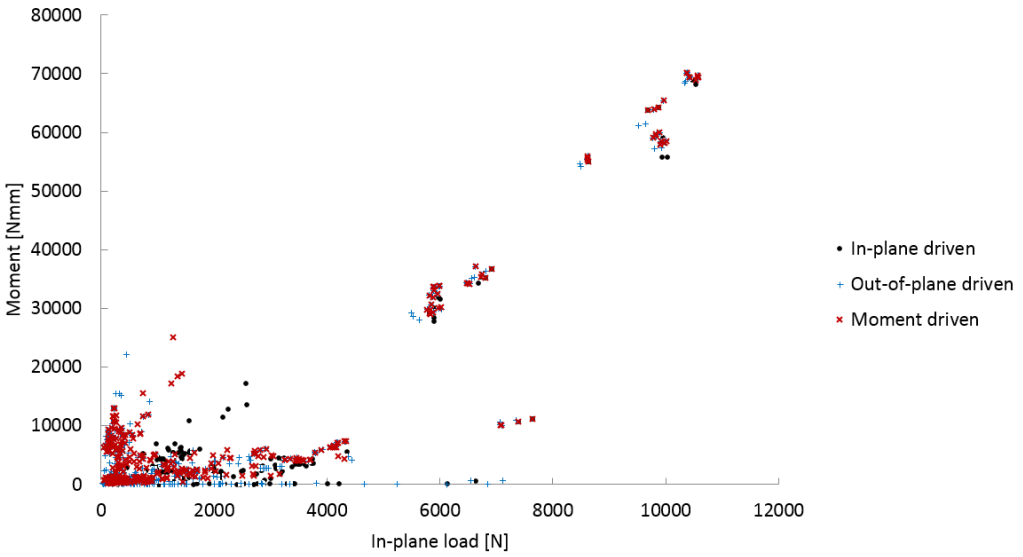

Figure 6.2: Highest load cases for all attachment points, in-plane and moment load only.

the relation between the in-plane and moment load is less apparent, but these loads are not of interest for proving the feasibility of the concept since the magnitudes are smaller. If the concept can support the highest loads, supporting the lower loads should not pose a problem.

Considering the above, an in-plane load offset from the neutral plane is selected. Since the highest in-plane load of all load cases is 10.6 kN, this is set as the strength goal.

6.2 Test setup design

To apply the offset in-plane load to an attachment point a custom test setup is required. The designed setup is shown in Figure 6.3.

The sample to be tested is cast in potting material and placed on the compression plate that is part of the test bench. The potting material is required to stabilize the lower end of the sample as the compression load is applied.

Since the attachment point can not be loaded directly, a steel fixture is made to extend past the part and introduce the load into the attachment point. The top of this fixture is clamped in the upper part of the test bench. This fixture is a rectangular steel bar, with a hole machined in one end for the bolt. The cross-section is 8 by 50 mm. Since the loads introduced into the bolt are quite high, the fixture is made from 1.2510 tool steel. This material is chosen since it provides a decent strength while still being easily machinable.

To eliminate as much play as possible in the bolted connection, shoulder bolts are selected. These bolts have an accurately machined shaft, and are commercially available in grade 12.9 high-strength steel. The used bolts can be seen in Figure 6.4. The selected bolts have an h8 shaft tolerance which, when combined with the K7 tolerance specified for the holes in the fixture and inserts, results in a K7/h8 transition fit. For a 12 mm bolt and hole the typical clearance of this fit is 11 μm and the maximum clearance is 33 μm. The main goal of this accurate fit is to reduce the possible impact the clearance can have on the measured bench

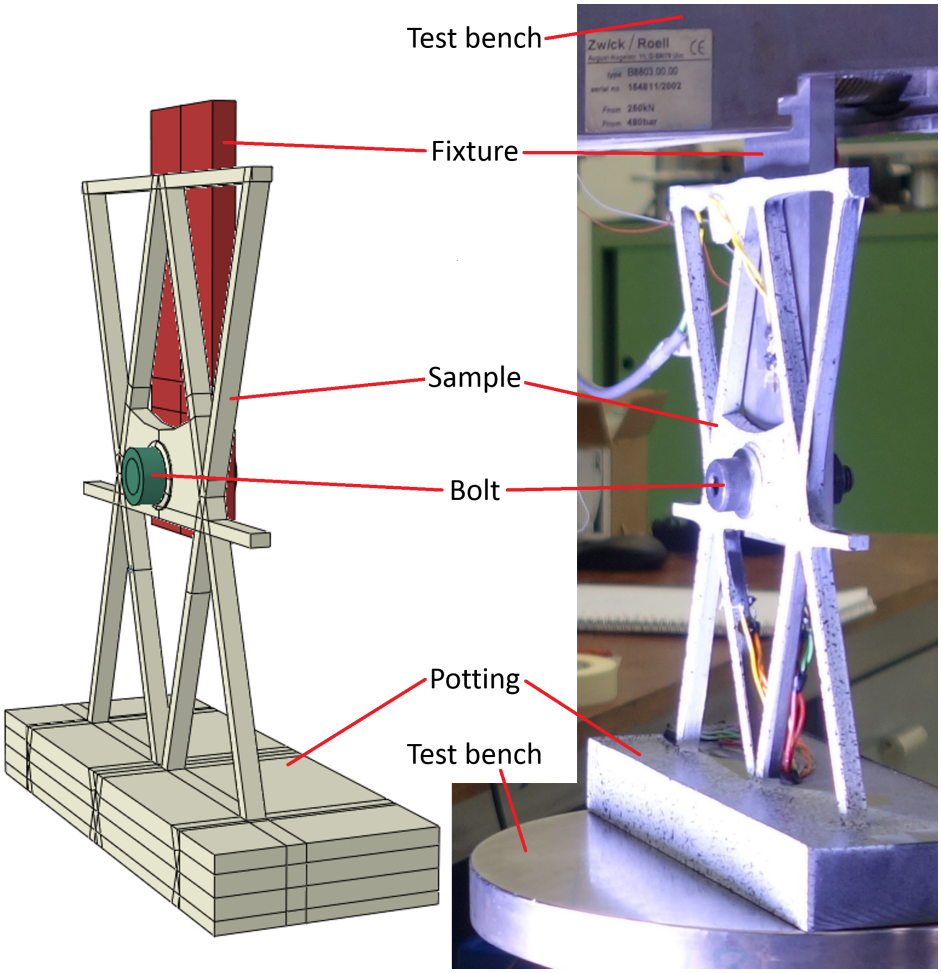

Figure 6.3: Test setup for the attachment points, CAD drawing and the actual setup.

displacement. The clearance is also well within limits to not have any negative effect on the bearing strength and stiffness, even in composites.[54]

Figure 6.4: Shoulder bolts used for the tests.

The free-standing nature of the sample results in somewhat different boundary conditions than are present around an attachment point in a SCT. This is considered not to be an issue since the goal of the tests is to obtain reference data for correlation of the model. Accurately reproducing all the boundary conditions, including far-field loads as are present in the SCT requires a much more elaborate test setup, and introduces more unknowns.

6.3 Material differences

The general optimization of the SCT was performed using properties of Hexcel's 954-6/M55J prepreg material, which consists of ultra-high modulus carbon fibers in a cyanate ester matrix. However, this material was not available for making the test samples. Instead, Hexcel 8552/IM7 is used, which consists of an intermediate modulus carbon fiber in an epoxy matrix. The properties of these materials are significantly different, the available strength properties are listed in Table 6.1. The factor by which the 8552/IM7 material is stronger is also listed.

Table 6.1: Material properties of SCT and test sample materials, and the factor by which the latter is stronger.

Property	Direction	954-6/M55J [59]	8552/IM7	Factor
Strength	0° Tension	2165 MPa	2590 MPa	1.2
	90° Tension	40 MPa	115 MPa	2.9
	0° Compression	896 MPa	1725 MPa	1.9
	In-Plane Shear	78 MPa	120 MPa	1.5
	0° Interlaminar	70 MPa	135 MPa	1.9

Depending on the property, the used material is 1.2 to 2.9 times stronger than the material of the SCT. To be able to claim that the concept can be used to take the highest loads of the SCT attachments the strength goal is multiplied by 1.9, to be 20.1 kN. While a fully conservative approach would use the factor 2.9, a 90° tension failure is not expected, so the factor 1.9 is used.

Additionally, it is recognized that differences in stiffness of the rib and patch are a possible cause for stress concentrations, and a different stiffness ratio can influence the magnitude of the concentration. To assess this difference, the ratio between the stiffness of a quasi-isotropic patch and a unidirectional rib are compared. For the SCT material, this ratio is 0.39, and for the test sample material it is 0.43, a 10% difference. This is considered sufficiently small not to require an additional correction on the strength goal.

6.4 Locations selected for testing

Given the large number of attachment points in the SCT, the base structure can not be made such that all of these points are in favorable locations on the grid, some will be at a location that might give some difficulties designing the attachment. To show that this does not prevent the concept from being used, two different locations in the grid are selected for testing.

The first of these locations is right next to a rib, with the in-plane load in the direction of that rib. When combined with high loads, this represents a worst-case location since the design space in the direction of the load is very limited. The strength goal for these samples is set at the overall strength goal of 20.1 kN. This location and the samples that are made for it are named DC1, where DC is short for design case.

The second location is in the middle of a cell, as far away from the ribs as possible. This will not only demonstrate the ability to reach any place on the grid, but also allows the behavior of the patch to be studied better, since the larger size of it will show the patch-specific effects

more clearly. This attachment will be designed for intermediate loads, so makes use of a partial thickness patch. This location and the corresponding samples are referred to as DC2. Figure 6.5 shows the locations of both the selected locations in the grid, and the direction of the in-plane load.

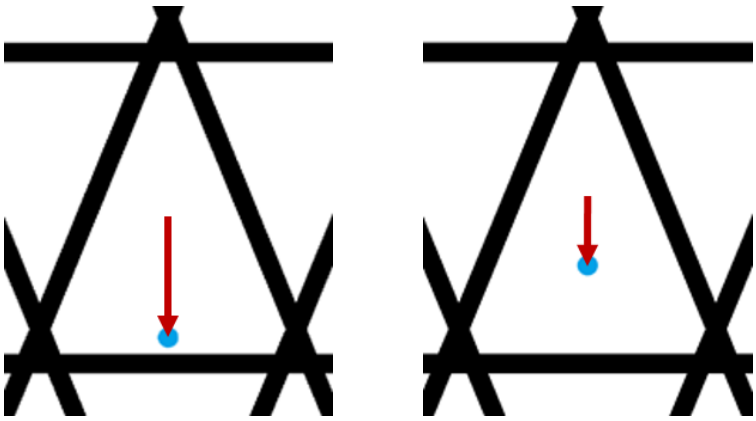

(a) DC1 (b) DC2

Figure 6.5: Location of attachment points in the grid, and direction of loads used for the test samples.

An issue not addressed in either of the aforementioned samples is that the attachment point should not negatively influence the strength of the base structure since it will have to carry the far-field loads. An additional set of samples is added to investigate the effect of a laminate patch on the strength of the ribs. This set contains two different sample types with the same basic design. Three samples will consist of only ribs, while three others have a patch between the ribs. These samples will be loaded in pure compression to test the differences in stiffness and strength resulting from the patch. Unlike the DC1 and DC2 samples, these samples will be made from a square grid. This allows the ribs to be loaded purely along their length. Additionally, both the tooling and the part itself are easier to make. These samples are further referred to as the ORTH samples, the name derived from the orthogrid panel they are cut from. The test samples can be seen in Figure 6.6.

Figure 6.6: The two types of ORTH test samples.

6.5 Test sample design and FE models

6.5.1 DC1

For the models of the attachment test samples, some changes are made to the scripted method that was presented in section 4.2. The modeling method for the composite part is mostly unchanged, but the boundary conditions and introduction of loads are different, so the approach there is changed. The model, highlighting the areas of the boundary conditions is shown in Figure 6.7.

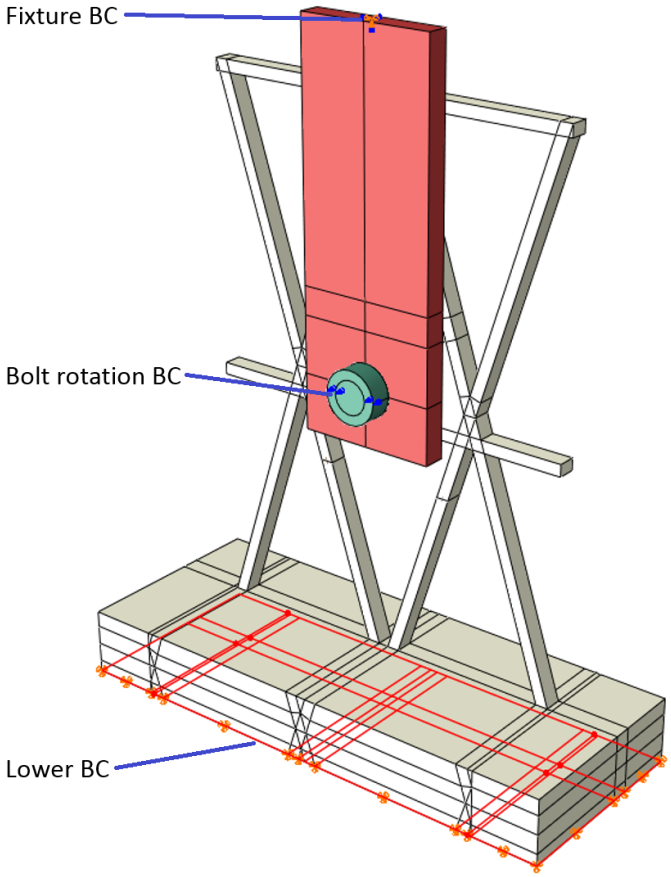

Figure 6.7: Geometry and boundary conditions for the DC FE models.

To accurately model the lower boundary, the potting material is added to the composite part. A 'pinned' boundary condition restricting all translational movement is then applied to the lower surface that is in contact with the test bench. While this surface is not actually fixed in the tests, the compressive load applied to the sample ensures that the surface remains in contact and that there is no movement.

The load introduction through the fixture, and the corresponding boundary conditions require additional changes. The fixture bends under the loading, thus introducing an out-of-plane load into the sample while taking up some of the bending load. To best include these effects the fixture is included in the model. The top of the fixture, at the height at which it is clamped in the test bench, is rigidly coupled to the center point of the cross-section. This point is then restricted from movement in any direction but the vertical, allowing it to move

in the direction of the load. The load on the fixture is applied as a point load on this boundary point.

To transfer the load from the fixture to the sample, the bolt is also modeled as a solid, and contact with friction is defined on the appropriate surfaces. The bolt preload is applied using the 'bolt load' in Abaqus. This load type shortens the bolt shaft until the set preload is reached, and then fixes the length of the shaft. This corresponds well to the actual process, where the bolt is preloaded before the test and then remains in place during further steps.

Properties used for the materials in the model are listed in section B.6

Additionally, a third boundary condition is applied to prevent the bolt from rotating along its axis, while leaving all other movements unrestrained. Application of this boundary condition results in less required computational time for contact initiation.

Comparison of a nonlinear and linear analysis showed a small difference in results due to a slightly nonlinear behavior. Therefore, the results from the nonlinear analysis are used, and any further analyses of the DC samples are also nonlinear.

For the test samples, the dimensions of the base structure are taken from the SCT optimization. The design of the attachment zone itself is performed manually, using the lessons learned from the trend study presented in section 5.1, and making use of the analysis methods presented in section 4.1. This design method ensures that a somewhat optimized attachment is made, without over-optimizing the design for one specific load case. The resulting design can be seen in Figure 6.8. It features an attachment point for a 12 mm diameter bolt, with two hat inserts to better spread the loads over the interface. The full-thickness laminate consists of equal parts 90° and ±45° plies. A curved edge is used for the laminate patch, and analysis showed that the patch can be kept relatively small, despite the high design load. The additional mass of the patch and the insert is 18 g.

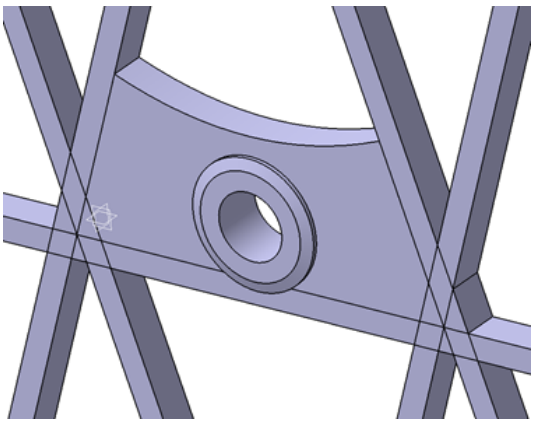

Figure 6.8: Patch design for the DC1 samples.

6.5.2 DC2

The DC2 model was constructed in a similar way, but with a different patch design and a smaller bolt. Like the DC1 design, the patch was designed manually using the lessons learned from the trend study. The patch design features a half-thickness patch consisting of equal parts of 90° and ±45° plies. A ring insert is used with an 8 mm inner diameter. The geometry is shown in Figure 6.9. The additional mass of the patch and the insert is 11 g.

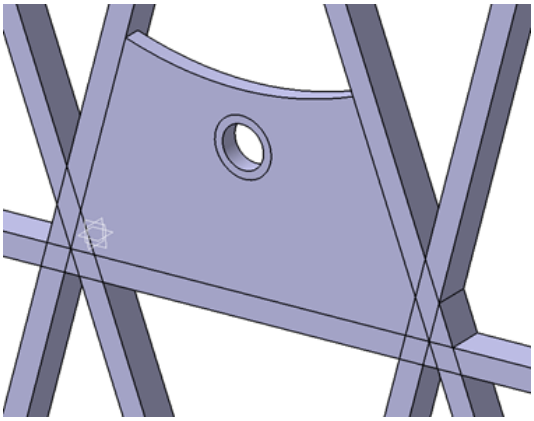

Figure 6.9: Patch design for the DC2 samples.

6.5.3 ORTH

Compared to the DC models, the model for the ORTH samples is relatively simple. There is only one part, as shown in Figure 6.10. The modeling method of the composite and the potting is the same as in the DC models, the dimensions of the ribs are also the same. Boundary conditions are also similar, the boundary condition on the lower surface is again 'pinned'. The methods used for the top boundary condition and load introduction are the same as used for the top of the fixture in the DC models.

Two models are set up, the only difference between them being the presence of the laminate patch. The spacing between the two horizontal ribs, which are embedded in the potting, is set at 60 mm. This is short enough to prevent buckling from occurring before the ribs fail in compression, but large enough to allow the silicone tooling to apply sufficient compaction to the ribs.

Again, both linear and nonlinear models were compared. The results are practically equal, so linear analyses are used to save on computational time.

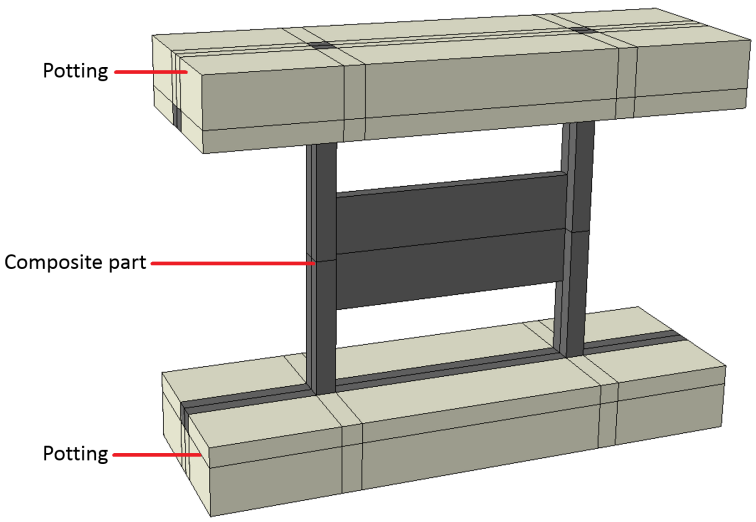

Figure 6.10: Model of an ORTH sample with a patch.

6.6 Expected failure loads

6.6.1 DC samples

For the designed attachment point samples, the expected failure loads are calculated using the methods discussed in chapter 4, the resulting expected failure loads are given in Table 6.2. Since the applied load is in-plane, only in-plane failure modes are considered, thus excluding pull-through.

Table 6.2: Expected failure loads for the attachment samples.

(a) DC1 samples

Failure type	Load
Shear-out	19 kN
First ply failure	19 kN
Bearing	24 kN
Bolt	55 kN

(b) DC2 samples

Failure type	Load
Bearing	8 kN
Shear-out	20 kN
First ply failure	23 kN
Bolt	24 kN

For both the designs, the indicated first ply failure is in in-plane shear on the rib-patch interface, near the node.

The expected failure loads for the DC1 sample fall just short of the 20.1 kN goal. There are however some conservative factors in the analysis methods, so the samples are expected to achieve the strength goal. Conservatism in the shear-out load lies in the influence of the insert. Since it is expected that the flanged insert spreads the load more evenly, the shear-out load is also expected to be higher as a result of adding it. It is unknown how large the influence of the insert actually is, so this is not taken into account in the estimations. The first ply failure load is considered conservative since a more detailed modeling of the interface, as shown in section 5.2, results in lower strains on the interface.

The order in which the failure modes are expected to occur in the DC1 samples is somewhat undesirable, since shear-out is a rather abrupt failure, with very little residual post-failure strength. Ideally, a progressive failure mode like bearing would occur first, as is the case for the DC2 samples. However, due to the location of the attachment point right next to the rib, there is very little space between the bolt and the edge of the cell in which the attachment is placed. In case the shear-out strength would be limiting the design, one can consider extending the patch into the adjacent cell to increase the design space at the cost of increased complexity.

6.6.2 ORTH samples

For calculating the strength of the rib test samples, multiple approaches can be taken. When multiplying the cross-sectional area of the ribs with the compressive strength of the material, the resulting sample strength would be 100 kN. However, the horizontal ribs, patch, and potting locally influence the distribution of the strains, reducing the strength. To account for this, the expected strengths are found from the FE models.

By modeling the samples with FE, the buckling loads can also be found easily with a linear buckling analysis. While the rib buckling load might also be determined analytically, esti-

mating the support given by the potting is difficult, so the FE results are used. The expected failure loads and buckling loads are shown in Table 6.3.

Table 6.3: Expected failure loads for the ORTH samples.

Sample type		Buckling	Rib failure	Location
W	(With patch)	118 kN	60 kN	Near node
WO	(Without patch)	87 kN	65 kN	Near node

In both cases the ribs are expected to fail before buckling occurs, which is as desired. While the patch does have a small influence on the local strain distribution of strain in the rib where it connects, the effect is not strong enough to move the failure location away from the node. A small reduction in strength is expected since the patch introduces a small amount of bending deformation in the ribs under loading. The buckling load is influenced significantly by the presence of a patch, since it stabilizes the ribs and increases their bending stiffness.

6.7 Instrumentation and data gathering

To better study the behavior of the structure under loading and to obtain the data necessary for correlation of the model, several types of instrumentation are applied to the samples.

6.7.1 DC tests

The main points of interest of these tests are the deflections and deformations under loading, and the failure behavior of the attachment.

The applied load and overall displacement are output by the test bench itself, and give information on the response of the entire test setup. To capture the displacements of the composite part, a speckle pattern is applied to the visible side of the sample, so digital image correlation (DIC) can be used to capture the deformation of the sample. This also allows the strains to be calculated on the visible area, which is advantageous since the strain field on the rib-patch interface is quite irregular. Use of DIC allows more of the local effects to be seen than would be possible with strain gages alone. While the strains on the other side of the sample are higher, the fixture on that side blocks a large portion of the view. This makes the data from the visible side more useful, since it gives a more complete image of the strains in the patch and rib-patch interface.

Additionally some strain gages are placed on the test sample, the locations of which are shown in Figure 6.11, their purpose is explained hereafter.

Three strain gages are placed on the ribs between the attachment and the potting. One is on the side of the speckle pattern, allowing the measured strain to be compared to the strain as measured with DIC. The other two strain gages are placed on the opposite side of the ribs, where the strains are expected to be higher. By placing these on two different ribs any unequal distribution of loads between the ribs is easily identified.

Another strain gage is placed on the side of the hoop rib, at the location of the attachment point. This serves to both capture the bending of the rib, and to capture any effects of shear-out damage, if present. The DC2 samples do not have this strain gage on the side of

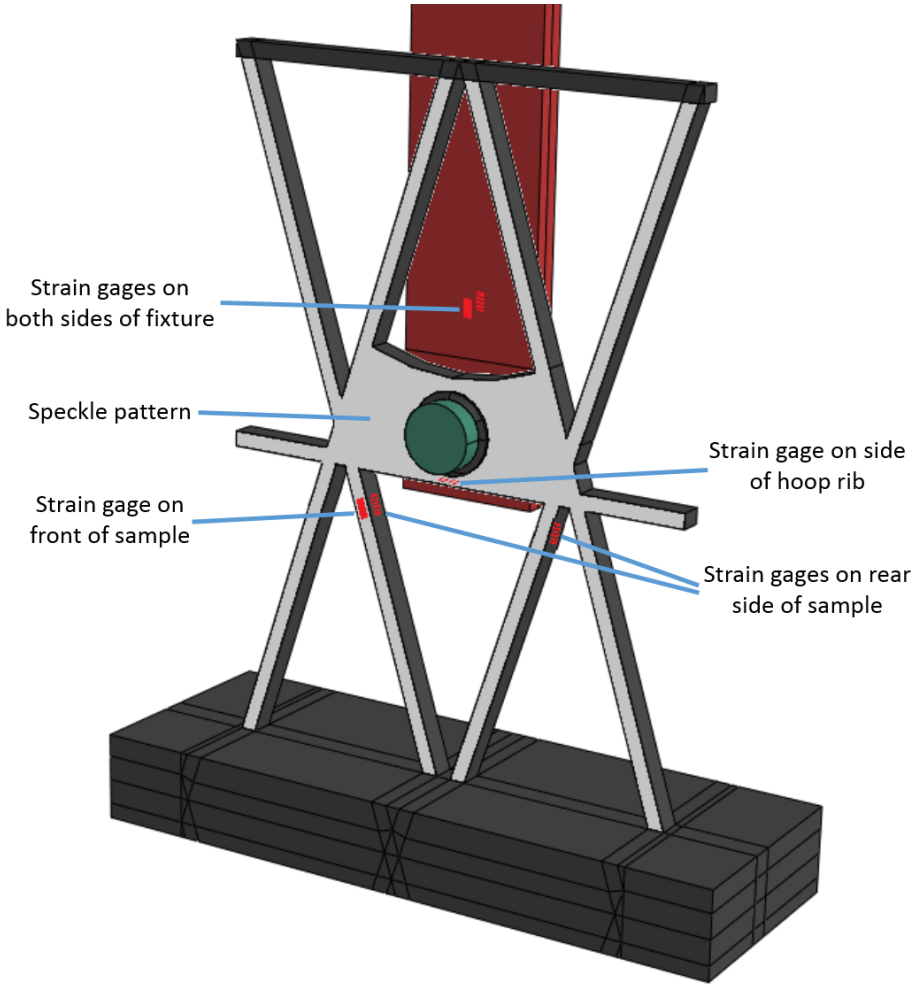

Figure 6.11: Instrumentation applied to the DC1 samples

the hoop rib, since the attachment point is further away from the rib, and shear-out is not expected as a failure mode.

Additionally, two strain gages are also placed on opposite sides of the steel fixture to capture the bending deformation under loading.

6.7.2 ORTH tests

The main point of interest for the ORTH samples is the behavior of the ribs, more specifically the stiffness and the strength difference between the samples with and without a patch.

This requires the applied load and displacement to be measured. The load is output by the test bench, but the displacement is measured using two linear variable differential transformers (LVDTs), also known as linear variable displacement transducers. The LVDTs are held by magnetic supports. The LVDTs are placed on opposite sides of the sample, so the average of the two measured values is the displacement that is applied to the sample. The LVDTs were placed as close as possible to the sample, since it was observed that placing them further away from the sample resulted in a different measured displacement. The location of the LVDTs in

the test setup can be seen in Figure 6.12. This figure also shows some other components of the setup. The steel bars that are placed on top of the lower compression plate are necessary because the samples are smaller than the test bench is designed for.

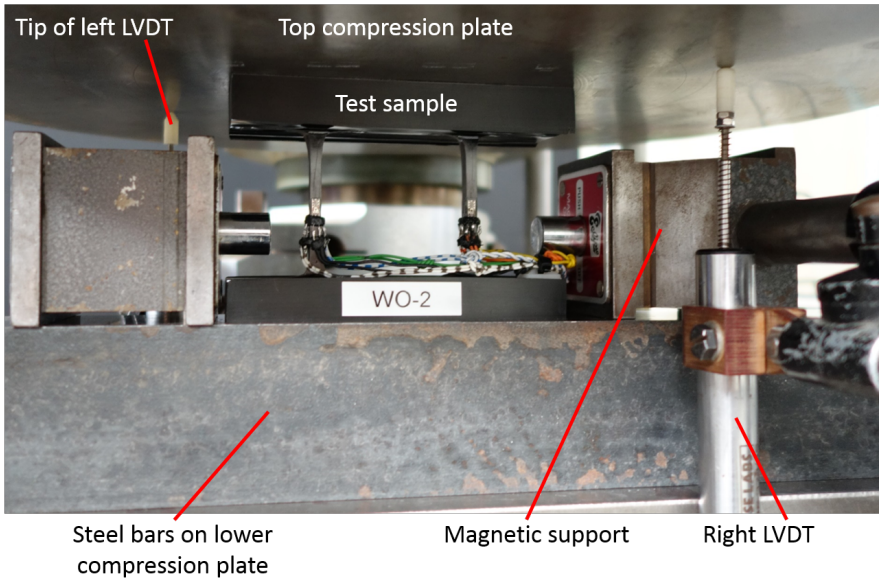

Figure 6.12: Detail of the test setup for the first ORTH samples, showing the LVDT locations.

Strain gages are placed halfway along the length of the test sample ribs, to measure the strain in the rib and to observe any bending behavior, if present. Since the patch stabilizes the ribs in the plane of the structure, the samples with a patch have strain gages only on the front and rear of the ribs, on the locations indicated in Figure 6.13. On the samples that do not have a patch, strain gages are placed on all four sides of the rib.

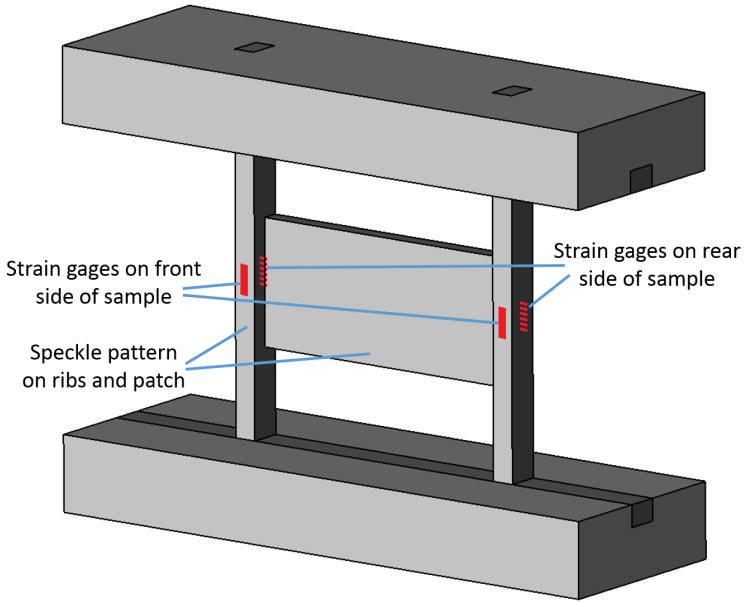

Figure 6.13: Instrumentation applied to the ORTH samples

Four of the samples are tested without DIC. The results of these tests showed a higher overall displacement and a significantly lower strength than predicted by the FE model. To obtain some additional data, DIC was also used for the final two samples, with the speckle pattern applied to both the ribs and the potting. By applying the speckle pattern to the ribs the strains in the entire rib can be measured, thus also at the location of failure. The speckle pattern on the potting was used as a second source of data for the overall displacement, since it was observed that the displacement measured by the LVDTs varied with the location at which they were placed, leading to doubts about the reliability of the data.

6.8 Test matrix

To give an overview of the tests, key elements from the preceding sections are summarized in Table 6.4.

Table 6.4: Test matrix.

Sample type	DC1	DC2	ORTH
Number of samples	4	4	3 without patch 3 with patch
Load type	Offset compressive load on attachment point	Offset compressive load on attachment point	Pure compression
Reason for test	To show high loads can be taken, even on an unfavorable location	Reach attachment point far away from rib, and study patch behavior	Comparison of compressive behavior of rib with and without patch.
Expected onset failure load	-	8 kN	-
Expected onset failure type	-	Bearing	-
Expected final failure load	19 kN	>8 kN	65 kN (without patch) 60 kN (with patch)
Expected final failure type	Shearout/First ply failure	Bearing	Rib fracture
Data to be recorded	Load Displacement Strains Failure type	Load Displacement Strains Failure type	Load Displacement Strains Failure type

Chapter 7

Manufacturing

To make the test samples, three larger composite panels are made, which are then cut into smaller samples:

- One panel containing all 6 rib test samples, size 390 by 270 mm.
- One panel containing all 4 DC1 test samples, size 630 by 300 mm.
- One panel containing all 4 DC2 test samples, size 630 by 300 mm.

Since the basic grid is the same, both the DC1 and DC2 test samples can be made in one panel but it is chosen not to do this. By making these parts separately they can be placed in separate vacuum bags, so in case of a punctured bag only one of the sets of samples is lost. This choice means a slight increase in the amount of tooling that is required, but the resulting redundancy is considered worth the effort.

7.1 Attachment point manufacturing steps

Most of the manufacturing steps taken for the test parts are the same as would be used to make a larger structure for a real application, other than the lack of automated equipment. And whereas the methods used might be somewhat different in a production environment, the basic steps remain the same.

7.1.1 Manufacturing of tooling

To ensure the outer dimensions of the part are as designed, metal tooling is used on all boundaries of the structure. Since the manufactured parts are flat panels, the metal tooling is rather easy to make. Samples are placed onto a 10 mm thick aluminum plate that is part of the autoclave equipment. The top of the sample is covered by a caul plate which is cut from 3 mm thick aluminum sheet. The dams surrounding the part are made from 15x15 mm square aluminum rod. To prevent separation of these dams, holes and threads are machined into them, allowing the dams on all four sides of the part to be bolted together. The caul plate and the dams are sanded with P1000 sandpaper to provide a smooth surface, cleaned, and then a chemical release agent is applied to them to ensure these parts separate after

curing of the structure. It must be noted that for a cylindrical structure this tooling would be more complicated to make.

To make sure the grid cures in the desired shape, the area between the ribs is filled with silicone rubber tooling. This tooling is cast in 3D-printed molds, covered with laser-cut acryl plates. Such a mold can be seen in Figure 7.1. The casting and initial cure are performed at room temperature. Afterwards, the parts are post-cured in an oven for three hours at 190 °C, which is 10 °C higher than the processing temperature of the composite material. This post-cure serves both as a method to ensure the cure is complete, and as a check to see if the tooling can handle the elevated temperature. A total of 233 rubber blocks are made, in 20 different shapes.

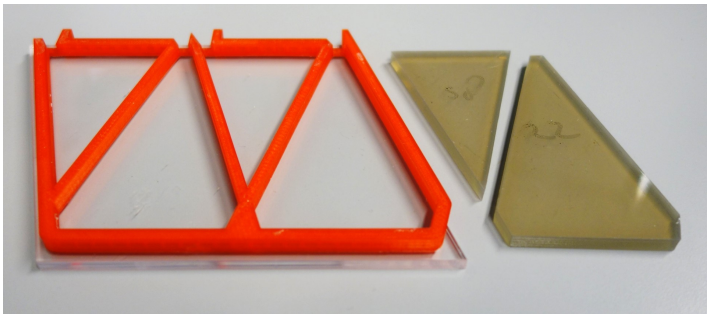

Figure 7.1: Rubber tooling mold and finished blocks.

7.1.2 Layup

Using a computer numerical control (CNC) cutting machine, the required tows and plies are cut from a 300 mm wide roll of unidirectional prepreg material. While this approach allows tows to be cut in practically any width, 6.35 mm (1/4") is selected. This is chosen since this is a width often seen for industrially available towpreg or slit tape, and thus can show the compatibility of the process with industrially available materials. A total of 2406 separate tows and plies are required to make the three panels.

The layup is done manually, since no automated methods are available. The layup is done free-standing on an aluminum plate covered with release film. A printed template is used to help align the plies. The rib plies are placed applying mild pressure when placing them on the nodes, in the area in between the nodes the plies are freely suspended, this means that care must be taken to prevent pushing down on the ribs during layup. The plies forming the patches are also placed applying mild pressure. No interim debulking is performed. A finished layup can be seen in Figure 7.2.

After layup the excess material at the edges is removed and the part is transferred to the plate used in the autoclave, after which all the rubber and metal tooling is placed.

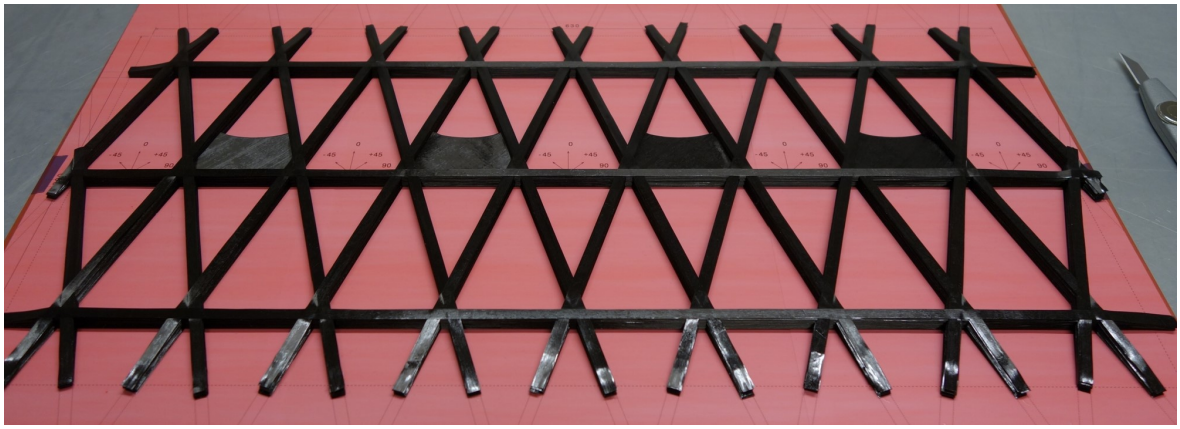

Figure 7.2: Finished layup of the DC2 panel.

7.1.3 Compaction under vacuum

After layup, the nodes are noticeably higher than the intended panel thickness. When the tooling is placed this can be clearly seen by the layup extending above the rubber tooling, as shown in Figure 7.3.

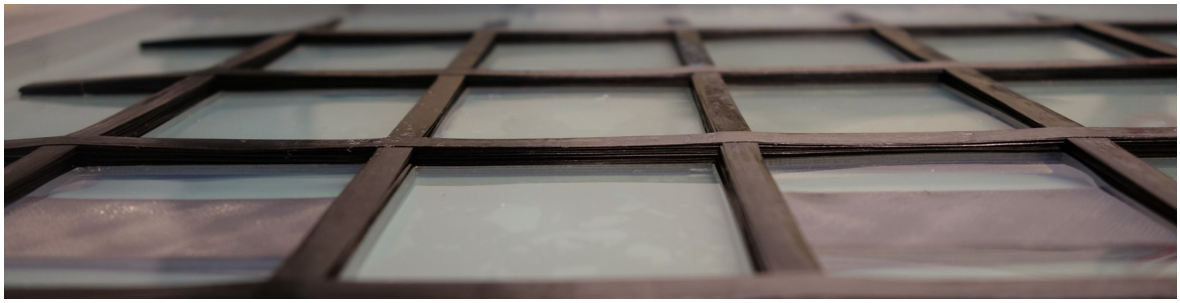

Figure 7.3: Layup extending above tooling before compaction.

To reduce this height a caul plate is put on top, the assembly placed in a vacuum bag, and vacuum is applied. The pressure difference results in a force pushing down on the caul plate, thus compressing the material at the nodes. In order to study the rate at which this occurs, the vacuum bag is opened several times during the process to measure the progress. The thickness of the panel is measured at the nodes, and since metal outer tooling is used the top and bottom of the panel remained practically flat. Despite this, there are some small differences in height over the panel. The progress of the compaction over time is shown in Figure 7.4.

It can be seen that after as little as half an hour under vacuum, there is already a significant reduction in panel height. As time goes by, the rate at which the panel is flattened decreases but compaction continues nonetheless. After almost a day under vacuum, the panel thickness has decreased to only slightly more than the height of the rubber tooling. The final difference is equalized during curing in the autoclave, where the higher pressure and increased resin flow due to the elevated temperature creates more favorable circumstances for compaction.

Another observation is that the ORTH panel shows a more rapid compaction than the DC panel. This is expected to be due to the layout of the panels. At each node, the ORTH panel has only one crossing of ribs, whereas the DC panel has three such areas per node, which

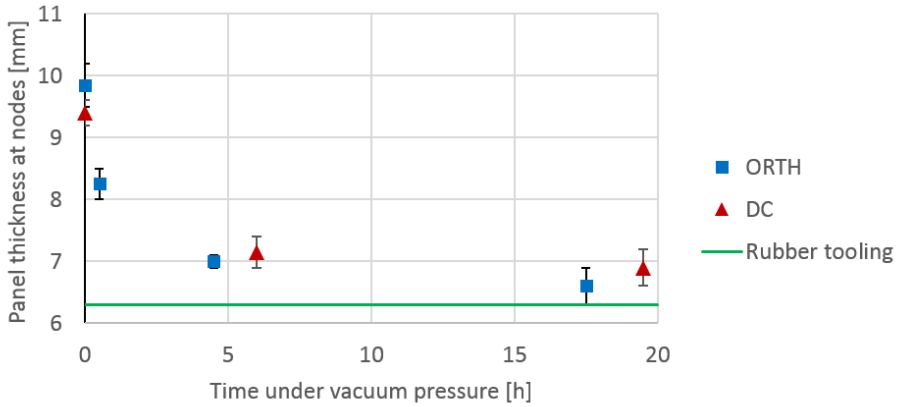

Figure 7.4: Height of nodes during debulking.

individually are also bigger since the ribs do not cross at a 90° angle. Then, when assuming that the total force due to the pressure load on the caul plate is equally spread over all areas where the ribs cross, the relatively small nodes of the ORTH panel experience a higher load, thus speeding compaction.

It was also noticed that some of the plies that were initially extending above the rubber tooling shift slightly during compaction and end up on top of the rubber tooling. To prevent this from happening, the nodal compaction would either have to take place during layup, or special tooling would have to be developed specifically for debulking, restricting the plies from shifting laterally.

7.1.4 Cure

After compaction, the parts are vacuum bagged for the autoclave. On a single base plate, two separate vacuum bags are made. One contains the DC2 panel, the other contains both the DC1 and ORTH panels. The DC2 panel has a thermocouple placed in a hoop rib to monitor the temperature in the composite part during curing. This thermocouple has to be extended outside of the vacuum bag, making it more likely to cause leaks. Therefore the DC2 sample is separated from the other samples.

The cure cycle used is the standard cure cycle as recommended by Hexcel, which consists of a one hour dwell at 110 °C, followed by a two hour cure at 180 °C.[60] The cooling and heating rates were set at 2.5 °C/minute.

Unfortunately, soon after starting the cure cycle the temperature data from the thermocouple in the composite part became highly erratic, likely due to a faulty connector. This did not have any effect on the temperature control of the autoclave itself, since another thermocouple inside the autoclave is used for that purpose. The recorded temperatures are shown in Figure 7.5

It is clearly seen that the temperature inside the autoclave accurately follows the set temperature, except for the final part of the cooling stage where the autoclave can't cool fast enough. At this time the composite is already cured and well below its glass transition temperature (Tg), so this is not an issue. While the overall data is erratic, the measured temperature inside the composite does indicate a stable temperature during the dwell and cure periods.

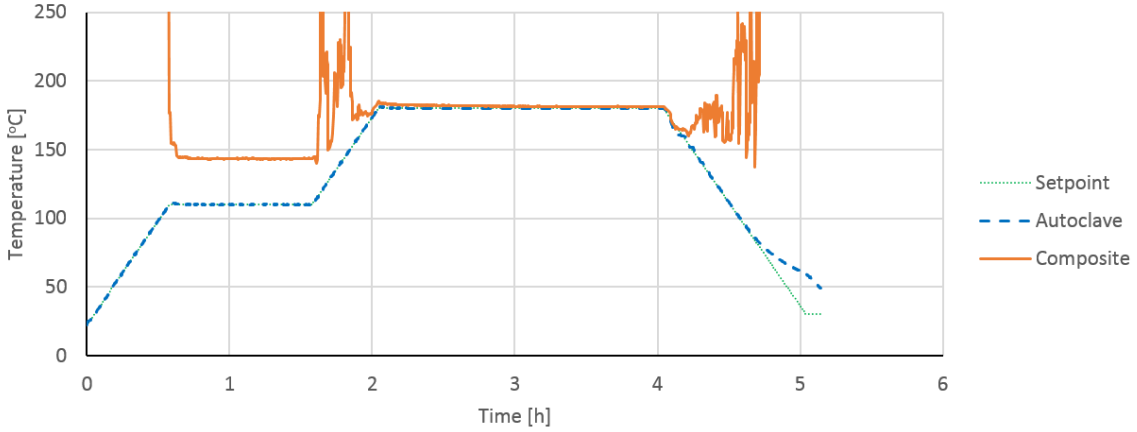

Figure 7.5: Temperatures during curing of the part.

Since the temperatures in the autoclave and composite are expected to equalize after a certain amount of time, this indicates that the part has experienced the cure temperature for the intended duration.

7.1.5 Placement of the inserts

Machining holes in the laminate

The holes in the laminate are made using a CNC milling machine. First a hole is drilled through the laminate using a 9 mm diameter drill which is specifically suited for composites. This allows the hole to be made with a reduced chance of creating delaminations in the composite. Afterwards, an 8 mm diameter router is used to further mill the hole to the specified diameter. Again, tools specifically designed for composites are used to prevent delaminations in the laminate. This results in a hole of constant diameter, with a smooth inner surface and no visible damages to the composite material.

Bonding the inserts

The surface preparation technique is practically the same for both insert types. The surfaces of the aluminum inserts that are in contact with the adhesive are sanded with P120 sandpaper and thoroughly cleaned and degreased. The composite parts received the same treatment, but a finer P240 sandpaper is used instead.

The used adhesive is 3M Scotch-Weld EC-9323 B/A two-part structural adhesive. A small quantity is mixed, and 1.5% by weight of 100-200 micron glass beads are added to control the bondline thickness to be between 0.1 and 0.2 mm. At this thickness, the highest shear strength is obtained.[61]

Suitable methods for bonding the inserts were found by trials using only 3D-printed parts. The approaches for bonding the two types of insert were slightly different. To bond the single ring insert in the thinner laminate of the DC2 samples the following approach was used:

- Apply masking tape to the surface of the laminate, leaving the hole in the laminate accessible.

- Apply a thin layer of adhesive to the surface of the hole in the laminate.
- Apply adhesive to the outside of the insert. Due to the small size of the insert the amount is somewhat hard to control.
- Place the insert in the hole.
- Use a small knife with a straight edge to align the insert with the laminate.
- Use the same knife to wipe away most of the excess adhesive.
- Place a bolt, nut and some washers covered in release agent to keep the insert in place while the adhesive cures.
- After curing, remove the bolt and the masking tape, this removes most of the excess adhesive.
- Carefully remove the remaining excess adhesive that is left on the side of the insert using mechanical methods (scraping, cutting, and sanding).

To bond two tapered hat inserts in the thicker laminate of the DC1 samples requires a somewhat different approach:

- Apply a thin layer of adhesive on the surface of the hole in the laminate and on the inserts. The amount of adhesive has to be such that a fillet is formed at the end of the insert flange after placement, this fillet can be seen clearly in Figure 7.6.
- Place one of the inserts on a bolt with the flange against the bolt head.
- Carefully place this assembly such that the insert rests in the composite structure, in the location where it should be. Manually apply some force to keep the bolt and insert in place during the next steps.
- From the other side of the structure, slide the second insert over the bolt and into the hole in the laminate.
- Screw a nut onto the bolt to keep the inserts in place.
- There is no need to remove any excess adhesive if the right amount was used.

Since the diameters of the inserts and the shoulder bolt used for testing are specified as a K7/h8 transition fit, a very small misalignment between the inserts can result in the inability to install the bolt for testing. To prevent this from happening, the same type of shoulder bolts are used for the installation of the inserts. These bolts are first cleaned and treated with a chemical release agent to ensure removal is possible after curing.

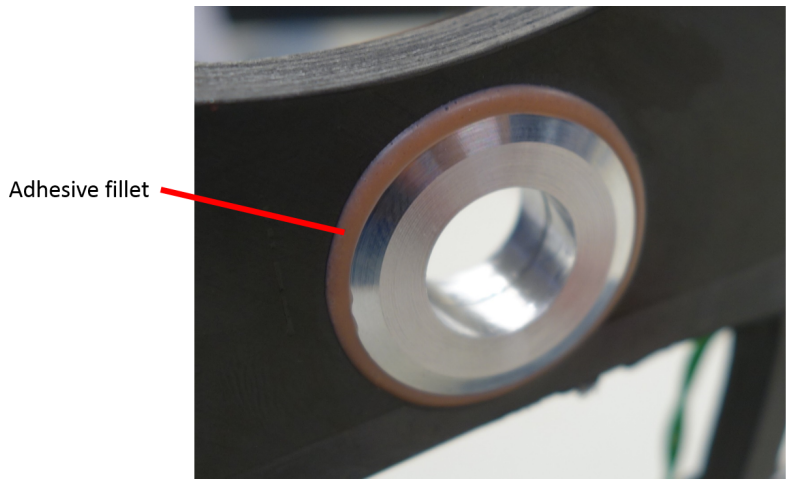

Figure 7.6: Bonded insert in a DC1 sample, after curing.

Accelerated adhesive cure

Since the full cure duration of the adhesive is 14 days at room temperature, an elevated-temperature cure is used to accelerate this process. According to the product technical data sheet, either a 2 hour cure at 65 °C or a 15 minutes 100 °C cure results in a full cure.[61] However, the potting material required for testing is cast before bonding the inserts, which gives some complications since the Tg of the potting material is at 60 °C. Both the accelerated cure temperatures then present issues since it is not desired to exceed the Tg. To resolve this issue an interpolation using an equation of the form $y = a * x^b$ is made through the three known cure profiles. At a temperature of 60 °C this indicates a 3 hour cure would suffice. To allow for some inaccuracy of this interpolation, and to not risk a partial cure of the adhesive, it is chosen to extend this cure for one additional hour. The interpolation used for this correction is shown in Figure 7.7.

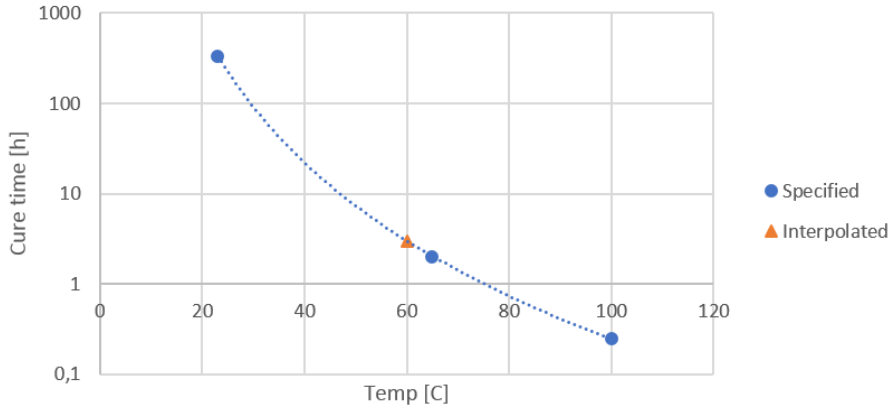

Figure 7.7: Interpolation used to determine the required cure at 60 °C.

7.2 Test-sample specific manufacturing steps

Some additional manufacturing steps are necessary to prepare the samples for testing, these are elaborated on in this section. These manufacturing steps are not necessary to make an attachment point in a structure for a real application.

7.2.1 Cast potting

To stabilize the samples in the test bench it is necessary to embed the ends of the samples in a potting material. The RenCast 2418 system was chosen for this purpose. This is a metal filled epoxy casting resin with a relatively high stiffness, so it can give sufficient support to the very stiff CFRP structure. It also has a low shrinkage, and can easily be cast, cured and machined making it ideal for processing.

The potting is cast after the holes are milled in the laminates, but before the inserts are bonded. The attachment test samples require potting material only on the lower side, since the load is applied using a steel fixture. The rib test samples need potting on both the top and bottom ends of the sample, so this requires the potting to be added in two steps. Sufficient

time is allowed between the separate castings to allow the potting to cure. Similar to the adhesive used for the inserts, the potting is cured at an elevated temperature to accelerate the cure, 14 hours at 40 °C as specified results in a full cure. [62]

First, custom molds are designed and fabricated to be able to cast the potting with the samples in an upright position. The molds consist of an aluminum plate and several angle profiles to create the space in which the potting can be cast. These parts are designed to be removable after the potting is cured so that the parts can be easily removed. A chemical release agent is applied before the potting is cast to ensure easy removal from the mold. The mold is completed by a wooden frame to keep the samples in an upright position.

Two such molds are made, one for the attachment samples and one for the rib test samples. One of the molds, with samples and cured potting can be seen in Figure 7.8, the molds are symmetric about the vertical wooden plate, so the shown mold can hold four samples simultaneously. It can be seen that both visible samples are cast into the same block of potting, these are separated by sawing through the potting between the samples after curing.

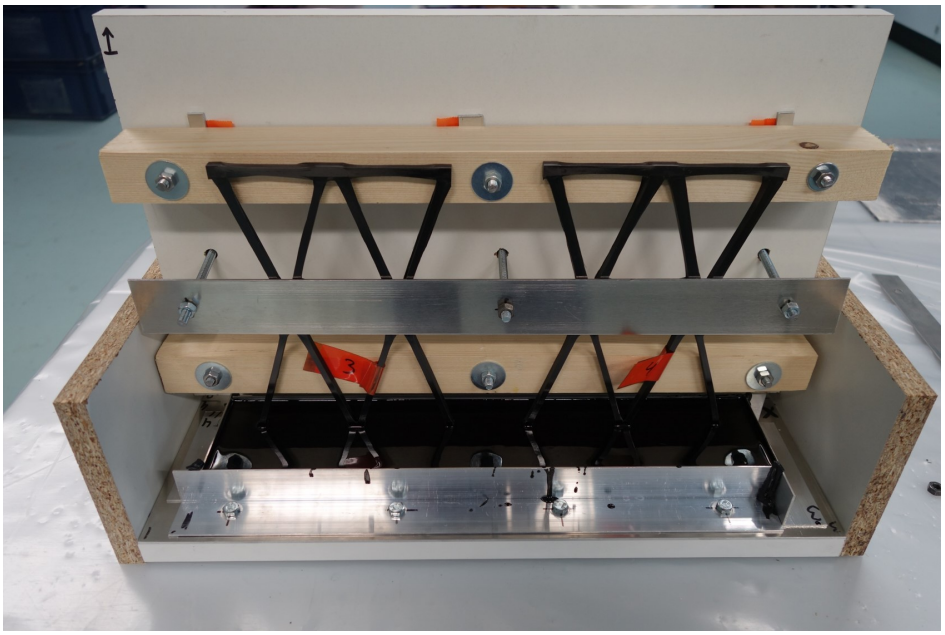

Figure 7.8: Custom mold for casting potting of the test samples.

After the potting is cast and cured, the surfaces that are to be in contact with the test bench are milled to provide a flat surface at a 90° angle with respect to the plane of the structure. This final milling operation also makes sure that the composite is extending through the potting up to the plane of contact, ensuring the load is properly introduced into the sample.

7.2.2 Instrumentation

The final step before testing the samples is applying the required instrumentation as defined in section 6.7. After marking, sanding and cleaning the intended locations, the strain gages are bonded to the samples using cyanoacrylate strain gage cement. Lead wires are soldered to the strain gage to facilitate connection to the test equipment.

The speckle pattern required for the DIC system is applied by first painting the surface with several light coats of matte white paint, the speckles are then created by lightly spraying

some black paint over the samples from a distance. Some of the finished samples are shown in Figure 7.9.

Figure 7.9: Instrumented DC1 samples ready for testing.

7.3 Inspection of manufactured parts

The overall quality of the manufactured parts is assessed after manufacturing, but before testing. The micro-structural (destructive) inspections are conducted after testing, since this requires cutting several samples into pieces. This also allows the inspection of failure regions, but those observations are discussed in chapter 8.

7.3.1 Overall sample quality

By visual inspection there are some manufacturing defects and imperfections to be seen. The largest visible defect is that the ribs on the edge of the panels are bent slightly away from the center of the panel. This is due to the flexibility of the rubber tooling allowing this movement. This effect is most noticeable in the rib test samples, as can be seen in Figure 7.10. The shown sample is cut from the edge of a larger panel, it clearly shows both ribs being bent to the left. Similar effects are noticed on some of the attachment samples, but since a somewhat larger part of the edge of the panel these were cut from is discarded the effect as visible in the samples is smaller.

On a somewhat smaller scale, it is noticed that some of the ribs have small flanges extending from the top of the ribs. These are a result of the occasional ply that ended up on top of the rubber tooling during compaction, an effect already identified in subsection 7.1.3. Generally these flanges are only loosely connected to the rest of the rib, and are easily removed with a thin, sharp knife. Since the amount of material in these flanges is very small, and the loose connection to the ribs means they will hardly contribute to the strength of the structure these flanges are removed. In some cases where the flange is somewhat thicker and hard to remove,

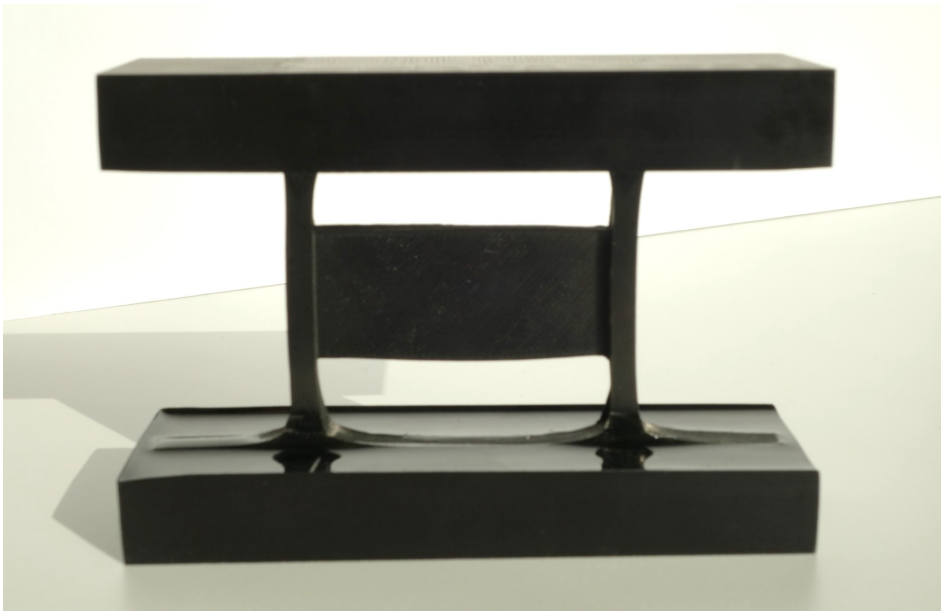

Figure 7.10: ORTH test sample cut from the edge of the larger panel, showing bent ribs.

it is left in place since the risk of damaging the structure associated with their removal is considered unacceptable. This was the case in only a couple of locations.

The removal of these flanges also makes it possible to more accurately measure the dimensions of the ribs. An overview of the measured dimensions is given in Table 7.1. These dimensions are as measured on the ribs at a distance away from the nodes and patches so as to rule out any effect these might have. Especially the nodes have a large effect on the local rib width. The ribs widen significantly near the nodes, a result of the tows in the nodes being spread wider and thinner to accommodate the fibers in the crossing rib. The dimensions of the different parts are listed in Table 7.1.

Table 7.1: Measured rib dimensions, away from nodes and patches.

	Rib height	Rib width
Designed	6.60 mm	4.40 mm
DC1 measured	6.55-6.60 mm	4.30-4.38 mm
DC2 measured	6.53-6.58 mm	4.28-4.32 mm
ORTH measured	6.27-6.46 mm	4.22-4.41 mm

In general, the actual dimensions are slightly smaller than designed. For the DC samples, this difference is small, with the rib height within 0.1 mm, and the rib width within 0.2 mm of the designed values. For the ORTH samples the rib width has similar deviations, but the rib height is occasionally over 0.3 mm smaller. This reduction in dimensions is accompanied by an increase in fiber volume fraction, with a higher increase in the parts that show larger reductions in dimensions. More details on the fiber volume fractions are given at the end of section 7.3.2.

Another interesting point is that there is more scatter in the rib dimensions of the ORTH samples. The highest reduction of the rib height is seen at the edge of the ORTH panel, in the ribs that are also slightly bent.

7.3.2 Microstructural quality

After testing, some small samples are cut from the test samples. These small samples are used for either investigation under a microscope, or determining the fiber volume fraction.

Microscopy

Figure 7.11 shows the locations of which the microscope images will be discussed in this section. The numbers correspond to the order in which they are discussed.

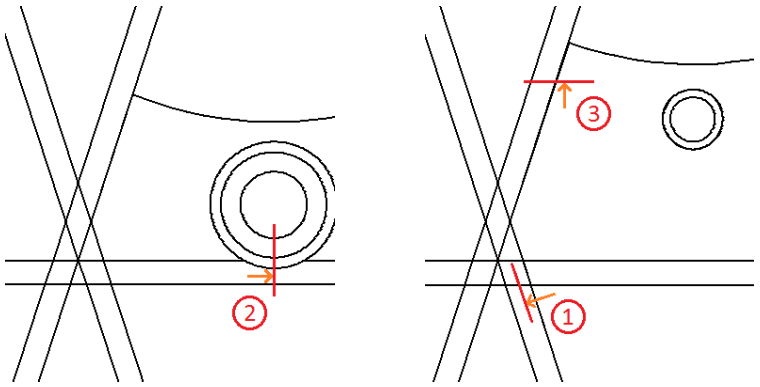

(a) From DC1 sample (b) From DC2 sample

Figure 7.11: Microscope samples cut from the attachment samples.

The microscopy samples are embedded in a resin and then polished to achieve the required surface finish. An optical microscope with a camera ia used to capture multiple pictures of each sample, which are then combined into larger pictures. This section only discusses the samples showing the quality of the structure. The failure-related samples are discussed in chapter 8.

(1) *Transition of a rib into a node*

Figure 7.12 shows a helical rib (left) as it crosses into a node (right), the visible plane is along the length of the rib. It can clearly be seen that the plies in the node are mostly straight and oriented along the length of the rib. Outside of the node this is different though. Here the plies deviate from their intended orientation into a wavy pattern. This effect reduces at a distance further away from the nodes.

The small brighter areas that can be seen just outside of the nodes are resin pockets. These are present because the plies in the rib are wider and thinner near the nodes to make room to accommodate the plies of the crossing rib. Since this transition can not be instantaneous there is a small area outside of the node where the created space is filled by resin.

Another point of interest is that the amount of voids is very small, indicating sufficient compaction pressure can be applied using the silicone rubber tooling.

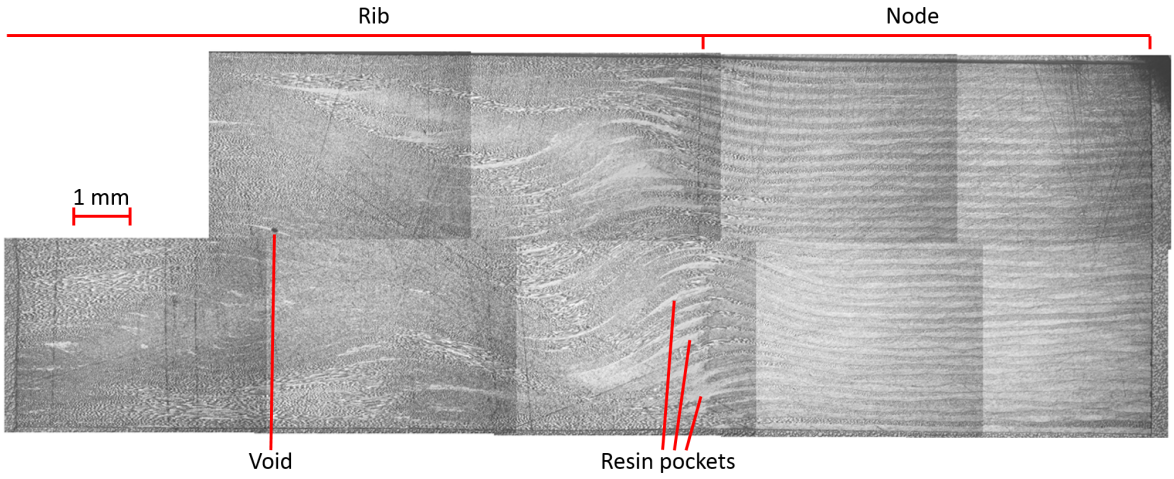

Figure 7.12: Microscopy image of a rib-node transition, 9 images combined.

(2) *Interface of a full thickness laminate and a rib*

The interface between a hoop rib and a laminate of equal thickness is shown in Figure 7.13. Due to the location at which this sample is cut this image also shows the hat inserts and the corresponding bondline.

Since the 90-degree oriented plies in the patch have the same orientation as the hoop rib, these plies show the same color as the hoop ribs and are thus indistinguishable. The lighter colored plies are the +45 and -45 degree oriented plies. The different distances that some plies were to extend into the rib are easily distinguished. At the top and bottom of the rib a set of plies is extending to the far side of the rib, and through the thickness several plies extend halfway into the rib. The plies extending into the rib remain almost straight, the small deviations that are present are due to the compaction that is applied by the rubber tooling to the other side of the rib.

From the distance between the termination of the plies that do not extend into the rib it can be seen that the horizontal distance between the leftmost and rightmost terminations of these plies is around 0.6 mm, meaning that the accuracy of the manual layup in this area is around +/- 0.3 mm.

This image also shows the bond between the aluminum inserts and the composite part. The bondline has a constant thickness between 0.1 to 0.2 mm, as desired. This is attributed to the accurately machined inserts and the addition of glass beads to the adhesive to control the bondline thickness. The adhesive fillets that are formed at the end of the flanges contain some relatively large voids, but since these areas are less highly loaded this is not an issue. In the bondline some of the aforementioned glass beads can be seen, as can some small darker spots. These spots can be either voids or locations where a glass bead was present, but was pulled out by the sanding or polishing. Considering the number of these areas visible, and knowing that only 1.5% by mass of glass beads was added it is likely that at least part of these spots are small voids. Considering their size is usually the same as the glass beads, their effect on the bondline strength is expected to be very small.

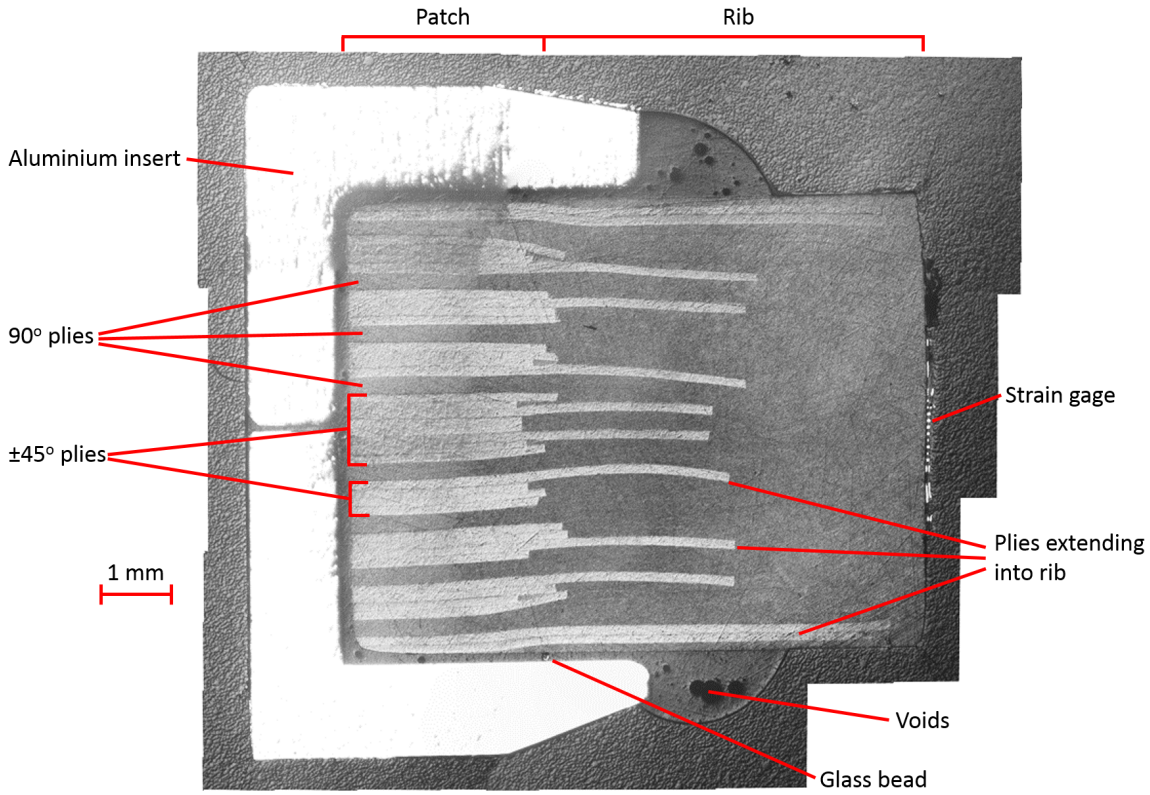

Figure 7.13: Microscopy image of the interface of a thick laminate with a hoop rib, also showing bonded inserts. 11 images combined.

(3) *Interface of a partial thickness laminate and a rib*

Figure 7.14 shows a similar interface of a partial thickness laminate into a rib. Since this shows the interface with a helical rib, the difference between the 90 degree plies of the patch and the plies in the rib can be seen clearly.

Most elements of this interface are similar, but some differences in behavior can be observed. The extending plies curve into the rib, and remain less straight than was the case for the thick laminate.

Another interesting point is the irregular surface of the laminate, which contains an imprint likely caused by the tooling. A surface roughness was observed on the rubber tooling that covered the laminate. In turn, this roughness was caused by the molds used to manufacture the tooling. These are 3D-printed, so the surfaces are not completely smooth. While the roughness on the vertical surfaces of the molds is only small, which can be seen from the imprint left on the side of the ribs, the horizontal surfaces showed a higher roughness. The depth of these imprints is still quite small though, approximately 0.1 mm, which is equal to the layer thickness of the 3D-printed part.

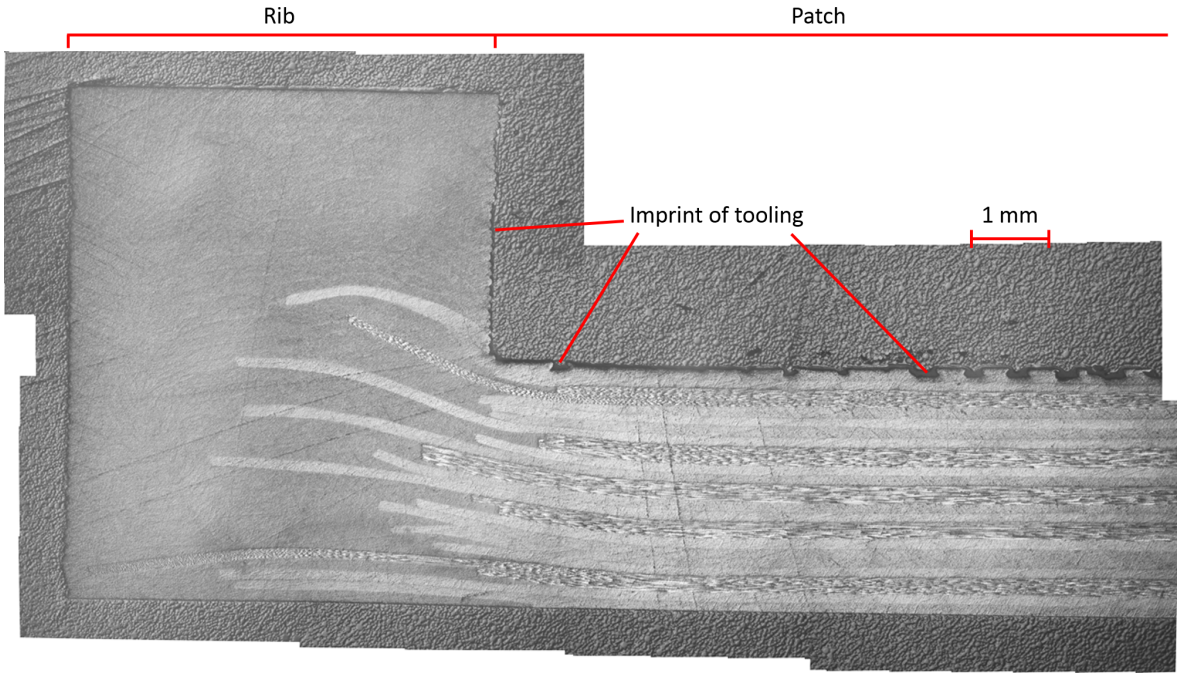

Figure 7.14: Microscopy image of the interface of a thin laminate and a helical rib. 10 images combined.

Fiber volume fraction

Parts are cut from all three types of samples to determine the fiber volume fractions. The parts cut from the DC1 sample are shown in Figure 7.15, the DC2 parts were cut from similar locations. For the ORTH samples, the center parts of some ribs were used.

The method used for determining the fiber volume is to first determine the density of the material. Knowing the individual densities of the fibers and the resin, the fiber volume percentage can then be calculated. Results are shown in Table 7.2.

Table 7.2: Measured fiber volumes in the attachment samples.

Location	DC1	DC2	ORTH
Node	62.0%	61.8%	-
Next to node	56.6%	57.4%	-
Rib	63.1%	63.4%	64.9%*
Patch	61.5%	61.6%	-

* Average of 4 samples

Generally the differences between the DC1 and DC2 samples are very small, the largest difference being in the area next to the node. Keeping in mind that the properties in this area vary locally due to the fiber waviness and resin pockets observed with the microscope, measuring a part cut in a slightly different location can easily result in a different measured fiber volume fraction. The abundance of resin pockets in this area is also the explanation for the significantly lower fiber content next to the nodes.

In all other areas, the measured fiber volume fraction is higher than specified by Hexcel.

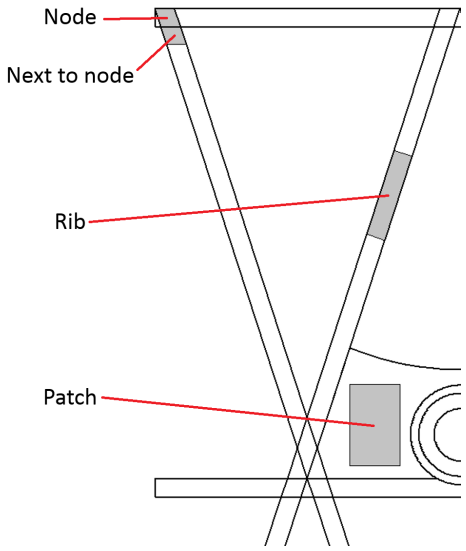

Figure 7.15: Parts of the DC1 sample used to determine the fiber volume.

59.9 vol% is specified, but values go as high as 65.5 vol% in the ribs of the ORTH samples. Three possible reasons can explain this difference:

- Resin flows out of the sample during curings.
- Resin flows into resin-rich areas in the sample during curing.
- The fiber volume fraction of the pre-preg material is not as specified.

The latter is considered the least likely of the three. Resin-rich areas in the rib right next to the node have already been identified. Additionally, small amounts of resin flowing out of the sample during curing were observed.

Chapter 8

Testing results and correlation

The manufactured samples were tested according to the approach described in chapter 6. This chapter covers the results, the comparison with the analysis method from chapter 4, and the resulting improvements that are made to the model.

8.1 Observed failure types and loads

This section gives a brief overview of the type of failure observed during the tests and the loads at which these occurred. Comparison of these results to the expectations is left for the following section.

8.1.1 ORTH tests

In all samples compressive fracture is observed in the ribs right next to the node. As can be seen in Figure 8.1 the presence of a patch does not affect the failure type. In addition to the shown rib fractures, occasionally a delamination extends from a fracture surface into the rib. This also occurs irrespective of the presence of a patch.

The loads corresponding to the failures are shown in Table 8.1. Both the load at the first audible sign of failure, and the highest taken load are given.

Table 8.1: Failure loads of the ORTH samples.

Sample	First cracking sound	Maximum load taken	Expected failure load
ORTH-WO1	23.0 kN	27.0 kN	65 kN
ORTH-WO2	-	30.0 kN	65 kN
ORTH-WO3	-	23.5 kN	65 kN
ORTH-W1	25.0 kN	27.5 kN	60 kN
ORTH-W2	26.5 kN	31.8 kN	60 kN
ORTH-W3	22.5 kN	26.0 kN	60 kN

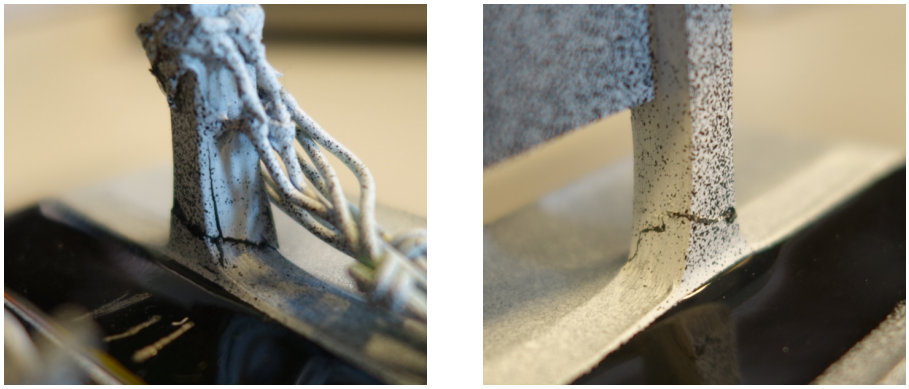

(a) Without a patch (b) With a patch

Figure 8.1: Typical failure in the ribs of the ORTH samples.

Final failure usually occurred at the highest load, accompanied with a load drop to between 5 and 10 kN. Only the W3 and WO3 samples showed a somewhat more progressive failure after the maximum load.

8.1.2 DC tests

All samples showed failure in the ribs underneath the patch, just outside of the node. The type of failure is highly similar to that of the ORTH samples. Additionally the DC2 samples showed some bearing damage in the laminate around the bolt.

In most cases the failure was not instantaneous, and some damage could be seen in the ribs before final failure. The first visible damage was a crack forming in the rib just outside of the node, on the side of the test fixture, this was usually accompanied by a small load drop. From this initial crack, damage progressed further through the thickness of the rib, either breaking through the entire rib, or causing delaminations along the length of the rib. A failed sample can be seen in Figure 8.2, the remaining load after failure is still applied, making the failed regions more clearly visible.

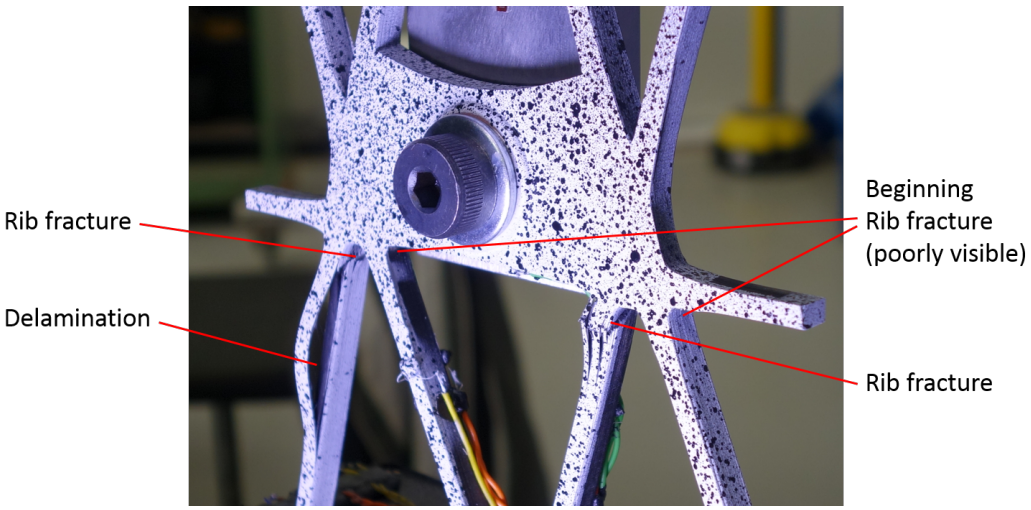

Figure 8.2: A DC1 sample after final failure.

The indicated delamination is exceptionally visible since its location close to the surface of the rib allowed the remaining thin part of the rib to develop a large out-of-plane deflection. The shown sample is the only one that showed this behavior, other delaminations were further away from the surface. The directional nature of the ribs makes it easy for cracks to propagate along the length. Also, this failure mode emphasizes the need for proper cure pressure control in the ribs. With an insufficient cure pressure, the void content will increase, which decreases the ILSS [63], allowing delaminations to grow more easily. Considering the low void content present in the samples, as identified in subsection 7.3.2, it is apparent that the samples experienced sufficient pressure during curing.

The loads taken by the samples are shown in Table 8.2. Similar to the ORTH test results, the first audible sign of failure and the maximum load are reported. Since several smaller load drops were usually observed before final failure, the first occurrence of these is also reported.

Table 8.2: Failure loads of the DC samples.

Sample	First cracking sound	First load drop	Maximum load taken	Expected failure load
DC1-1	18.8 kN	21.2 kN	22.3 kN	19 kN
DC1-2	18.0 kN	21.5 kN	21.6 kN	19 kN
DC1-3	18.9 kN	19.7 kN	21.2 kN	19 kN
DC1-4	17.7 kN	21.1 kN	-	19 kN
DC2-1	16.9 kN	21.3 kN	22.4 kN	8 kN (onset)
DC2-2	19.2 kN	21.7 kN	23.0 kN	8 kN (onset)
DC2-3	18.6 kN	22.0 kN	22.0 kN	8 kN (onset)
DC2-4	16.7 kN	-	-	8 kN (onset)

From both test series the fourth sample was not loaded to final failure. The DC1-4 sample was loaded to the first load drop and then immediately unloaded. This allowed microscopic investigation of the structure to find the location of initial failure. The DC2-4 sample was loaded to only 17.5 kN to be able to see the extent of the bearing damage at a lower load.

All samples that were loaded to final failure showed a progressive failure, showing the ability of lattice structures to take up additional load after initial failure. This is in line with observations of high damage tolerance and redundant load paths in grid structures. [6]

8.2 Comparison to initial model

The comparison with the initial model is made by comparing the measured displacements and strains. Given the large amount of data, only some of the interesting comparisons will be discussed. Additional displacement and strain gage data can be found in Appendix C.

The focus of the correlation is the patch and attachment point behavior, as well as the effects caused by the presence of the patch. Although the base structure does influence the measurements, its behavior is not the main focus of this research and correlation of all the effects there is not a main goal.

8.2.1 ORTH tests

The goal of these tests was to see the influence of a patch on the strength and the stiffness of a rib, this is necessary since far-field loads must be transferred through the attachment.

Failure load and type

Overall, the actual failure load is lower than expected. With the prediction of failure at 60 or 65 kN and actual values between 23.5 and 31.8 kN, the difference is significant. It will later be identified that the reduced strength is caused by an increase in strain just outside of the node, leading to premature failure of the sample.

Noteworthy is also the relatively large difference in strength between samples of the same design. With the data from Table 8.2 presented differently in Figure 8.3, it is clearly seen that the second samples are noticeably stronger than the first and third from a series. This can be attributed to the slightly bent ribs of the weaker samples. Since the second samples are cut from the center of the panel, these samples have the straightest ribs.

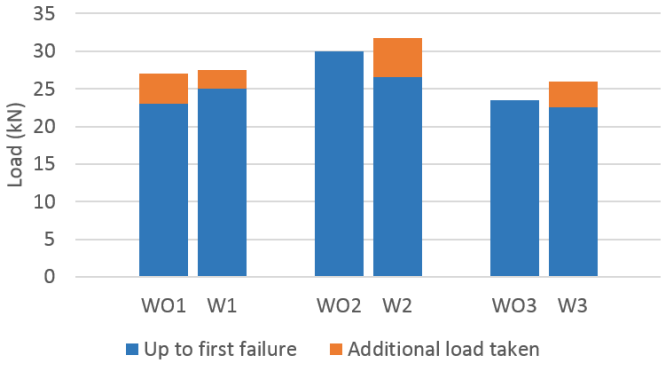

Figure 8.3: Strengths of the ORTH samples, comparing samples cut from similar places in the panel.

Comparing the samples from the same location in the panel it can be seen that the final failure load of the samples with a patch is higher, but in two out of the three cases the initial failure load is somewhat lower. Here, initial failure is determined as the load at which the first audible cracking sound is heard. This is usually not yet accompanied by a load drop, the first nonlinearity is at a higher load.

Given the similarity in the strengths, the effect of the patch on the strength of the ribs can be considered small.

Overall stiffness

The relation between the load and overall displacement applied to the WO samples is shown in Figure 8.4. The expectation from the initial FE model is also included.

Up to 5 kN the results show some settling, as expected, and from 5 kN up to the onset of failure the samples show linear behavior.

The first and third sample show a somewhat lower stiffness than the second one, again this can be attributed to the ribs being initially bent. This difference is less in the samples with a patch, which can be caused by the stabilizing effect the patch has on the ribs. This reduces the amount of bending under load, thus also reducing the difference in overall stiffness.

Looking at the slope of the graphs between 5 and 20 kN, the actual sample stiffness is less than predicted by the FE model. An overview of these stiffnesses is given in Table 8.3.

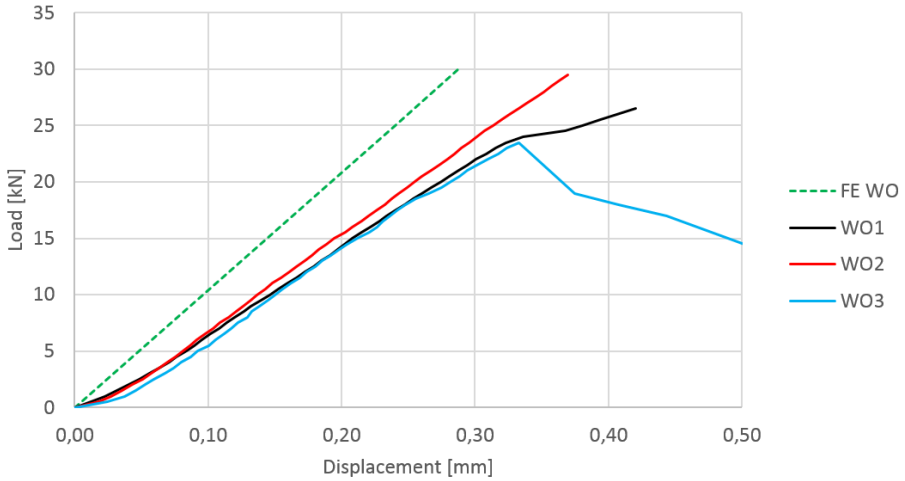

Figure 8.4: Overall stiffness of the samples without a patch, compared with FE expectations.

Table 8.3: Stiffness of the ORTH samples, compared with FE expectations.

Sample	5-20 kN stiffness	Difference
WO FE	104 kN/mm	–
WO1	79 kN/mm	-25%
WO2	86 kN/mm	-17%
WO3	79 kN/mm	-24%
W FE	106 kN/mm	–
W1	84 kN/mm	-21%
W2	90 kN/mm	-16%
W3	82 kN/mm	-23%

The large mismatch in stiffness, earlier doubts about the reliability of the LVDT data, and the fact that the strain gage data does correlate well, resulted in the decision to test some samples with DIC to obtain a secondary source of displacement measurements. A speckle pattern was applied to the potting faces, and DIC was used to measure the relative displacement between the top and bottom potting. A comparison of these measurements to the LVDT data from the same tests is shown in Figure 8.5.

The displacements agree very well, showing that the doubts about the correctness of the LVDT data are ungrounded. The measured stiffness mismatch is therefore also actually present.

To be able to see if the patch has an influence on the error, the difference between the averages of the two datasets is compared with predictions from both FE models. This is shown in Figure 8.6.

Despite the large absolute error, the difference between the samples with and without patch is very small. This shows that the presence of a patch only has a very small influence on the stiffness of a rib. Furthermore, the difference agrees well with the difference seen in the FE predictions. This makes it quite certain that the error in overall stiffness is caused by something in the base structure, and is not caused by the patch.

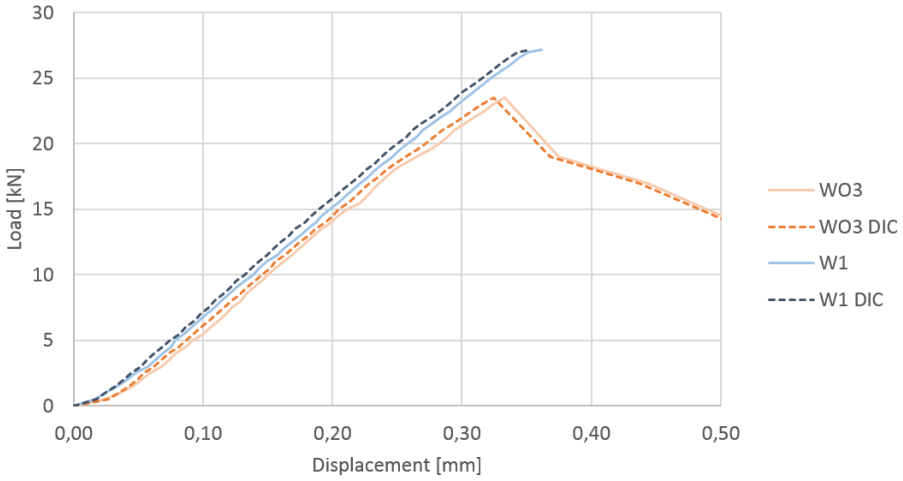

Figure 8.5: Comparison of displacements measured with LVDTs and DIC.

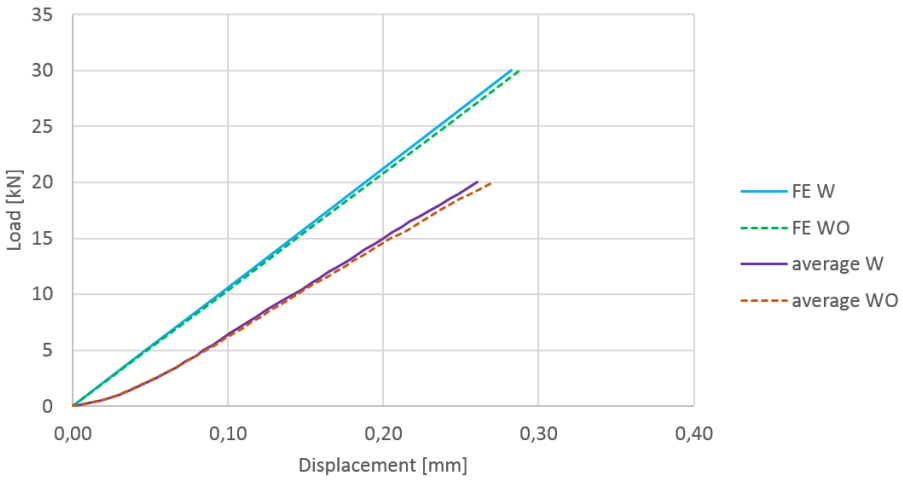

Figure 8.6: Average displacements compared with FE predictions.

Strains

The effect of the initially bent ribs, which has been mentioned several times before, can be clearly seen in the bending of these ribs under load. With strain gages on all sides of the rib, bending shows as a difference between the measured strains. To illustrate this the measured strains in the ribs of two different samples are shown in Figure 8.7.

In the left rib of the WO1 sample, a large difference can be clearly seen between the strains on the left and right sides of the rib, indicating bending. In the straight rib from the WO2 sample, the effect is a lot less visible, although some bending is still observed. Bending increases the strain significantly on one side of the rib. While this could lead to premature failure, the maximum observed strain is still below half of the material allowable of 1.2% compressive strain. This alone is therefore not an explanation for the lower failure load.

It can be seen that, on average, the FE results over-predict the strain somewhat, although the error is not as large as the overalls stiffness error. This is not only true for the WO

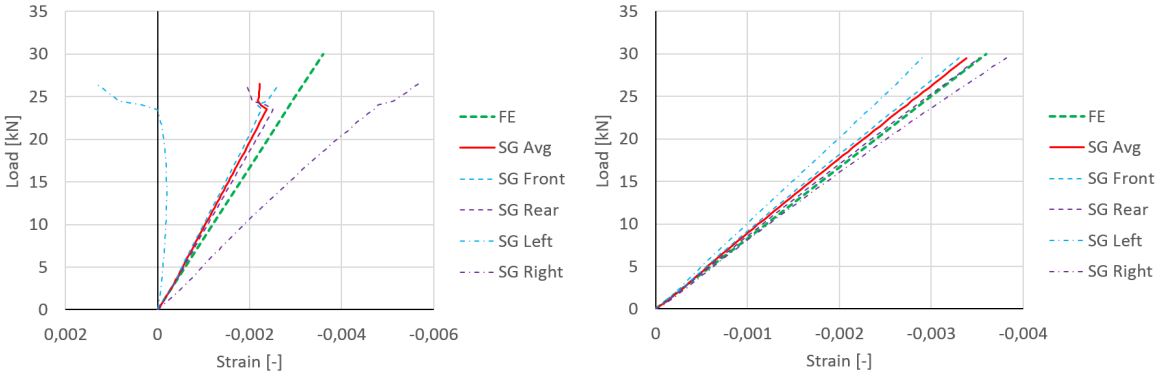

(a) WO1 left rib (bent) (b) WO2 left rib (straight)

Figure 8.7: Strain gage measurements in ribs of two samples without a patch, compared with FE predictions.

samples, but also true for the W samples, which do contain a patch.

While a patch may stabilize the rib against bending in-plane, the asymmetry it introduces may be cause for out-of-plane bending of the ribs. This effect showed in the FE predictions, but as can be seen in Figure 8.8 the test samples hardly experienced this. The strains measured on the front and rear of the ribs are almost equal.

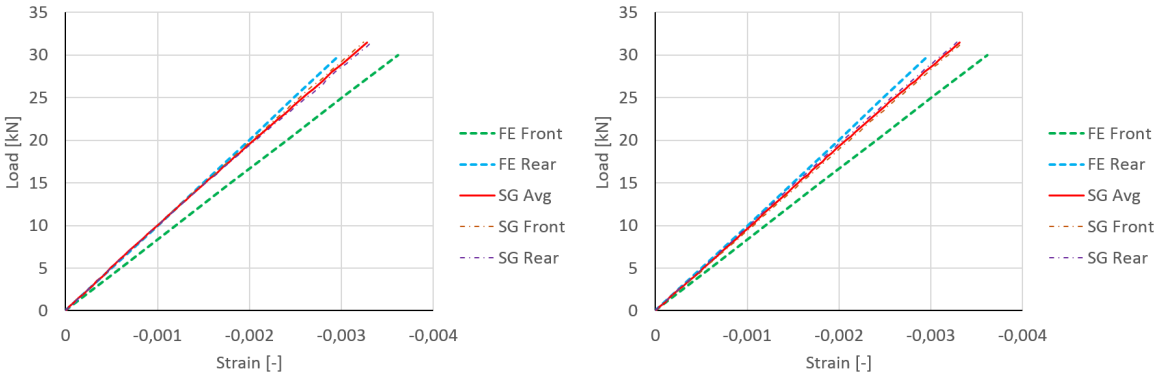

(a) Left rib (b) Right rib

Figure 8.8: Strain gage measurements in the ribs of the W2 sample, compared with FE predictions.

It is suspected that this is caused by the more gradual distribution of the plies extending into the ribs. As already identified in section 7.3.2 these plies curve into the rib, resulting in a reduced stiffness difference over the rib height.

To find a reason for the early failure, the strain field found with DIC is investigated. A comparison with FE results is shown in Figure 8.9. In this figure the results are mirrored over the dividing line, that is: the leftmost side of the DIC results corresponds to the rightmost side of the FE results.

Overall, the strain field is very similar, except for the area at the end of the rib just outside of the node. There, a large increase in strain is seen locally. The strain at this location can

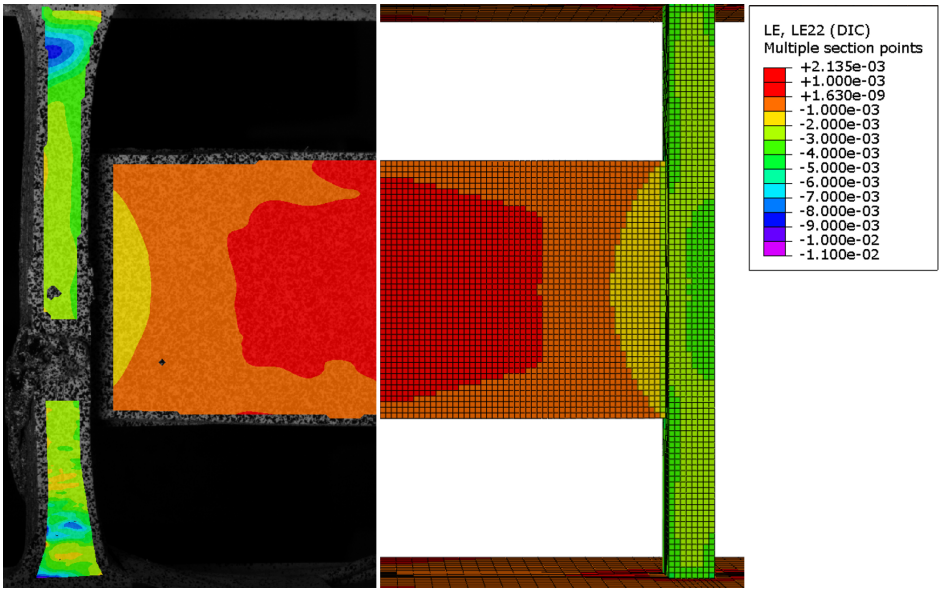

Figure 8.9: Strain in the direction of the vertical ribs at 25 kN load, DIC measurement (left) and FE results (right).

be extracted and plotted, as shown in Figure 8.10. Also shown in this graph is the strain as measured by the DIC at the location of the strain gage, and the strain gage measurement itself. These strains match very well, showing the accuracy of the DIC system.

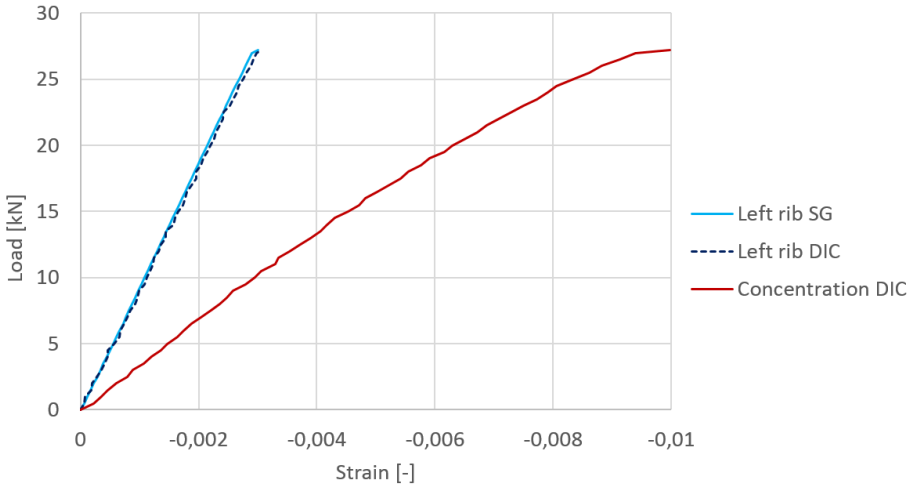

Figure 8.10: Comparison of strain measured by strain gage and DIC at the same location, and DIC measured strains at the concentration next to the node.

The measured strain at the concentration next to the node is around three times higher than strain further along the rib. Strain goes as high as 1% before failure occurs. This approaches the material allowable, and when considering that increased transverse strain and shear are also present in this location this explains failure at that location. Since this effect is identified in both samples with and without a patch, it is clear that his is an effect of the base structure, and therefore outside of the scope of the presented research.

8.2.2 DC1 tests

The main goal for these tests was to show that a high-strength attachment point can be made even in an unfavorable location. Furthermore the test data is used to correlate the model.

Failure load and type

The strength goal for these samples was set at 20.1 kN. All samples exceeded this strength. As was already shown in subsection 7.3.2, the inserts, laminate and rib in the direction of the load show no damage at all. Also the fit of the bolt in the insert is unchanged, there is no noticeable additional play. This confirms that there is no damage in the attachment itself.

The predicted failure at 19 kN, either in shear-out or first-ply failure on the rib-patch interface, did not occur. The higher shear-out strength can be attributed to the inserts. It was expected that these would have a beneficial influence by spreading the loads over a larger area, but since no reference data was available this was not taken into account in the predictions. And as was already shown in section 5.2 the modeling method used for the interface is conservative, explaining the higher strength there.

At the final failure load around 21 to 22 kN, an unexpected failure type occurred, the fracture of the ribs next to the node. In the FE model predictions, the strain in the fiber direction at the load and location of failure is around 0.6%, half of the allowable strain. In the ORTH samples discussed earlier, the actual strength was also around a factor two lower than expected. Since the type of failure and the location of failure are also very similar it is therefore likely that the same effect causes the reduced strength in both sample types.

To investigate the origin of this failure one sample was loaded up to the first sign of damage, and a microscope sample was cut at the failure location. Its location and the resulting image are shown in Figure 8.11.

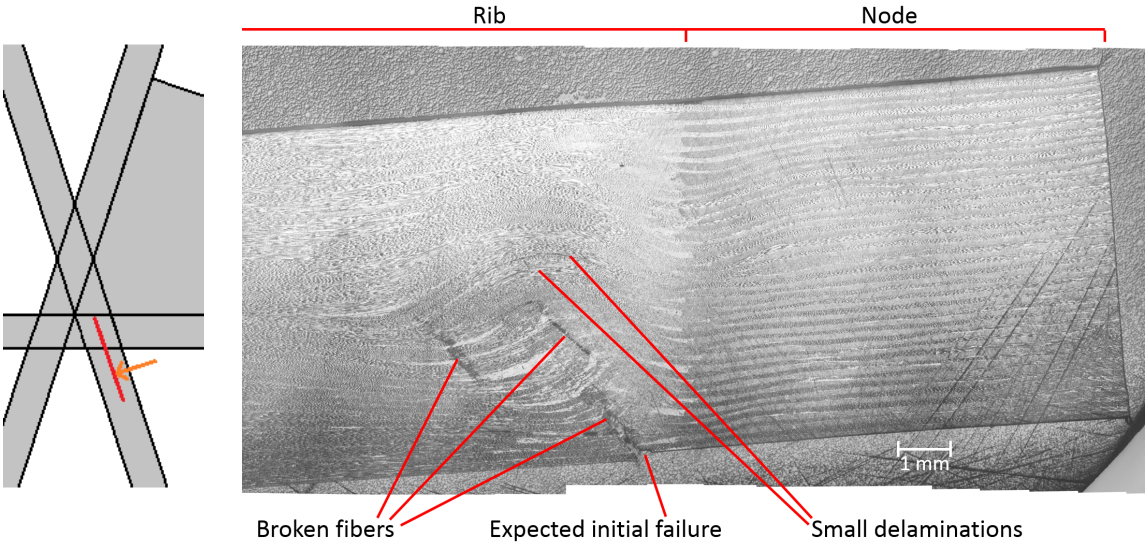

(a) Location in sample

(b) Rib cross-section

Figure 8.11: Microscope image of the location of initial failure, 15 images combined.

Damage can be seen in the wavy area just outside the node, both broken fibers and small delaminations can be seen. The damage is local and does not extend outside of a small area. This damage is thus not a propagation of damage from somewhere else (like the patch for instance) but an isolated failure.

Overall stiffness

The overall stiffness of the attachment is investigated by comparing the applied displacement to the expectations from the FE model. Figure 8.12 shows the measured displacement of all four DC1 samples and the FE expectations. To allow a better comparison, the measured displacements are corrected to be zero at 200 N.

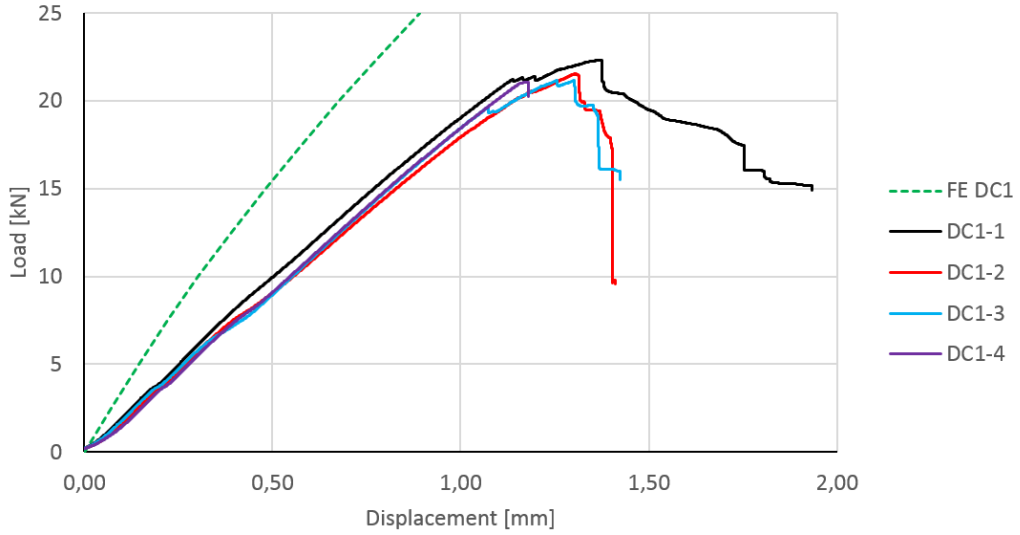

Figure 8.12: Overall applied displacement on the test setup with the DC1 samples.

The scatter between the samples is low, and all show a similar behavior up to the start of failure (around 19 kN). A major point to note is the large difference in overall stiffness with respect to the FE model. A linear part of the data is identified between 10 and 15 kN, allowing for a stiffness comparison with FE predictions, which is shown in Table 8.4.

Table 8.4: Stiffness of the DC1 samples, compared with FE expectations.

	10-15 kN stiffness	Difference
FE	27.7 kN/mm	–
DC1-1	18.8 kN/mm	-32%
DC1-2	18.3 kN/mm	-34%
DC1-3	19.4 kN/mm	-30%
DC1-4	19.3 kN/mm	-30%

At no less than 30%, the difference is significant. Since the displacement is measured by the test bench, all components in the load path influence the measurement. A single responsible is therefore not easily identified. To see if the extra displacement is taken up in the sample, the displacements as measured by DIC are compared with the FE model, a side-by-side comparison is shown in Figure 8.13.

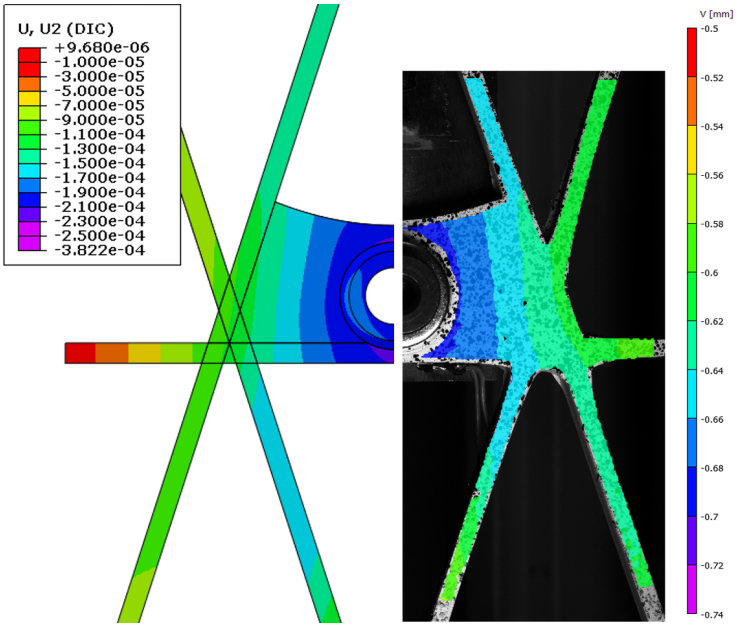

Figure 8.13: Vertical displacement at 15 kN in the test sample. As modeled (left) compared with DIC measurements (right), corrected for initial offset.

Note that the scale for the DIC results is corrected for the initial offset, which is due to the initial travel of the sample towards the lower plate of the test bench. The range of both scales is identical. The displacements agree very well, so the cause for the difference is not found in the sample.

At loads below 10 kN, some small nonlinearities are seen in the overall displacement. At loads between 7 and 10 kN, depending on the sample, a small increase of around 0.03 mm in displacement is seen. This displacement is of the same magnitude as the bolt clearance. This, and the load at which the displacement occurs, make the expectation that this is the settling of the bolt in the hole.

Additionally, there is a slight increase in displacement at 3.8 kN. Since the magnitude of the displacement and the load at which this occurs is exactly the same for all four samples, this is expected to be caused by an effect outside of the sample, so either in the test fixture, test bench, or measurement equipment. This is indicative of effects outside of the test sample influencing the displacement data, and lead to a possible explanation of the observed differences.

Strains

Strain gages were placed on several ribs and on the fixture, their locations were shown in Figure 6.11. Figure 8.14 shows the data from a strain gage on the rear side of a rib between the patch and the potting, and from the strain gage on the side of the hoop rib at the point where the attachment point is.

Both datasets show some scatter between the different samples, but overall differences are quite low. A slight difference with respect to the FE results can be seen, but its magnitude is also small. Other strain gage data shows a similar correlation, and is given in section C.2 for reference.

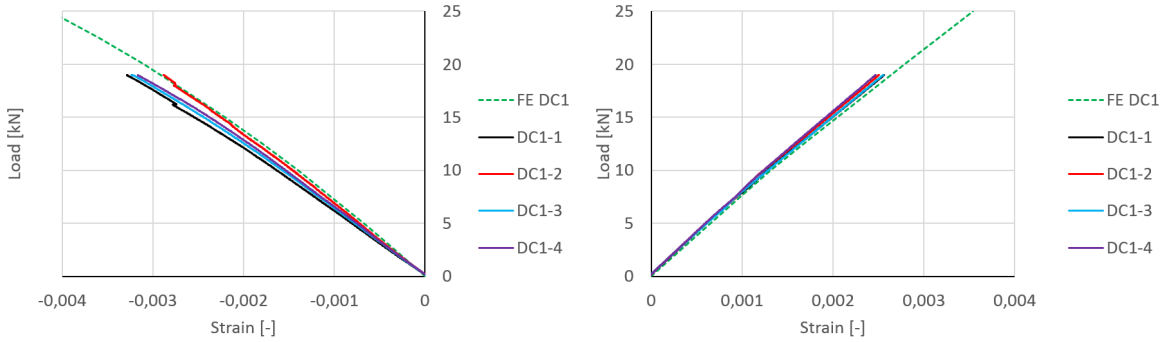

(a) Rear side of rib (b) Side of hoop rib

Figure 8.14: Strain gage measurements in the test samples. (truncated at 19 kN)

The data from the strain gages on both sides of the fixture are shown in Figure 8.15. The scatter between the different tests is very small, which is not surprising given that the same fixture is used for all four tests. The correlation with the FE model is excellent for the strain gage on the front of the fixture, but a large difference can be seen for the strain gage on the back of the fixture. It was later discovered that this is due to an improperly bonded strain gage, rendering this dataset useless.

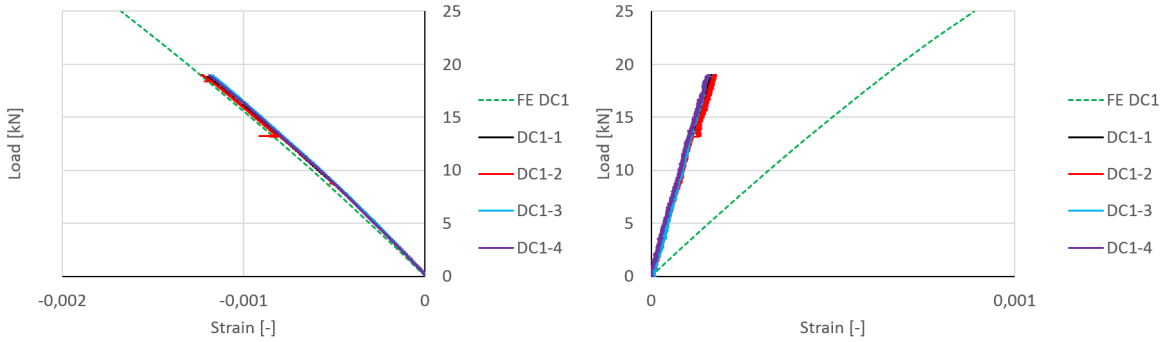

(a) Front of fixture (b) Rear of fixture

Figure 8.15: Strain gage measurements in the test fixture. (truncated at 19 kN)

The strain field on the patch interface is more complex than can be measured with strain gages, therefore DIC was used to get the strains in this area. With the fixture blocking the view of one side of the sample, the data is obtained from the visible side of the sample. This side shows lower strains in general, but allows a larger area to be viewed.

Of high interest is the strain in the vertical direction, since failure occurs primarily in this direction. The comparison of strains and FE results is shown in Figure 8.16. To facilitate the comparisons, the FE results are first transformed to the same coordinate system as is used for the DIC results.

Overall both the shape and magnitude of the strain field are very similar. Both the concentrations at the corner of the node, and the top of the rib-patch interface are captured. On the interface of the patch and the hoop rib some differences can be seen, mostly in the shape of the strain field, with the FE model showing a sharper transition. This is in line with

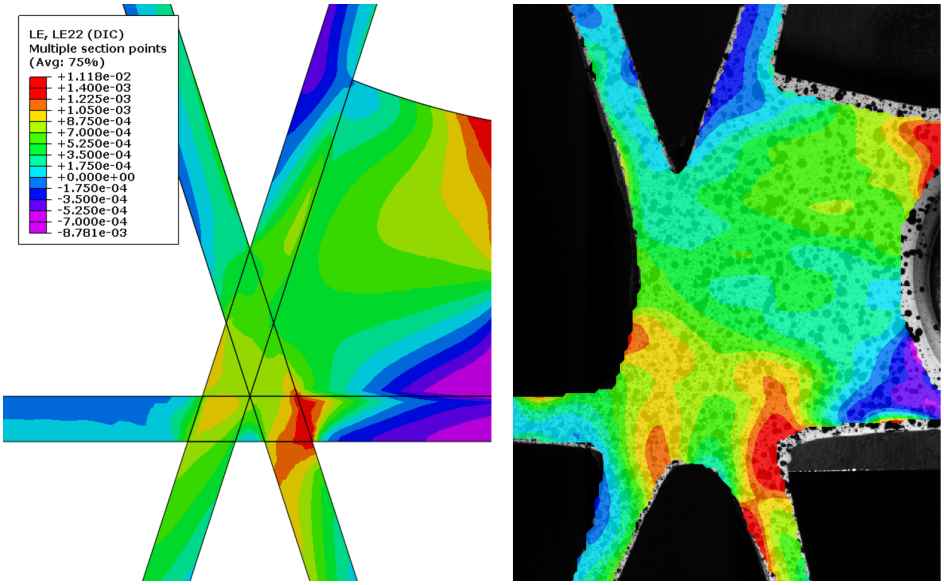

Figure 8.16: Strain in the vertical direction at 15 kN in the test sample. As modeled (left) compared with DIC measurements (right)

expectations, since the FE model has a very sudden transition from patch to rib, whereas the test sample has a more gradual transition.

The other strains and displacements as measured with DIC show a similar level of correlation, with the exception of the shear strains, which show a larger difference as can be seen in Figure 8.17.

The FE results show high strain concentrations in the ribs on the interface, which are not seen in the test sample. This is in line with what was seen in section 5.2, where more detailed modeling of the plies extending into the ribs showed to reduce the shear strains significantly in these areas. Aside from these areas, the actual shear strain is also lower in other locations such as the node, patch edge, and ribs.

On the edge of some of the ribs the DIC data shows some local peaks in shear strain. These are edge effects caused by the DIC software having difficulty calculating the strains on these edges, and are not actual strains.

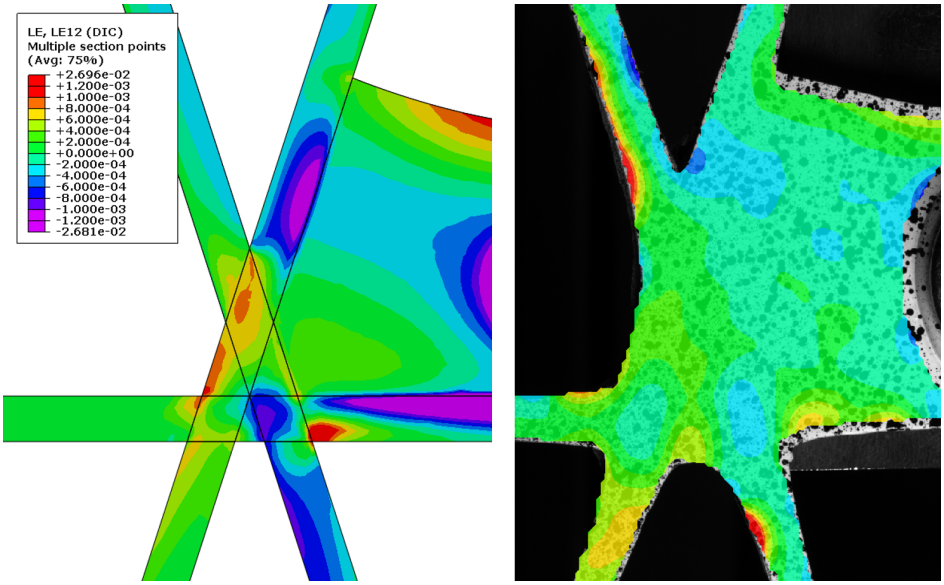

Figure 8.17: Shear strains at 15 kN in the test sample. As modeled (left) compared with DIC measurements (right)

8.2.3 DC2 tests

The goal of these tests was to show that an attachment point can be made as far away from the ribs as possible, with the use of a patch. This also allows better studying of the patch behavior since it plays a larger role in this attachment than it did in the DC1 case, where the patch was smaller.

Failure load and type

The final failure type was the same as for the DC1 samples: fracture of the ribs just below the nodes. Additionally, some bearing damage was observed as well. This is apparent from some visible damage in the laminate around the insert and a noticeable increase of clearance of the bolt after testing, indicating plastic deformation in the insert. Bearing failure was expected, but the expected onset strength of 8 kN is vastly exceeded. While final bearing failure is generally at a higher load than the onset, the observed strength is significantly higher, so the onset can't realistically have been at 8 kN.

The bearing onset load can not be easily seen from the overall displacement, since the preloaded bolt suppresses any stiffness loss due to the initial damage. This makes it difficult to identify the failure onset load, however it is observed that the stiffness does decrease slightly as damage accumulates. A single sample was loaded to 17.5 kN, which is well below the final failure load, but at a load where a slight decrease of stiffness is already observed. Microscopy samples were cut from both this sample and from one that was loaded to final rib failure at 23 kN. The location of these microscopy samples is shown in Figure 8.18, it is at the bolt hole in the direction of the load. The resulting images are shown in Figure 8.19.

The sample loaded to 17.5 kN shows some minor damage in the outer plies of the laminate, next to the insert. Additionally, some plastic deformation is seen in the aluminum insert. The 17.5 kN load corresponds to an average bearing stress of 685 MPa, but since the load is applied offset from the plane of the structure, the peak bearing stress will be higher.

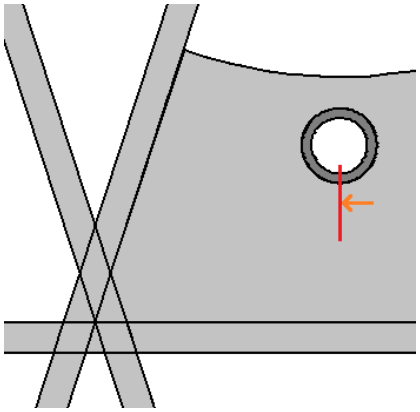

Figure 8.18: Location of the microscope images in the sample.

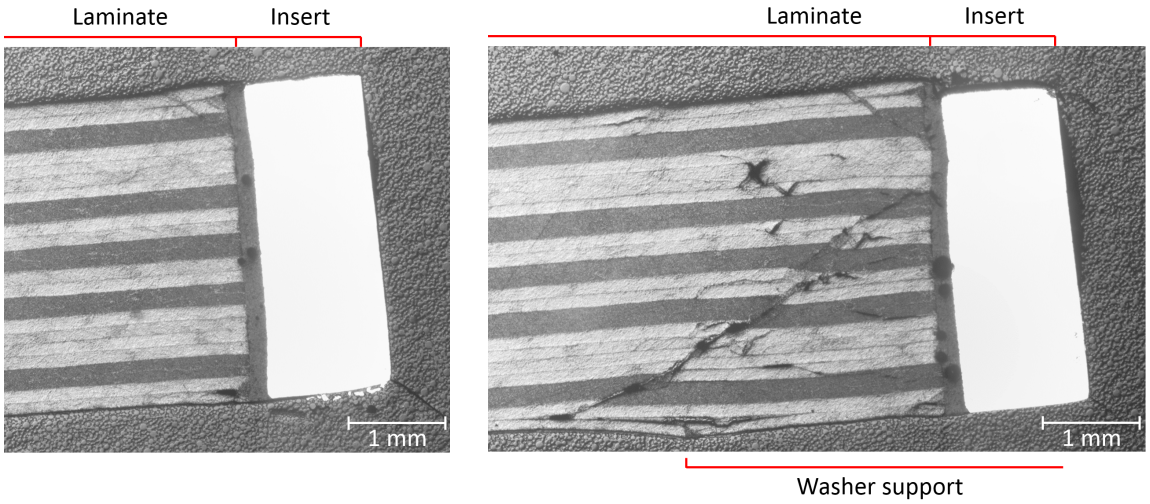

(a) Loaded to 17.5 kN (b) Loaded to 23.0 kN

Figure 8.19: Microscope images of the laminate loaded in bearing.

The damage seen in the sample loaded to 23 kN is much more extensive. Damage is seen in all the plies of the laminate, and additional delaminations are present. Furthermore the adhesive layer shows yielding and damage as well, and more plastic deformation in the insert is observed. The damage in the laminate extends past the area clamped by the washers, which results in the inability of the bolt preload to suppress the loss of stiffness due to further damage. This is one of the reasons the displacement curve levels off at high loads, the other factor influencing this is the initiation of failure in the ribs of the sample. The 23 kN load equals an average bearing stress of 900 MPa.

Comparing these images to microscopy images found in literature[50,64], it is estimated that the 17.5 kN sample is around 10% past the onset of bearing damage. The 23 kN sample is estimated to be at around 85% of final bearing failure. This makes the estimates for bearing onset and final bearing strength 15.5 and 27 kN, or 600 and 1050 MPa when expressed as average bearing stress. This is significantly more than the expected onset at 8 kN. Looking back at the calculation method presented in chapter 4, several possible reasons can be identified.

The expected failure load was calculated from a base bearing allowable, and multiplied by two factors to account for the insert and the load offset. It was already identified that the influence of the insert was an increase in strength of between 20 and 55%. With a conservative 20% increase used for the analysis, this can account for up to a quarter of the difference. A similarly small part can be attributed to the effect of layup, since laminates with more or less equal portions of ±45° and 90° plies show an excellent bearing strength.[47] Since the base allowable originates from a laminate that also performs quite well in bearing, it is not able to account for the rest of the difference though. This leaves the effect of the load offset, which was initially implemented by dividing the strength by a conservative factor of two. Now considering the test results, it is apparent that this factor 2 is too high. Dividing by 1.5 is more realistic, yet still conservative. This can then explain the remaining difference in strength. Since many factors influence the strength, it is not possible to identify exactly the contributions of each of the separate effects until more test data is available.

The difference between the onset and final bearing load is exceptionally high. A possible reason for this lies in the aluminum insert, which shows plastic deformation at higher loads. This plasticity redistributes the load over the interface with the composite, thus reducing the stress concentration on the side of the patch on which the load is introduced. This further postpones failure.

Not only the expected bearing strength is exceeded, the expected shear-out at 20 kN, and first-ply-failure on the interface at 23 kN did not occur. This is in line with results from the DC1 samples, and similar reasons apply.

Noteworthy as well is that the strength of the attachment is so high that it approaches the strength of the bolt.

Overall stiffness

The total applied displacements are shown in Figure 8.20

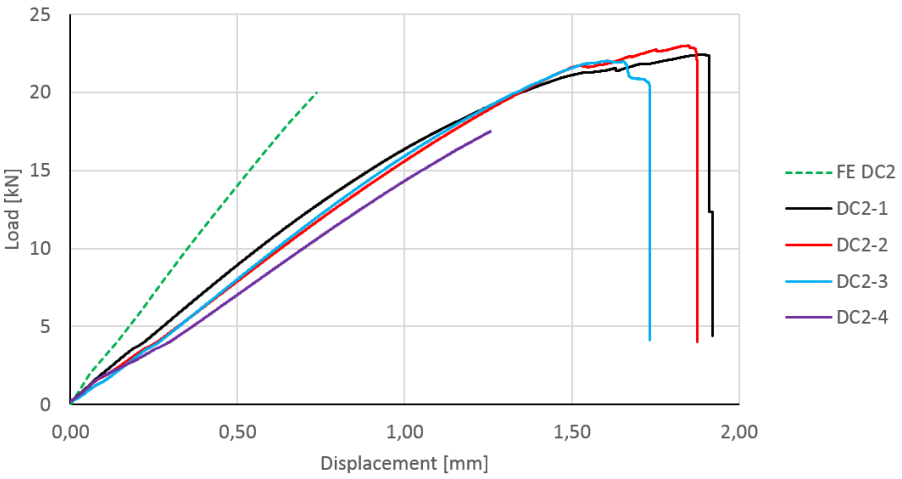

Figure 8.20: Overall applied displacement on the test setup with the DC2 samples.

Similar to the DC1 results, a low scatter between the samples is seen. At 3.8 kN the small displacement increase is again observed. Its occurrence also with different sample types confirms that this is an effect outside of the sample.

Since the bolt preload is significantly lower for these samples, any settling of the bolt shows between 1 and 2 kN, so it is less clearly seen. Another difference is the less linear behavior up to final failure, which can be explained by the bearing damage accumulating at higher loads.

Again, there is a large difference with the FE results, the magnitude of the overall stiffness and displacement error similar to what was observed with the DC1 samples. A comparison of the stiffness between 6 and 12 kN is given in Table 8.5.

Table 8.5: Stiffness of the DC2 samples, compared with FE expectations.

	6-12 kN stiffness	Difference
FE	28.1 kN/mm	–
DC2-1	16.9 kN/mm	-40%
DC2-2	16.1 kN/mm	-43%
DC2-3	16.9 kN/mm	-40%
DC2-4	14.9 kN/mm	-47%

Strains

Both the strain gage data and DIC data show a similar quality of correlation as the DC1 samples, so these are not further elaborated on here.

Noteworthy though are the strains that are measured in the test fixture. On the DC1 fixture one of the strain gages was not properly bonded, but the DC2 fixture did have both strain gages installed correctly. The measured strains are shown in Figure 8.21, showing excellent agreement with the FE model. This leads to the conclusion that the fixture is accurately modeled, which is not surprising considering the simple geometry and material. This also implies that the fixture is not the cause for the large difference in overall stiffness.

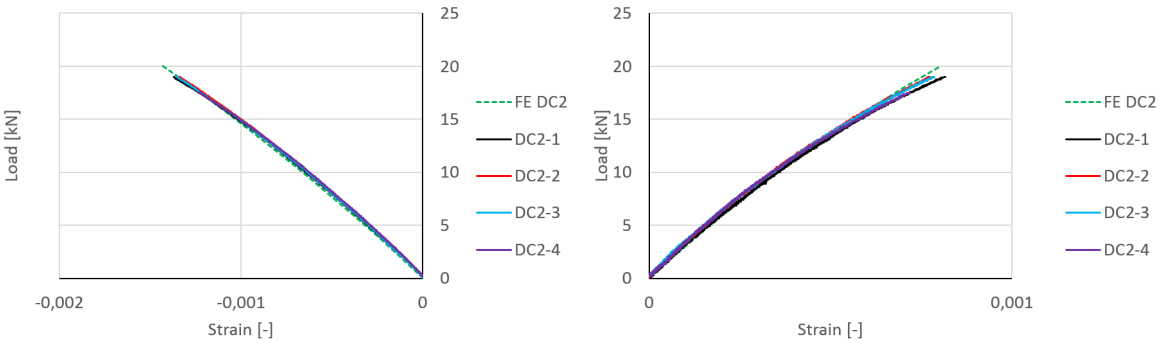

(a) Front of fixture

(b) Rear of fixture

Figure 8.21: Strain gage measurements in the test fixture. (truncated at 19 kN)

8.3 Correlation goal and strategy

While the strains as measured by the strain gages match the model quite well, some improvements can still be made, especially on the rib-patch interface. Additionally, the overall stiffness shows a significant difference. It was already identified that this is an effect in the base structure and therefore not the main focus of the research. Nonetheless, some changes are made to the models to investigate the cause for the overall stiffness. Here, obtaining a perfect correlation of the overall stiffness is not the goal, these changes are only performed to identify the likely cause for the stiffness difference.

If it proves impossible to reduce the errors to an acceptable level, the remaining errors should at least be explained. Furthermore, the changes to the model should not result in a bad correlation of the strains, since the correlation is good before the implementation of any changes.

8.3.1 Correlation strategy

Given the lower complexity of the samples and test setup of the ORTH samples, less factors will be influencing the results. Therefore these models are improved first.

The first step is changing the geometry of the ribs to the measured values, and correcting for the higher fiber volume fraction. Since it is recognized that the fiber dominates the stiffness in the fiber direction, the stiffness in that direction is changed linearly with the fiber volume fraction. Because a strain gage is bonded on the rib-patch interface, the plies extending into the ribs were already modeled for the ORTH samples, so there is nothing to be improved there. As a final step, an attempt is made to include the fiber waviness next to the node in the model.

If the changes to the ORTH model show to improve or change the correlation, these are also implemented in the DC models. Additionally, another correction is made to the DC models to more accurately represent the boundary conditions at the top of the fixture, where it is clamped in the test bench. This is done because the top of the fixture is clamped between circular pistons, whereas it is modeled as a straight boundary in the initial model. The distance from the bolt to this boundary was also slightly larger in the tests than in the models, so this is corrected as well. Additionally, the plies extending into the ribs will be modeled, since it was shown earlier in section 5.2 that this leads to different results on the rib-patch boundary.

8.4 Improvements made to the models

The improvements to the FE models are implemented as discussed previously in section 8.3. The changes are presented in the order in which they were implemented, and afterwards their applicability to the general modeling method is discussed.

8.4.1 ORTH models

The changes to the model are applied in several steps, to be able to see the effect of the separate changes. The names used and the changes included in these models are shown in Table 8.6.

Table 8.6: Nomenclature used for the different ORTH FE models.

Name	Changes to model
FE orig	None, this is the original model
FE+DIM	Actual rib dimensions and fiber volume
FE+WAV	FE+DIM with additional soft area in ribs next to node

The improvements are shown only for a part of the datasets here, section C.1 contains all the strain gage and displacement datasets, showing also the results from the initial and the final (FE+WAV) models.

Rib dimensions and fiber volume

The dimensions of the ribs are adjusted to 6.4 by 3.2 mm, which is within the range of actual dimensions as were identified in subsection 7.3.1. The rib material properties are corrected to a fiber volume of 64.9%, the average as identified in section 7.3.2. The material properties in the patch are adjusted to 61.5% fiber volume.

The effect of these changes on the overall displacements is very small, showing only a very slight reduction. The difference in the strains in the rib is more significant, as can be seen in Figure 8.22 for the strains in a rib with a patch.

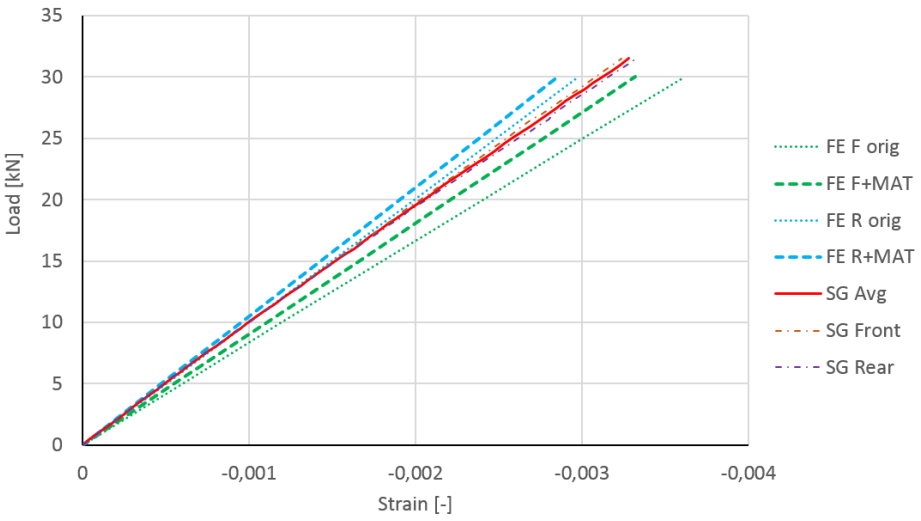

Figure 8.22: Strains in the rib of a sample with a patch, original FE model compared with the +MAT model.

Both the expected strains on the front and the rear of the ribs are reduced. On average, the FE results are closer to the measured strains. While the changes also reduce the strain difference between the two sides of the rib, the predicted difference is still larger than the measured values.

Waviness in ribs next to node

The wavy layout of the fibers in the rib next to the node presents quite a challenge to model if all the actual fiber orientations are to be modeled. It was also observed that the waviness varies from rib to rib, so the practical use of such an extensive modeling method can be doubted. The waviness is therefore implemented as an area with reduced stiffness in fiber direction.

Judging from the microscope images shown in Figure 8.11 and Figure 7.12, the size of the reduced stiffness area is selected to be 5 mm along the rib length, starting right next to the node. This area covers all the very wavy parts, but not much more.

The knockdown factor to use for the stiffness in this area is not easily determined since DIC data showed that the strains in this area vary very locally. As was shown in Figure 8.10 the strains are up to three times as high as the strain further along the rib. Lacking further details to determine a factor more accurately, a factor two is selected since it is the average between the minimum and maximum. This factor also corresponds well with the samples failing at around half the predicted load, since it will result in strains that are twice as high.

Implementation of these lower-stiffness areas results in a negligible change in the strains halfway along the length of the rib. As might be expected, the overall stiffness is affected by this change, as shown in Figure 8.23.

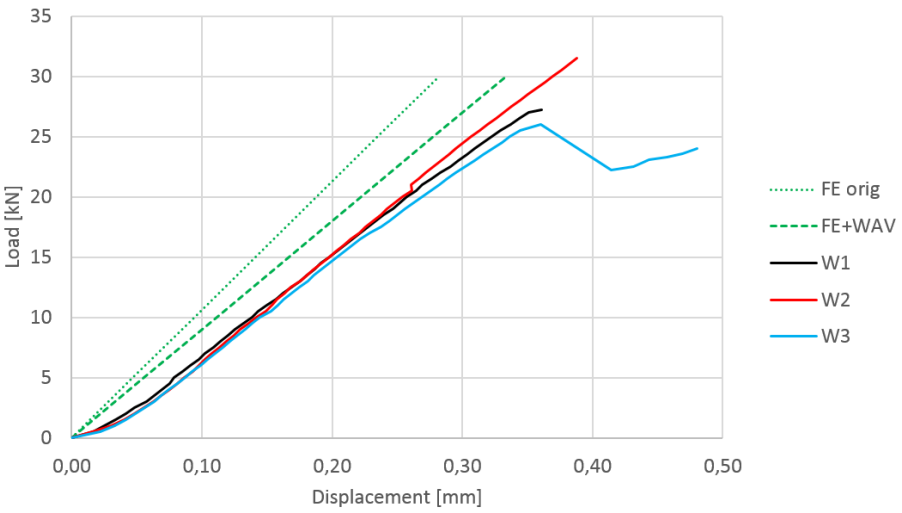

Figure 8.23: Overall displacement of the ORTH tests, original model compared with the +WAV model.

As can be seen in Table 8.7, the overall stiffness now matches quite well with the second samples from both sets of samples. There is still a difference with the first and third samples. The FE models do not take the effect of bent ribs (as are present in the first and third samples) into account, explaining the difference between the individual samples.

While the accuracy of both the stiffness reduction factor and the area on which it is applied can be doubted, this approach does show that the waviness is able to cause the overall stiffness mismatch. Given the simple geometry of the samples and the fact that the strain in the ribs matches well, it is not expected that other factors of significant influence exist.

Table 8.7: Stiffness of the ORTH samples, compared with original and improved FE models.

	5-20 kN stiffness	Difference with FE Original	+WAV
WO FE orig	104 kN/mm	–	–
WO FE+WAV	88 kN/mm	–	–
WO1	79 kN/mm	-25%	-13%
WO2	86 kN/mm	-17%	-2%
WO3	79 kN/mm	-24%	-12%
W FE	106 kN/mm	–	–
WO FE+WAV	90 kN/mm	–	–
W1	84 kN/mm	-21%	-7%
W2	90 kN/mm	-16%	0%
W3	82 kN/mm	-23%	-9%

8.4.2 DC models

Again, the changes to the model are applied in several steps, the names used and the changes that are included in these models are listed in Table 8.8. The effects of the changes are very similar for the DC1 and DC2 models, hence these are not treated separately.

Table 8.8: Nomenclature used for the different DC FE models.

Name	Changes to model
FE orig	None, this is the original model
FE+DIM	Actual rib dimensions, fiber volume and fixture BC
FE+PLY	FE+DIM with plies into ribs modeled
FE+WAV	FE+PLY with additional soft area in ribs next to node

Rib dimensions, fiber volume and fixture boundary

In a similar manner as done for the ORTH models, the rib dimensions and fiber volume fraction are adjusted to the actual values as reported in section 7.3. Additionally, the shape of the edge of the fixture, which represents the clamping by the test bench, is adjusted. The change in geometry is shown in Figure 8.24.

These changes result in practically no change in strains at the strain gage locations. A slight increase is seen in the overall displacement, but no other noteworthy changes are observed.

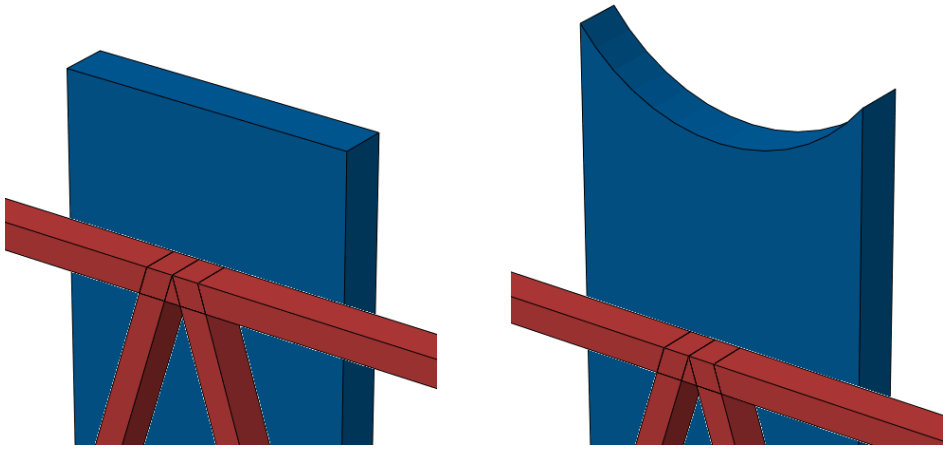

Figure 8.24: Different geometries of the boundary of the test fixture, uncorrected(left) and corrected (right).

Plies extending into ribs

The plies extending into the ribs are modeled using the method described in section 5.2. Just as was observed before, the strains on the interface change noticeably as a result. Comparing to the DIC data, this results in an improved correlation. This effect is most visible in the shear strains, which initially had a poor correlation with the initial model on the rib-patch interface. Figure 8.25 shows the comparison of the shear strain with both the original model and the model with plies extending into the ribs.

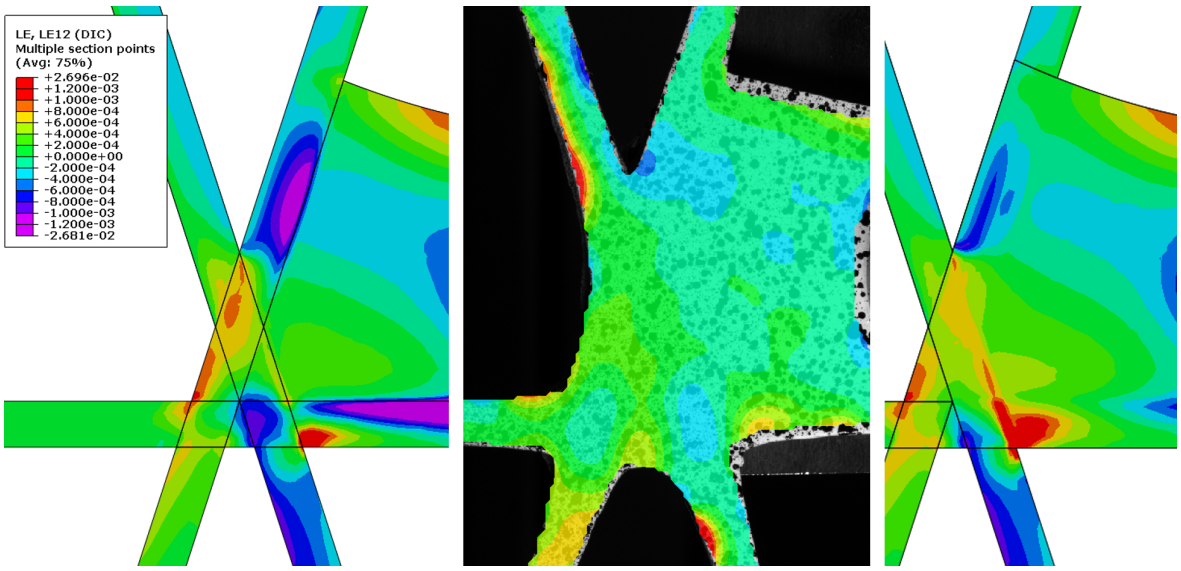

Figure 8.25: Shear strain in the test sample. DIC measurements (center) compared with the initial model (left), and the model with plies extending into the ribs (right).

The large concentrations of shear strain present in the ribs of the initial model have been vastly reduced by the improved model, and the overall correlation is improved. It is not perfect however, still showing some shear strains around the node, which are not measured in the sample.

The difference is less noticeable for the other strains, mostly because the initial difference was a lot lower, but some improvements are still seen.

Other than the strains at the interface, hardly any differences are seen. Both the overall displacement and strains at the strain gage locations are not significantly changed.

Waviness in ribs next to node

The softer area in the nodes next to the ribs is implemented in the same way as in the ORTH models. This reduced the difference in overall displacement somewhat, as can be seen in Figure 8.26. There is however a large remaining difference, even with all the implemented changes.

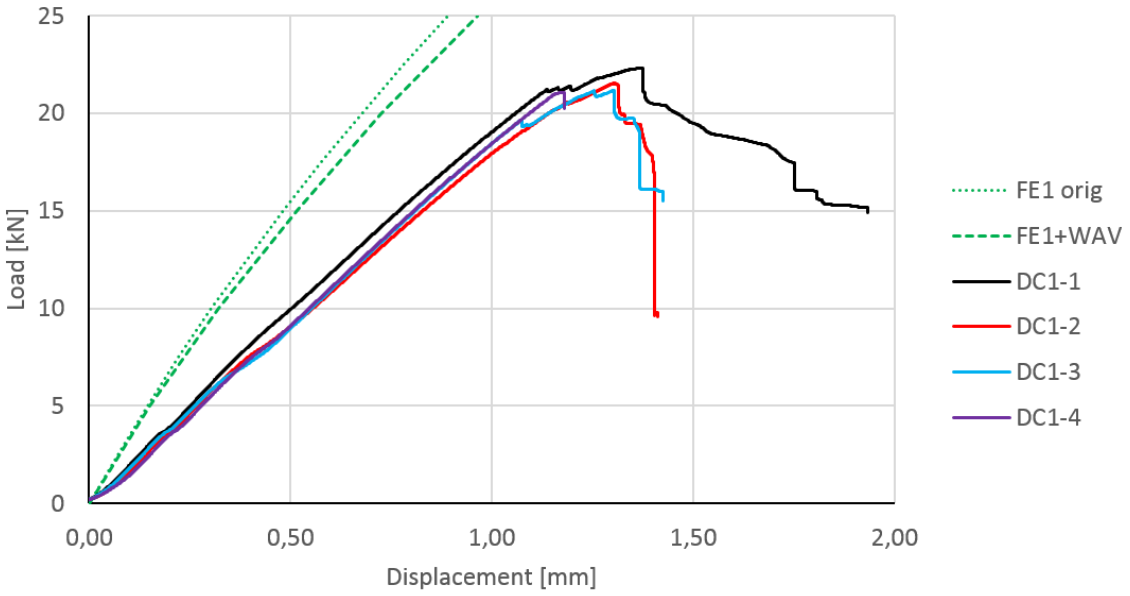

Figure 8.26: Overall displacement of the DC1 tests, with predictions from the original and +WAV FE models.

Around half of the gained improvement is attributed to the softer area outside the nodes, the rest of the improvement is due to the other changes. The relative effect of the softer areas outside the nodes is smaller here than it was for the ORTH model. This is due to the longer ribs, so the part of a rib that is assigned softer properties is relatively small. Table 8.9 and Table 8.10 give a comparison of the stiffness differences for the DC1 and DC2 samples respectively.

Strains at the strain gage locations are affected very slightly by this implementation, but the difference is not noteworthy.

Table 8.9: Stiffness of the DC1 samples, compared with original and improved FE models.

	10-15 kN stiffness	Difference with FE Original	+WAV
DC1 FE orig	27.7 kN/mm	–	–
DC1 FE+WAV	25.6 kN/mm	–	–
DC1-1	18.8 kN/mm	-32%	-27%
DC1-2	18.3 kN/mm	-34%	-29%
DC1-3	19.4 kN/mm	-30%	-24%
DC1-4	19.3 kN/mm	-30%	-25%

Table 8.10: Stiffness of the DC2 samples, compared with original and improved FE models.

	6-12 kN stiffness	Difference with FE Original	+WAV
DC2 FE orig	28.1 kN/mm	–	–
DC2 FE+WAV	25.7 kN/mm	–	–
DC2-1	16.9 kN/mm	-40%	-34%
DC2-2	16.1 kN/mm	-43%	-37%
DC2-3	16.9 kN/mm	-40%	-34%
DC2-4	14.9 kN/mm	-47%	-42%

Remaining differences

Despite the made improvements, a large difference in overall displacement still remains for the DC tests, the difference being as large 0.4 mm at the onset of failure.

Several components exist in the load path, each of which is a possible cause for the higher displacement, going from the bottom of the test setup upwards:

- *The test sample.* Comparison of the measured and predicted displacements in the sample showed a good agreement even before improvements were made to the model, as seen in Figure 8.13. So the difference is not here.
- *Adhesive used for the insert.* Given that the bondline thickness is only a third of the displacement error, this can't be the cause.
- *The metal insert.* The DC1 samples showed no signs of plastic deformation in the insert, and the plasticity occurring in the DC2 samples shows as a nonlinearity. Furthermore, the displacement error grows linearly with the applied load, whereas any plasticity would show only after the yield load is reached.
- *The bolt.* No permanent deformation is seen in any of the bolts. Almost half a millimeter of additional displacement in the bolt should have caused some visible effect. So again, this is not the cause. Clearance in the bolted connection also can't be the cause, since the typical bolt clearance is around 11μm.
- *The test fixture.* As was shown in Figure 8.21, the strains in the fixture match excellently with the model, so this is also not the cause.

This leaves the test bench itself. Some other influences outside of the components listed above were already identified to be occurring at 3.8 kN, so it is considered plausible that the other displacement mismatches are caused by the test bench as well.

8.4.3 Analytical failure analysis methods

The analysis methods used for the bolted connection are not changed. The factors used to account for the effects on the bearing strength are changed slightly.

As already discussed in subsection 8.2.3, the factor to account for the increased bearing stress due to the load offset is overly conservative. It was initially set at 0.5, it is changed to 0.67. While it is expected that several other factors can also be changed slightly, the combination of several influences makes it uncertain if the change is justified.

The same argumentation applies to the calculations used for shear-out. While the current strength is higher than expected, it is unknown if this is due to a higher base strength, or due to the influence of the insert.

8.4.4 Applicability of changes to the general model

The discussed changes that are made to the analytical methods are definitely applicable to the general model, and are also easily implemented. The changes made to the FE models are partly specific to the test samples, and partly generally applicable.

The implemented changes of rib dimensions and fiber volume fractions are specific to the test samples and are therefore not applied to the general model.

The modeling of plies in the ribs is applicable to the general model, and the relevance was already identified before the comparison with test data. At the time it was decided not to implement the detailed model of the interface in the parametric model, since including this in the scripts presented difficulties. Not only is the number of interface areas dependent on the patch shape and location, the properties are also different depending on the rib direction. To implement this it would be required to have the script identify the different interfaces, and adjust all following steps to take the varying number and properties thereof into account. While this is considered possible, the amount of work required is prohibitive. Also, the current method was shown to be conservative.

The necessity to implement the waviness next to the nodes is debatable since the waviness itself is undesirable in the structure. So instead of implementing the effects in the model, it is recommended to investigate the origin of the waviness, and explore possibilities to prevent it from occurring. Should this prove to be impossible, implementation of areas of reduced stiffness next to the nodes is relatively easy outside of the cell containing the attachment. In the cell with the attachment, implementation difficulties similar to the ones outlined for the plies extending into the ribs are expected.

Chapter 9

Closing remarks

Based on the presented research and the observations that were made, conclusions on the feasibility of the in-panel attachment method can be drawn. Some additional conclusions are presented, followed by the recommendations for further research.

9.1 Main conclusions

As stated in chapter 1, the goal of the research was to develop a universal in-panel attachment concept for fiber-placed grid structures, with a rapid analysis method for initial design.

The main conclusion that can be drawn is that the novel concept of adding a laminate patch between the ribs is a feasible method for making in-panel attachments in grid structures, and that rapid analysis is possible using an approach combining analytical and FE analyses.

This is supported by the following sub-conclusions:

- The manufacturability of parts with a laminate patch is proven by the manufacturing of multiple samples, with different grid and patch shapes.
- For a reference case, an attachment point has been shown to be able to take the highest required loads without any sign of damage in the attachment, even at an attachment location which is considered undesirable. For the point in the grid that is furthest away from the ribs, it is shown that making an attachment point is possible using a laminate patch. This makes it plausible that an attachment point can be made at any location in the grid.
- The effect of a patch on the rib stiffness and strength was investigated by compressive testing of ribs with and without a patch attached. The differences in strength and stiffness are very small, proving that far-field loads can be transferred through the attachment zone.
- Both the analytical and FE analysis methods can be fully parametrized, so changes to an attachment design are easily made. Combined with the limited runtime of an analysis, this allows a rapid design. Further acceleration of the initial design is possible by using design graphs which can be constructed for a given combination of materials.

9.2 Secondary conclusions

Several other conclusions can be drawn that do not directly relate to the feasibility of the concept, but do result from the performed research. This includes some conclusions and observations that are outside of the focus of the research.

9.2.1 Attachment-related

The following conclusions can be drawn regarding the modeling, manufacturing, and behavior of the attachment point:

- Modeling the strain concentrations on the rib-patch interface using FE methods is troublesome, since that area occasionally shows singular behavior. This is likely caused by the sharp stiffness transitions in this area. At the singular points the results are unreliable.
- The shape and layup of the patch can be tailored to reduce the strains on the interface with the rib.
- By extending the patch plies to the far side of the rib, the shape of adjacent cells is changed slightly. By extending the patch plies halfway into the rib, the shape of adjacent cells is unchanged. Therefore extending patch plies halfway into the rib is preferred. This does require an accurate placement of the plies, which might increase cost.
- The patch plies that extend into the rib remain almost straight when a full thickness patch is used, with a partial thickness patch the plies slightly curve into the rib.
- In general, the lightest initial design is the one with the smallest possible bolt diameter, since the bolt is heavy compared to the laminate patch.
- Ribs which are slightly bent are stabilized by a patch, resulting in less bending and stiffness loss when loaded in compression.
- Bearing failure is very progressive when a ring insert is used, and the stiffness loss after initial failure is low when a bolt preload is applied. This results in significant load-carrying capability after the onset of bearing failure.
- For the attachment point tests, the obtained strength exceeds the goals and expectations. The loads at which bearing, shear-out, and first-ply failure on the rib-patch interface were expected to occur are exceeded. This is attributed to conservatism in the used analysis methods.

9.2.2 FE model correlation

Before implementing any changes in the FE models, the strain gage data already correlates well with the models. The horizontal and vertical strains, as measured with DIC, also correlate quite well. Exceptions are the strains in the rib-patch interface, where the measured strains show a smoother transition than the FE model results, and the rib area just outside of the node. The overall magnitude of the shear strain as measured by DIC is lower than in the FE models, and in the rib-patch interface it shows some additional differences. The overall

displacement as measured during the tests is higher than the displacements obtained from the FE models. This difference in overall stiffness is largest for the attachment test samples.

The following effects were identified as being possibly responsible for the differences:

- The modeling method for the rib-patch interface, which does not model the plies into the ribs. The method is inaccurate but gives conservative results on the interface, results at a distance from the interface are not affected.
- The dimensions of the ribs and the thickness of the patch are slightly smaller than designed.
- The ribs, nodes, and patch have a slightly higher fiber volume fraction, likely caused partly by resin flowing into resin-rich areas during curing, and partly by resin flowing out of the sample.
- There is significant fiber waviness in the ribs next to the nodes. This causes the stiffness in the rib to be reduced locally, resulting in strains up to three times higher than further along the rib. Although some strain concentration is expected at this location, the severity far exceeds expectations. Due to the higher strains, fracture occurs in the ribs just outside of the node, this failure is seen in all test samples. For the rib test samples this was the expected failure mode, but due to these effects it occurred at a significantly lower load than expected. For the attachment test samples this is an unexpected failure mode. Microscopic investigation of the failure location confirmed that this is an isolated failure, and not a propagation of damage from elsewhere.

The latter three are defects and other effects in the base grid structure. And although these are not the focus of this research, these did have a significant influence on the test results.

Several changes are made to the test sample FE models as a result of the identified sources:

- A more detailed modeling method of the rib-patch interface, also modeling the plies that extend into the ribs. This leads to a better correlation of strains on the interface, but has little effect on results elsewhere.
- Changing the dimensions to the measured dimensions and correcting the material properties for the higher fiber volume fraction. This results in only a very small change, since the stiffness changes due to these two effects mostly cancel out.
- The waviness is implemented in a simplified way, by applying an overall reduction of the stiffness in these zones. This affects the overall sample stiffness and results in higher strains in the changed areas.

With all the changes implemented, the rib test FE models still show a good correlation of the strain gage data. With the implementation of the waviness, the overall displacement now also shows a good correlation. Although the accuracy of the method used to model the waviness can be doubted, it does show that the waviness can be responsible for the overall sample stiffness error.

The attachment sample models show an improvement in correlation of the strains on the interface due to the more accurate modeling of the plies that extend into the ribs. The error in overall displacement is reduced somewhat, but the remaining difference is still significant. However, it is identified that this difference is not caused by an effect in the test sample, since the displacement field measured with DIC shows a good correlation with the model. The bolt, insert, bondline and test fixture are ruled out as well. This implies that the

remaining difference is caused by an effect that is well outside of the scope of the current study, and is probably related to the test bench.

9.3 Recommendations

Based on the observations and conclusions of the current research, the following recommendations for future research are made:

- Expand the bolt and pull-out failure calculations, since those are rather basic in the current method. This will make the model better applicable to cases where these failure modes become of influence.
- By testing, obtain more accurate allowables and multiplication factors for use in the analysis. These multiplication factors are used to take the effect of inserts, load offset, preload and other influences into account, and are currently known to be conservative.
- Implement the more detailed modeling method for the rib-patch interface in the parametric model.
- Implement more advanced failure criteria in the FE model.
- Test attachment samples using another measurement technique for the overall displacement, to be able to correlate the stiffness behavior of the attachment point, including the bolt.
- Test the effects of a patch on the strength and stiffness of a rib just outside of a node, to see if a patch has an effect there.
- Test attachment points with other typical load combinations, including out-of-plane loading.
- Improve the surface quality of the silicone tooling, since the current approach results in a poor surface quality, leaving imprints on the ribs and patch.
- Investigate the cause of the fiber waviness in the ribs, and investigate possibilities to prevent it. If this proves impossible, look into methods to predict it, and more accurately model it.
- Improve manufacturing process understanding and control, to be able to better predict and control the dimensions of the structure. The improved understanding will also allow refinement of the manufacturing constraints.

References

[1] Vasiliev, V. V., Barynin, V. A., and Razin, A. F., "Anisogrid composite lattice structures–development and aerospace applications," *Composite structures*, Vol. 94, No. 3, 2012, pp. 1117–1127.

[2] Vasiliev, V. V. and Razin, A. F., "Anisogrid composite lattice structures for spacecraft and aircraft applications," *Composite structures*, Vol. 76, No. 1, 2006, pp. 182–189.

[3] ISO, EN, "898-1: 2009, Mechanical properties of fasteners made of carbon steel and alloy steel – Part 1: Bolts, screws and studs with specified property classes – Coarse thread and fine pitch thread," .

[4] Huybrechts, S. and Meink, T. E., "Advanced grid stiffened structures for the next generation of launch vehicles," *Aerospace Conference, 1997. Proceedings., IEEE*, Vol. 1, IEEE, 1997, pp. 263–270.

[5] Rutan, B., Hiel, C., and Goldsworthy, B., "From Complete Chaos To Clear Concepts-Part I," *SAMPE journal*, Vol. 32, No. 5, 1996, pp. 19.

[6] Huybrechts, S. M., Hahn, S. E., and Meink, T. E., "Grid stiffened structures: a survey of fabrication, analysis and design methods," *Proceedings of the 12th International Conference on Composite Materials (ICCM/12). Paris, France*, 1999.

[7] Maes, V. K., "Design, Analysis, Optimization and Testing of Grid-Stiffened Composite Structures," 2015.

[8] te Kloeze, I., "Design, Analyis, Manufacturing and Testing of Load Introductions in Grid-Stiffened Composite Structures," 2015.

[9] Bakhvalov, Y. O., Petrokovsky, S. A., Polynovsky, V. P., and Razin, A. F., "Composite irregular lattice shells designing for space applications," *Proceedings of the 17th int conf on composite materials (ICCM-17), Edinburgh, Scotland*, 2009.

[10] Vasiliev, V. V., Barynin, V. A., and Rasin, A. F., "Anisogrid lattice structures–survey of development and application," *Composite structures*, Vol. 54, No. 2, 2001, pp. 361–370.

[11] Wegner, P. M., Higgins, J. E., and VanWest, B. P., *Application of advanced grid-stiffened structures technology to the Minotaur payload fairing*, Defense Technical Information Center, 2002.

[12] Lane, S. A., Kennedy, S., and Richard, R., "Noise transmission studies of an advanced grid-stiffened composite fairing," *Journal of Spacecraft and Rockets*, Vol. 44, No. 5, 2007, pp. 1131–1139.

[13] Rehfield, L. W., "A brief history of analysis methodology for grid-stiffened geodesic composite structures," *44th International SAMPE Symposium and Exhibition*, SAMPE Society for the Advancement of Material Process Engineering, 1999, pp. 956–964.

[14] Chen, H.-J. and Tsai, S. W., "Analysis and optimum design of composite grid structures," *Journal of composite materials*, Vol. 30, No. 4, 1996, pp. 503–534.

[15] Huybrechts, S. and Tsai, S. W., "Analysis and behavior of grid structures," *Composites Science and Technology*, Vol. 56, No. 9, 1996, pp. 1001–1015.

[16] Fan, H. L. and Fang, D. N., "Anisotropic mechanical properties of lattice grid composites," *Journal of composite materials*, 2008.

[17] Totaro, G., "Local buckling modelling of isogrid and anisogrid lattice cylindrical shells with triangular cells," *Composite structures*, Vol. 94, No. 2, 2012, pp. 446–452.

[18] Wang, D. and Abdalla, M., *Buckling Analysis of Grid-Stiffened Composite Shells*, Springer, 2016.

[19] Weber, M. J. and Middendorf, P., "Semi-analytical skin buckling of curved orthotropic grid-stiffened shells," *Composite Structures*, Vol. 108, 2014, pp. 616–624.

[20] Higgins, J. E., Wegner, P. M., VanWest, B., and Viisoreanu, A., *Post-buckling test response and analysis of fiber composite grid-stiffened structures*, Defense Technical Information Center, 2002.

[21] Totaro, G. and Gürdal, Z., "Optimal design of composite lattice shell structures for aerospace applications," *Aerospace Science and Technology*, Vol. 13, No. 4, 2009, pp. 157–164.

[22] Totaro, G., De Nicola, F., Vasiliev, V. V., and Rasin, A. F., "Anisogrid conical adapters for commercial space application," *13th AIAA International Space Planes and Hypersonics Systems and Technologies Conference, Capua, Italy*, 2005, pp. 16–20.

[23] Jadhav, P. and Mantena, P. R., "Parametric optimization of grid-stiffened composite panels for maximizing their performance under transverse loading," *Composite structures*, Vol. 77, No. 3, 2007, pp. 353–363.

[24] Wodesenbet, E., Kidane, S., and Pang, S.-S., "Optimization for buckling loads of grid stiffened composite panels," *Composite Structures*, Vol. 60, No. 2, 2003, pp. 159–169.

[25] Totaro, G. and De Nicola, F., "Recent advance on design and manufacturing of composite anisogrid structures for space launchers," *Acta Astronautica*, Vol. 81, No. 2, 2012, pp. 570–577.

[26] Goldsworthy, W. B. and Hiel, C., "Thermoplastics technology applied to manufacturing of grid-stiffened structures," *Society for the Advancement of Material and Process Engineering, Evolving and Revolutionary Technologies for the New Millenium*, Vol. 44, 1999, pp. 931–942.

[27] Del Olmo, E., Grande, E., Samartin, C. R., Bezdenejnykh, M., Torres, J., Blanco, N., Frovel, M., and Canas, J., "Lattice Structures For Aerospace Applications," *12th European Conference on Spacecraft Structures, Materials and Environmental Testing*, Vol. 691, 2012, p. 6.

[28] Huybrechts, S. M., Meink, T. E., Wegner, P. M., and Ganley, J. M., "Manufacturing theory for advanced grid stiffened structures," *Composites Part A: Applied Science and Manufacturing*, Vol. 33, No. 2, 2002, pp. 155–161.

[29] Van West, B. and Wegner, P., "Fiber-placed composite grid-stiffened structures," *33 rd International SAMPE Technical Conference*, 2001, pp. 782–791.

[30] Maes, V. K., Pavlov, L., and Sahak, M., "An efficient semi-automated optimisation approach for (grid-stiffened) composite structures: Application to Ariane 6 Interstage," *Composite Structures*, 2016.

[31] Pavlov, L., Smeets, B., and Simonian, S. M., "Optimization of a Composite Lattice Satellite Central Cylinder Structure Using an Efficient Semi-automated Approach," *57th AIAA/ASCE/AHS/ASC Structures, Structural Dynamics, and Materials Conference*, 2016, p. 1497.

[32] Koot, M. J., "Feasibility study on the design, manufacturing and economic potential of fibre reinforced polymer lattice structures for wind turbine towers," 2016.

[33] Bakhvalov, Y., Molochev, V., Petrokovskii, S., Barynin, V., Vasiliev, V., and Razin, A., "Proton-M composite interstage structures: design, manufacturing and performance," *European Conference for Aerospace Sciences (EUCASS)*, 2005.

[34] Aerospace committee (Kazcosmos) Ministry of Investment and Development of Republic of Kazakhstan "Republican center of space communication" JSC, "KazSat-3," `http://www.rcsc.kz/images/for_news/25112012_1.jpg` (visited: 2016-05-01).

[35] JSC Academician M.F. Reshetnev Information Satellite Systems, "Lybid," `http://www.iss-reshetnev.com/media/photo/photo-detail?ids=1925&gid=4` (visited: 2016-05-01).

[36] Shanygin, A. N. and Kondakov, I. O., "Application of Lattice Composite Technologies to Aircraft Primary Structures," Presented at the 18th International Conference on Composite Structures (ICCS18). Lisbon, Portugal.

[37] Koelle, D. E., "Specific transportation costs to GEO – past, present and future," *Acta Astronautica*, Vol. 53, No. 4, 2003, pp. 797–803.

[38] Nilsson, S., "Increasing strength of graphite/epoxy bolted joints by introducing an adhesively bonded metallic insert," *Journal of composite materials*, Vol. 23, No. 7, 1989, pp. 642–650.

[39] Herrera-Franco, P. J. and Cloud, G. L., "Strain-relief inserts for composite fasteners-an experimental study," *Journal of composite materials*, Vol. 26, No. 5, 1992, pp. 751–768.

[40] Camanho, P. P. and Matthews, F. L., "Bonded inserts for cfrp bolted joints," *European Space Agency-Publications-ESA SP*, Vol. 468, 2000, pp. 207–212.

[41] Camanho, P. P., Tavares, C. M. L., De Oliveira, R., Marques, A. T., and Ferreira, A. J. M., "Increasing the efficiency of composite single-shear lap joints using bonded inserts," *Composites Part B: Engineering*, Vol. 36, No. 5, 2005, pp. 372–383.

[42] Turan, K., Gur, M., and Kaman, M. O., "Progressive failure analysis of pin-loaded unidirectional carbon-epoxy laminated composites," *Mechanics of Advanced Materials and Structures*, Vol. 21, No. 2, 2014, pp. 98–106.

[43] Adam, L., Bouvet, C., Castanie, B., Daidie, A., and Bonhomme, E., "Discrete ply model of circular pull-through test of fasteners in laminates," *Composite Structures*, Vol. 94, No. 10, 2012, pp. 3082–3091.

[44] Steeve, B. E. and Wingate, R. J., "Aerospace Threaded Fastener Strength in Combined Shear and Tension Loading," *NASA/TM–2012–217454*, 2012.

[45] Hung, C.-L. and Chang, F.-K., "Bearing failure of bolted composite joints. Part II: model and verification," *Journal of composite materials*, Vol. 30, No. 12, 1996, pp. 1359–1400.

[46] Egan, B., McCarthy, M. A., Frizzell, R. M., Gray, P. J., and McCarthy, C. T., "Modelling bearing failure in countersunk composite joints under quasi-static loading using 3D explicit finite element analysis," *Composite Structures*, Vol. 108, 2014, pp. 963–977.

[47] Collings, T. A., "On the bearing strengths of CFRP laminates," *Composites*, Vol. 13, No. 3, 1982, pp. 241–252.

[48] Wang, H.-S., Hung, C.-L., and Chang, F.-K., "Bearing failure of bolted composite joints. Part I: experimental characterization," *Journal of Composite Materials*, Vol. 30, No. 12, 1996, pp. 1284–1313.

[49] Collings, T. A., "The strength of bolted joints in multi-directional CFRP laminates," *Composites*, Vol. 8, No. 1, 1977, pp. 43–55.

[50] Camanho, P. P. and Lambert, M., "A design methodology for mechanically fastened joints in laminated composite materials," *Composites Science and Technology*, Vol. 66, No. 15, 2006, pp. 3004–3020.

[51] Garbo, S. P. and Ogonowski, J. M., "Effect of Variances and Manufacturing Tolerances on the Design Strength and Life of Mechanically Fastened Composite Joints. Volume 1. Methodology Development and Data Evaluation," Tech. rep., DTIC, 1981.

[52] Niu, M. C., "Airframe Structural Design. Practical Design Information and Data on Airframe Structures," 1988.

[53] Duthinh, D., "Connections of fiber-reinforced polymer (FRP) structural members: a review of the state of the art," *National Institute of Standards and Technology*, 2000.

[54] McCarthy, M. A., Lawlor, V. P., Stanley, W. F., and McCarthy, C. T., "Bolt-hole clearance effects and strength criteria in single-bolt, single-lap, composite bolted joints," *Composites Science and Technology*, Vol. 62, No. 10, 2002, pp. 1415–1431.

[55] Elder, D. J., Verdaasdonk, A. H., and Thomson, R. S., "Fastener pull-through in a carbon fibre epoxy composite joint," *Composite Structures*, Vol. 86, No. 1, 2008, pp. 291–298.

[56] Banbury, A., Kelly, D. W., and Jain, L. K., "A study of fastener pull-through failure of composite laminates. Part 2: Failure prediction," *Composite structures*, Vol. 45, No. 4, 1999, pp. 255–270.

[57] Banbury, A. and Kelly, D. W., "A study of fastener pull-through failure of composite laminates. Part 1: Experimental," *Composite structures*, Vol. 45, No. 4, 1999, pp. 241–254.

[58] Sun, C. T., Quinn, B. J., and Oplinger, D. W., "Comparative evaluation of failure analysis methods for composite laminates," Tech. rep., DOT/FAA/AR-95/109, 1996.

[59] Hexcel, *HexPly 954-6 Product Data Sheet*, 2005.

[60] Hexcel, *HexPly 8552 Product Data Sheet*, 2013.

[61] 3M, *Scotch-Weld EC-9323 B/A Two Part Structural Adhesive, Technical Data Sheet*, 2013.

[62] Huntsman, *RenCast CW2418-1/ Ren HY 5160 or HY 5161 or HY 5162 or HY5118 casting resin Product Data Sheet*, 2007.

[63] Koushyar, H., Alavi-Soltani, S., Minaie, B., and Violette, M., "Effects of variation in autoclave pressure, temperature, and vacuum-application time on porosity and mechanical properties of a carbon fiber/epoxy composite," *Journal of Composite Materials*, Vol. 46, No. 16, 2012, pp. 1985–2004.

[64] Xiao, Y. and Ishikawa, T., "Bearing strength and failure behavior of bolted composite joints (part I: Experimental investigation)," *Composites Science and Technology*, Vol. 65, No. 7, 2005, pp. 1022–1031.

[65] Kress, G., Naeff, P., Niedermeier, M., and Ermanni, P., "The onsert: A new joining technology for sandwich structures," *Composite structures*, Vol. 73, No. 2, 2006, pp. 196–207.

[66] Gebhardt, J. and Fleischer, J., "Experimental investigation and performance enhancement of inserts in composite parts," *Procedia CIRP*, Vol. 23, 2014, pp. 7–12.

[67] Ferret, B., Anduze, M., and Nardari, C., "Metal inserts in structural composite materials manufactured by RTM," *Composites Part A: Applied Science and Manufacturing*, Vol. 29, No. 5, 1998, pp. 693–700.

[68] Kim, J., Yoon, J.-C., and Kang, B.-S., "Finite element analysis and modeling of structure with bolted joints," *Applied mathematical modelling*, Vol. 31, No. 5, 2007, pp. 895–911.

[69] Montgomery, J., "Methods for modeling bolts in the bolted joint," *ANSYS User's Conference*, Vol. 5, 2002.

[70] Tanlak, N., Sonmez, F. O., and Talay, E., "Detailed and simplified models of bolted joints under impact loading," *The Journal of Strain Analysis for Engineering Design*, Vol. 46, No. 3, 2011, pp. 213–225.

[71] Penado, F. E., "Analysis of singular regions in bonded joints," *International journal of fracture*, Vol. 105, No. 1, 2000, pp. 1–25.

[72] Kurowski, P., "Easily made errors mar FEA results," *Machine Design*, Vol. 13, 2001.

Appendix A

Concept selection

This appendix gives an overview of the trade-off that led to the selection of the used concept. Both the used approach and an overview of the results are presented.

A.1 Approach taken

The first step was the identification of possible attachment methods. Since it was recognized that a solution that is also applicable to GSS would have additional value, this search was not limited to lattice structures alone. A few concepts were found from literature, and many others were thought up. This resulted in a large group of concepts, either applicable to both GSS and lattice structures or only one of these.

The concepts were evaluated on multiple criteria, in a quantitative way where possible, and qualitative elsewhere. The following criteria were considered the most important and were driving the selection:

- *Far-field load continuity*, the ability of loads on the base structure to transfer across the attachment. This can also be seen as the influence of the attachment on the strength of the base structure. This is evaluated by investigating the changes made to the base structure. Since it consists of highly directional composite ribs, interrupting or moving any fibers there is expected to lead to a loss of strength.
- *Obtainable strength of the attachment point.* This is evaluated by simplified calculations of the in-plane and out-of-plane strengths. The in-plane loads on the attachment points of the SCT are usually an order of magnitude higher than the out-of-plane loads. This is considered when comparing the strengths, giving the in-plane strength a larger influence. While the actual loads are rarely in one direction only, calculating the strength under combined loading requires significantly more effort and adds little value since the obtained values are for comparison purposes only. In case the strength depends on the dimensions of the base structure, the dimensions from the SCT are used for reference. Above a certain strength level there is little added value since it already is strong enough to be used for all points on the SCT.

- *Mass efficiency*, or the required mass per unit of strength. Since this would require a more or less completed design for each concept, a simplified method is again applied. Performance in this field is based on the specific strengths of the used materials, taking into account that a weak link in the load path has a large influence on the overall strength thus lowering the mass efficiency.
- *Manufacturability.* A relative score based on how difficult the additional parts of the attachment are to make. This also takes any changes that need to be made to the base manufacturing method into account.
- *Cost.* This is a relative estimation, and includes the cost of materials, manufacturing process, and tooling required specifically for a concept. The cost of launching any extra mass into space, or the cost of required development are excluded.

Several more criteria were used, but these did not drive the selection. These served mostly to increase the understanding of the concepts, also reducing the chance of some factors being overlooked.

A.2 Results overview

Taking a step back and looking at all the considered concepts, it was recognized that most are variations of some more general ideas. This allows the concepts to be grouped, so the results can be presented in a more organized overview. Instead of going into all the fine details, an overview of the results is presented, focusing on the lessons learned from the trade-off.

A.2.1 Hole in the base structure

In case enough strength will be left to carry the far-field loads, a hole can be drilled through the unchanged base structure, and a bolt can be used to attach another part. Additionally, a bonded insert may be used to increase the bearing or pull through strength if necessary. The most suitable locations would be in the skin, and while it is possible to drill a hole in a node or rib, the structure's strength will probably decrease too much as a result.

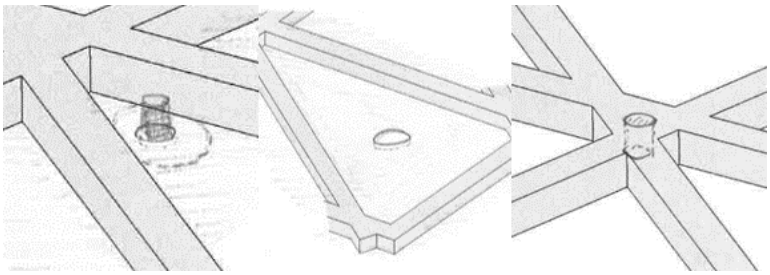

Figure A.1: Some early drawings of the hole in base structure concept.

Strength

Quantifying the strength, even on a very basic level, is not really possible since the achievable strength is not only dependent on the dimensions of the base structure but also on the far-field loads that need to be transferred. Their magnitude determines the maximum size of the hole, since it greatly influences the strength of the structure.

Other disadvantages made it quite clear that this was not a good concept, so even if the strength was high it would not have been selected.

Advantages

- The attachment can be added after manufacturing of the grid, meaning no changes will have to be made to the manufacturing method.
- This is a very easy method of attaching, no complex steps are required. This means that the cost will probably be low as well.
- Since barely any material is added, this is a very light-weight solution.

Disadvantages

- Strength of the attachment is highly dependent on the base structure.
- The attachment likely negatively influences the strength of the base structure.
- The practical applicability is limited to structures with a skin, since drilling a hole in a rib or node will result in a severely reduced strength of the base structure.
- This method is applicable to only a limited number of locations, this is especially true for lattice structures.

A.2.2 Clamped metal part

A metal part consisting of two pieces with some flanges that at least partially grab around a rib is placed. A bolt can then be used to keep the parts in place, while simultaneously attaching to the part that needs to be attached to the grid structure.

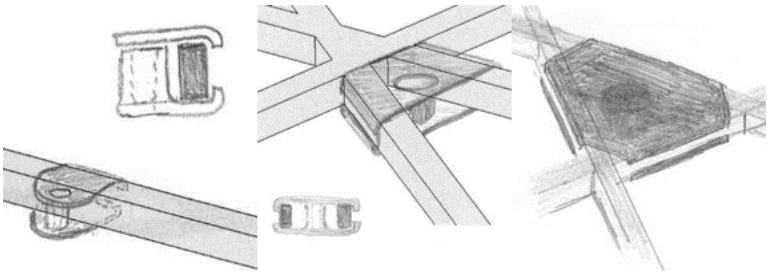

Figure A.2: Some early drawings of the clamped metal part concept.

Strength

Again, it is hard to give any numbers. This is because of the large role friction plays in the attachment. Since this is so dependent on bolt preload, surface roughness and other factors it is considered unreliable. This is especially true in systems where temperature differences are high since thermal expansion might result in a change in the clamping force, and thus the load-bearing capability.

Like the hole in the base structure, the apparent disadvantages made it clear early on that this was a bad concept.

Advantages

- The attachment can be added after manufacturing of the grid, meaning no changes will have to be made to the manufacturing method.
- Expected to have no influence on the strength of the base structure.
- This is a very easy method of attaching, no complex steps are required, only machining of a metal part and attaching it to the structure. This means that the cost will probably be low as well.
- The metal parts can easily be removed if necessary.

Disadvantages

- Clamping forces might be unreliable and/or offer limited strength. For instance if this method is used to attach to a single rib, the metal parts can slide along the rib at a relatively low load.
- For the strength it provides, this is a relatively heavy attachment method.
- Only usable for open lattice structures, and limited to locations near one or multiple ribs unless large and heavy metal parts are considered acceptable.

A.2.3 Bonded metal part

As an alternative to clamping a metal part, one can also bond a part onto the base structure. Since this no longer relies on clamping forces, different shapes can be used, and this attachment is no longer limited to open lattice structures only. For instance, a thread with a wide flange on one end (also known as an onsert [65]) can be bonded onto the structure, or a part can be bonded around a node. Another possibility is to use the metal parts from the clamped metal part concept, but additionally use adhesive.

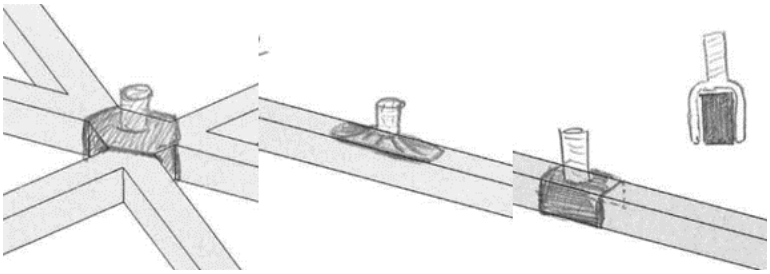

Figure A.3: Some early drawings of the bonded metal part concept.

Strength

For the strength estimation it is assumed that the metal part can be made strong enough, so the limiting part is the adhesive layer between the metal part and the grid structure.

Consider a threaded part with flanges on the side of a rib, as shown in the rightmost of the sketches in Figure A.3. A cross-section of such an attachment, and FBDs used for the strength estimations are shown in Figure A.4.

Assume the flanges cover the rib over 40 mm along its length. Calculating the out-of-plane strength then is quite easy. Neglecting the contribution of the adhesive part being loaded

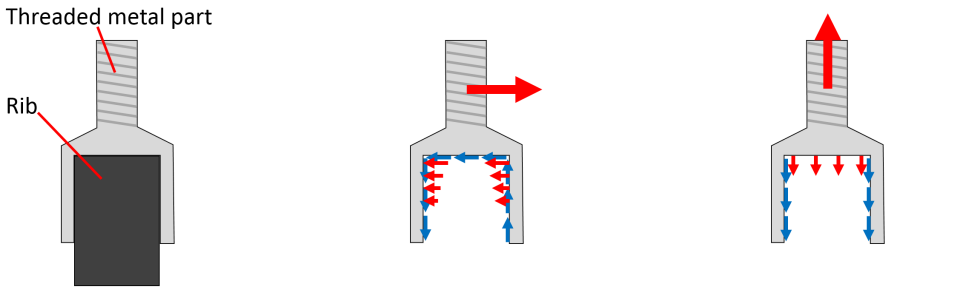

(a) Different parts (b) In-plane load (c) Out-of-plane load

Figure A.4: FBDs of a bonded metal part subjected to out-of-plane and in-plane loading. Red: applied load or normal force. Blue: shear force

in tension to be conservative, the area of adhesive in shear is just over 500 mm^2. At 25 MPa shear strength, typical for an aerospace-grade adhesive, this results in an out-of-plane strength of over 13 kN, way more than loads present in the SCT. The differences in CTE likely reduce the strength at the elevated or reduced temperatures which are often encountered in space. However, given the high strength a significant strength will still remain after taking this into account.

Calculation of the in-plane strength is more complicated, since the offset of the load from the rib results in a more complex load on the adhesive layer, with some parts in combined shear and compression or tension. Despite these additional secondary effects the in-plane load is expected to be quite high as well. Knowing that the strength might be further increased by using differently shaped metal parts, this makes it a feasible method for most attachment points on the SCT.

Advantages

- The attachment can be added after manufacturing of the grid, meaning no changes will have to be made to the manufacturing method.
- Expected to have no influence on the strength of the base structure.
- This is an easy method of attaching, no complex steps are required, only milling of a metal part and bonding it to the structure. This also means that the cost will probably be low as well.

Disadvantages

- Relies heavily on adhesive, which is relatively weak and thus limiting strength. Additionally, thermal cycling requirements may impose difficulties.
- Some bonded metal parts will have a thread extending out from the structure, this is not usable for all types of attachment zones.
- Requires accurate grid structure dimensions, small deviations can cause a change in bondline thickness, reducing strength. Especially the dimensions of the nodes show some variation.

A.2.4 Insert in or between ribs

If there is a small gap between some ribs, or if they are moved slightly to the side, a part can be added in this space. This part contains a hole, possibly threaded, and can be made of practically any material as long as it is compatible with the manufacturing method, and adhesion to the structure is not compromised. This part can be co-cured with the base structure.

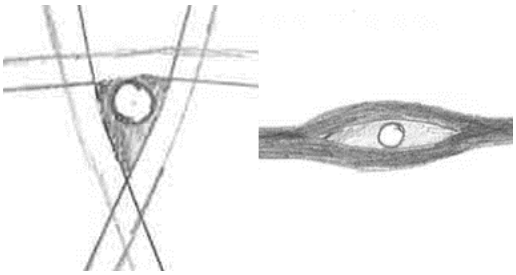

Figure A.5: Some early drawings of the insert concept.

Strength

A possible cross-section of an insert placed in the structure is shown in Figure A.6, along with two FBDs showing the forces acting on the insert when loaded by an in-plane or out-of-plane load.

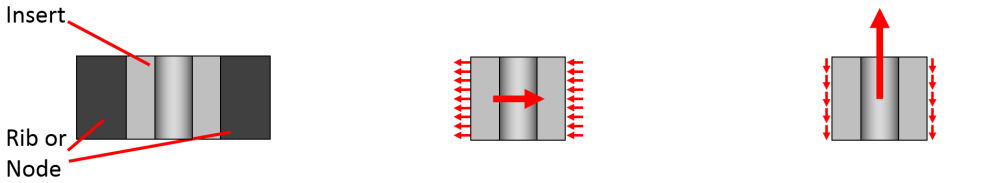

(a) Different parts (b) In-plane load (c) Out-of-plane load

Figure A.6: FBDs of a co-cured insert subjected to in-plane and out-of-plane loading.

For the calculations assume that the length of the interface between the insert and the composite is 40 mm, this results in an interface surface of 264 mm^2

The out-of-plane strength is strongly influenced by the adhesion between the insert and the composite. A single value can not be given since it depends on the selected material for the insert. However with the assumed interface area a shear strength as low as 5 MPa is already sufficient to take the highest out-of-plane load present in the SCT. This makes it likely that any well-picked combination of materials results in a sufficient strength.

When loaded in-plane, parts of the interface are loaded in shear, compression, tension, or a combination thereof. The ratio between these is dependent on the insert shape and load direction. Compared to shear and tension, compression is a relatively strong component. Since the insert is surrounded by composite ribs, some part of the interface will always be in compression, this makes the overall in-plane strength considered to be high. The in-plane strength might be limited by the surrounding ribs, since their unidirectional layout makes them poorly loadable in shear. But again, this is dependent on the layout of the structure locally.

Advantages

- No additional significant steps are required after curing of the structure. Before curing, the only extra steps are making and placing the insert.
- Can be made quite strong.
- Because of very little added material, the attachment total weight will be low.

Disadvantages

- Ribs have to be moved to make room for the insert in the SCT design. This will complicate manufacturing.
- Moving the ribs possibly influences the strength of the base structure.
- Compaction of the ribs in contact with the insert is applied from only one side, perhaps resulting in poor local properties.
- Only applicable to a limited number of locations, at or in between ribs.

A.2.5 Add a skin patch

Locally, a small patch of skin is added on top of the grid. This patch can be used to attach a part, by either drilling a hole and using a bolt and possibly an insert, or by bonding a metal part to the patch. This is a method which allows one to attach to points where there is no structure present. This does have some similarities with the *hole in base structure* concept, the difference being that a piece of skin is added specifically for the attachment. In case a skin is already present, the usefulness of this concept can be questioned since one could also attach to the already present skin if that can provide the required strength.

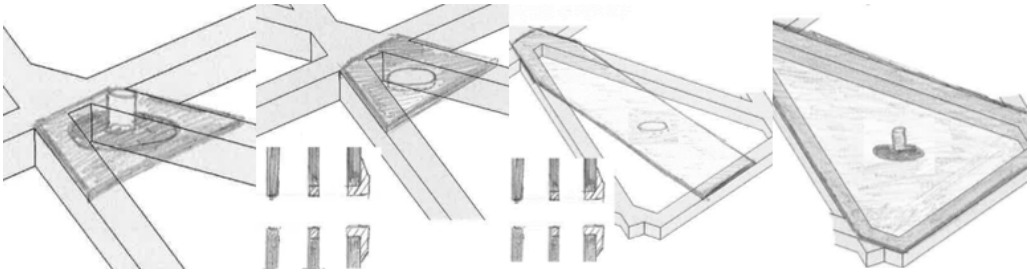

Figure A.7: Some early drawings of the skin patch concept.

Manufacturing method

Before discussing (dis)advantages of this concept, the manufacturing method is discussed first. Three options are available:

- Co-cure the skin with the grid. This has the advantage of curing the entire structure in one cycle, but this would require expensive changes to the hard tooling that is used since it would need to accommodate the local skin.
- Co-bond the skin onto the already cured grid. This has the disadvantage of requiring two curing cycles, with associated extra tooling, complex vacuum bagging, significantly increasing cost while having no strength advantage over co-curing.

- Bond the cured skin onto the cured grid. This has many advantages regarding manufacturing, it does not change the method used for the base structure, it is easier, and requires less additional or adapted tooling. However, the strength will be lower since the adhesive strength is usually less than the interlaminar strength.

Considering the above, and recognizing that better co-cured options are available (a laminate patch), the most suitable choice is to bond the patch onto the grid.

Strength

Consider a skin patch between two ribs as shown in Figure A.8, with a bolt used to introduce the load into the patch.

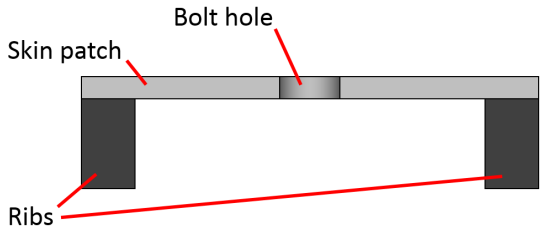

Figure A.8: Cross-section of a skin patch between two ribs.

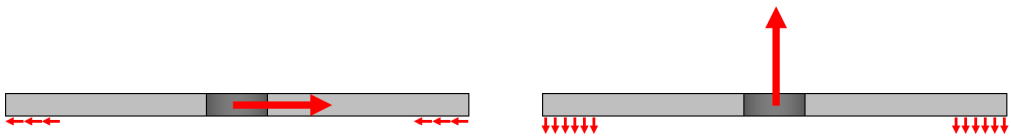

(a) In-plane load (b) Out-of-plane load

Figure A.9: FBDs of a skin patch subjected to in-plane and out-of-plane loading.

Now assuming that the weak point of the attachment is the bondline between the rib and the patch, the FBDs shown in Figure A.9 can be drawn.

Looking at the in-plane load case, this shows a shear load in the adhesive layer. When assuming that the patch covers 50mm of each of the ribs, this results in an adhesive area of 440 mm^2. With a shear strength of 25 MPa the overall strength then is 11 kN. This is more or less equal to the highest in-plane load present in the SCT, but a combined load will likely fail the adhesive layer at a lower load, especially since the out-of-plane load will result in tensile stresses in the adhesive. These tensile stresses are not very high on average, the highest out-of-plane load (around 1200 N) results in an average stress lower than 3 MPa. However, the load is rarely evenly spread, resulting in a higher peak tensile stress.

Despite falling just short of the highest strengths, this is still a feasible method for most of the attachment points.

Advantages

- The attachment is added after manufacturing of the grid, meaning no changes have to be made to the manufacturing method.
- Widely applicable and flexible concept, almost all locations on the structure are suitable.
- Expected to have no influence on the strength of the base structure.
- Quite easy to make.

Disadvantages

- Adhesive limits the maximum strength.
- Use of this concept in case a skin is already present is questionable.

A.2.6 Add a sandwich patch

Similar to the skin patch, one could make a local sandwich patch with facesheets on either side of the grid. In case a skin is already present, it can be used as one of the facesheets. As core materials, honeycomb, foam, and balsa are considered. Honeycomb has the advantage in strength and weight, with foam as a second choice, balsa is relatively heavy while offering only limited strength. Considering the application, honeycomb is the preferred choice. Different options exist for the insert, but a single best choice can not be given.

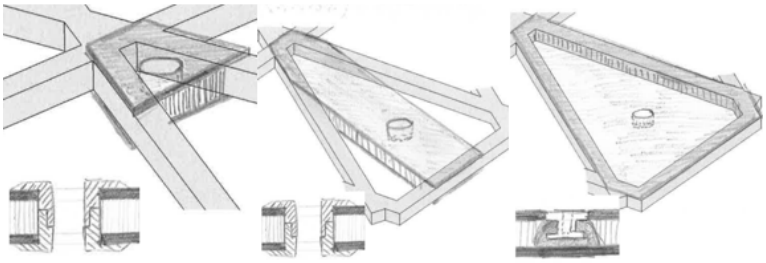

Figure A.10: Some early drawings of the sandwich patch concept.

Manufacturing method

Again, multiple manufacturing methods are possible, the same as for the skin patch. The (dis)advantages are similar, with an additional disadvantage for co-curing since rib compaction will be difficult for ribs with core material on one side. This is especially true for honeycomb core. So again, bonding is chosen as the best manufacturing method.

Strength

Given the similarities with the *skin patch* concept, most parts of the analysis are also similar. The FBDs shown in Figure A.12 also show some similarities with the ones of the skin patch.

The in-plane load is again transferred through the adhesive layer, but since the sandwich patch has facesheets on both sides of the ribs the strength is doubled. This makes this concept strong enough to take the highest loads occurring in the SCT. While the core material is also

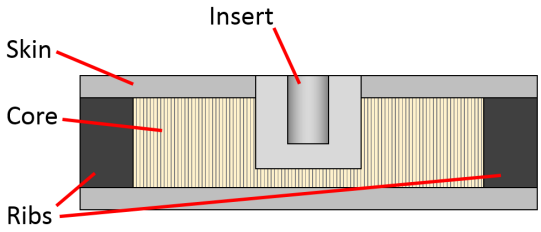

Figure A.11: Cross-section of a sandwich patch between two ribs.

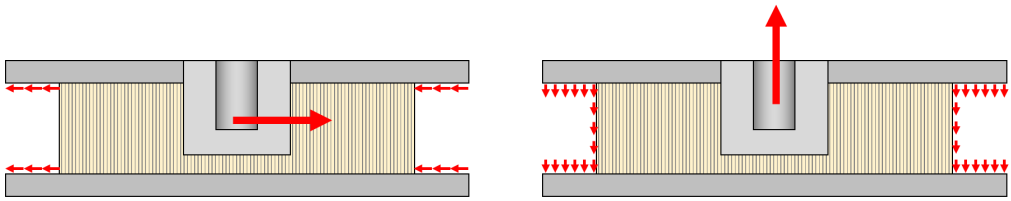

(a) In-plane load (b) Out-of-plane load

Figure A.12: FBDs of a sandwich patch subjected to in-plane and out-of-plane loading.

connected to the ribs, the multiple orders of magnitude lower in-plane stiffness of it makes the load being almost fully taken by the facesheets.

The out-of-plane shear stiffnesses are a lot more similar, resulting in the core material transferring a part of the out-of-plane load into the ribs. Combined with the additional facesheet, this makes the out-of-plane strength more than high enough as well.

Another part possibly limiting the strength is the insert and its placement in the sandwich panel. Since current SCTs are often a sandwich structure, it is clear that inserts do not limit the applicability of the concept.

Advantages

- The attachment is added after manufacturing of the grid, meaning no changes will have to be made to the base structure manufacturing method.
- Widely applicable and flexible concept, almost all locations on the structure are suitable.
- Can be made very strong.
- Expected to have no influence on the strength of the base structure.

Disadvantages

- The introduction of loads into a sandwich panel usually requires densification of the core to improve stability and strength. This adds more mass and additional manufacturing steps.

A.2.7 Add a laminate patch

An alternative is to co-cure a patch within the height of the grid with plies interweaving with the rib plies, resulting in a very large interface area through which loads can be transferred

into the structure. This patch can be any thickness up to the height of the grid, which is the upper limit.

In case a skin is already present, this concept can be combined with the *hole in base structure* concept. A patch can be added between the ribs on the skin to provide some reinforcement in case the skin alone can not provide enough strength.

This is the concept that is selected.

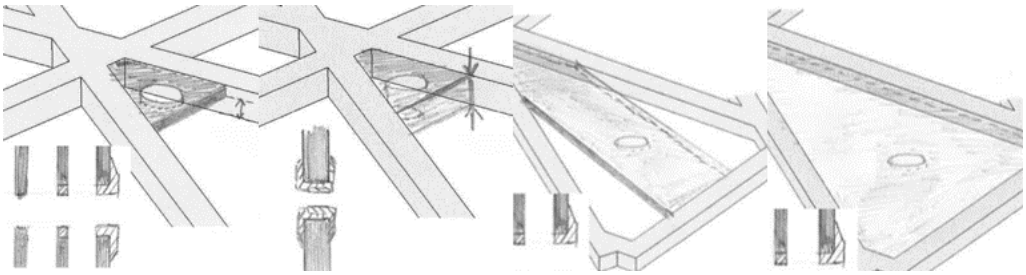

Figure A.13: Some early drawings of the laminate patch concept.

Strength

Focusing again on the interface with the rib, FBDs are shown in Figure A.15.

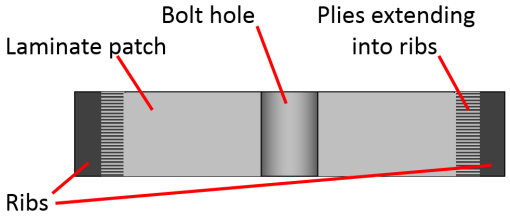

Figure A.14: Cross-section of a laminate patch between two ribs.

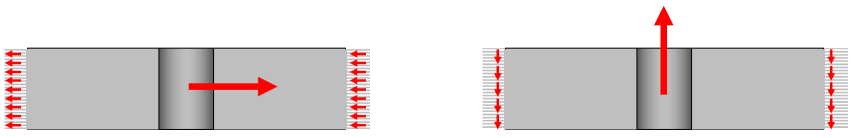

(a) In-plane load (b) Out-of-plane load

Figure A.15: FBDs of a laminate patch subjected to in-plane and out-of-plane loading.

The strength of this concept exceeds that of the other concepts. The load is transferred through interlaminar shear, which is usually stronger than adhesive. Additionally, the surface over which this is done is many times greater. Consider a full thickness patch, consisting of 52 0.127 mm thick plies and assume that 20 plies extend halfway into the rib. Over an interface length of 2 x 40 mm this then results in an interface area of 7040 mm^2. If one were to look only at the interlaminar strength, using an interlaminar shear strength of 70 MPa, typical for the material used for the SCT, this would result in an in-plane strength of 493 kN. This is a strength that can not be obtained since the laminate itself will fail well before this load. Still, with a maximum thickness of 6.6 mm, this laminate can also be made more than strong

enough to take the highest loads, even when considering that at the interface the load has to be taken by a part of the plies. With out-of-plane loads being much lower, the out-of-plane strength is also not a problem.

Advantages

- Relatively few manufacturing steps, the composite structure is cured at once, and afterwards only a few relatively easy steps are required.
- Very widely applicable and flexible concept, almost all locations on the structure are suitable.
- Can be made very strong, since the only limit is the available space within the height of the grid. The area through which stress is transferred into the ribs is very large, and is thus not limiting the strength.
- Since the obtainable strength is very high and the used materials are lightweight, the mass efficiency is also high.
- No changes to the solid outer tooling are required.
- Expected to have little to no influence on the strength of the base structure.

Disadvantages

- Some changes need to be made to the base manufacturing process.

A.2.8 Miscellaneous other concepts

Some concepts are not related to any of the previously mentioned groups and will be shortly mentioned here. These concepts all perform poorly due to various reasons. Currently, the following concepts do not fit in other groups:

- A metal part with small pins that is co-cured with the structure, placeable on a rib or a node. This has many disadvantages, the most important one is that the pins can impact rib or nodal compaction, and fibers might be damaged when placing the part. Required adapted outer tooling is another big disadvantage.
- A metal plate embedded in the skin, with a thread attached.[66,67] Difficult manufacturing, required adapted tooling, and risk of delaminations are the main disadvantages.
- Adding one or multiple short rib(s) in order to be able to use a solution that usually only works next to a node or rib in another location. This adds unnecessary complexity for a location where better solutions are available.

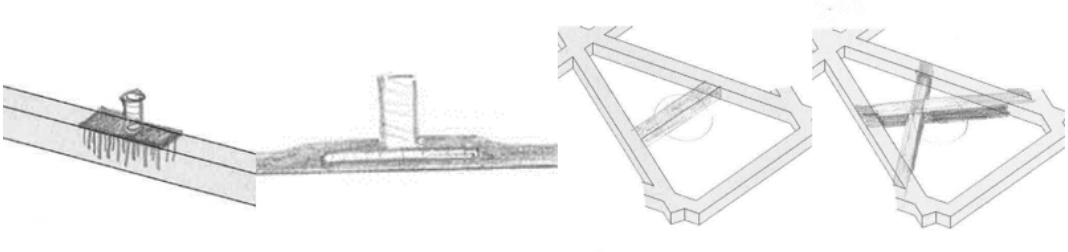

Figure A.16: Some early drawings of concepts that do not fit into other groups.

Appendix B

Finite element model particularities

B.1 Mesh convergence

An essential step for a finite element analysis is to determine the point at which the mesh is sufficiently fine such that the results are converged. The taken approach and the obtained results are presented in this section.

Two parameters are chosen to determine the mesh of the entire model. The first is an overall mesh size based on the number of elements in the width of a rib. The second parameter controls the aspect ratio of the elements in the ribs that are not adjacent to the cell containing the laminate patch. A higher value of this parameter results in elements that are longer in the direction of the rib, while the number of elements in the rib width and height remain unchanged.

While the use of only two parameters may result in a mesh which is finer than required in some locations, this quite general approach ensures that the found mesh size is applicable to other patch designs as well, not only to the design for which the mesh study was performed. An additional benefit is that it is easily implementable in the scripted model.

A combined in-plane, out-of-plane and moment load was applied to an attachment point using the simplified method explained in section B.4. Then, to determine convergence, the following results are compared:

- The total internal energy of the model.
- Displacement of a load introduction point, which is coupled to several surfaces at the bolt interface. The point for the out-of-plane load is used, since it is slightly offset from the plane of the structure, thus also capturing bending effects. This point is labeled OOP.
- Displacement at a point on the edge of the patch. This point is labeled TOP.
- Strains at the point N1, a point in the rib next to the patch.
- Strains at the point N2, a point in the rib away from the patch, next to a region where the aspect ratio of the elements is changed.

The aforementioned points are shown in Figure B.1. In this image, the number of elements in the width of the ribs is 2, and there is no change to the aspect ratio of the ribs.

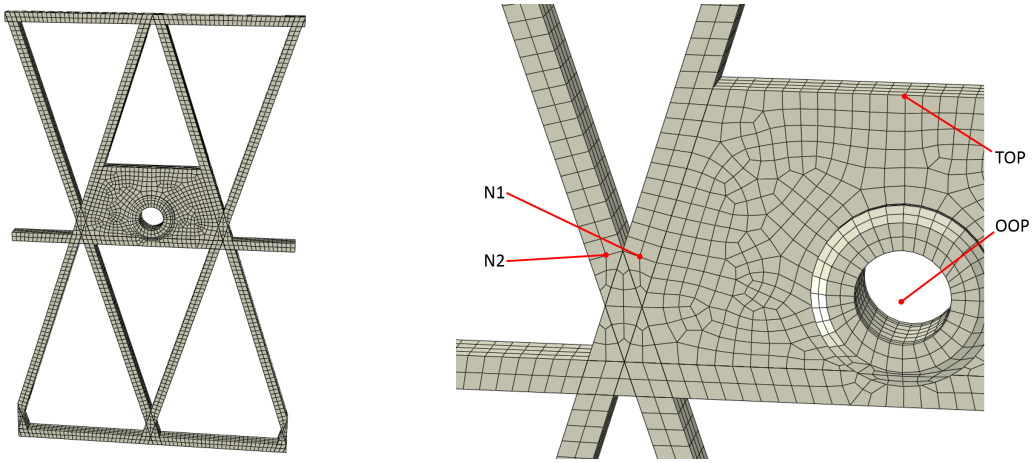

(a) Size of the used model. (b) Detail showing the points from which results were used.

Figure B.1: Locations at which displacements or strains were extracted for the mesh convergence study.

Initially the overall mesh size is reduced while keeping the length multiplier for the elements in the rib set at one. The amount of elements in the width of the rib was varied from 2 to 10. This was not increased beyond 10 since solving a more refined model required more memory than was installed in the computer, thus resulting in an excessively long calculation time.

Since no analytical reference values are available, the results are normalized to the results obtained from the finest model for comparison. An overview of the normalized results is shown in Figure B.2. It must be noted that there is no strain data for odd numbers of elements in the rib width, since in those cases there are no nodes from which the data can be extracted at the points of interest.

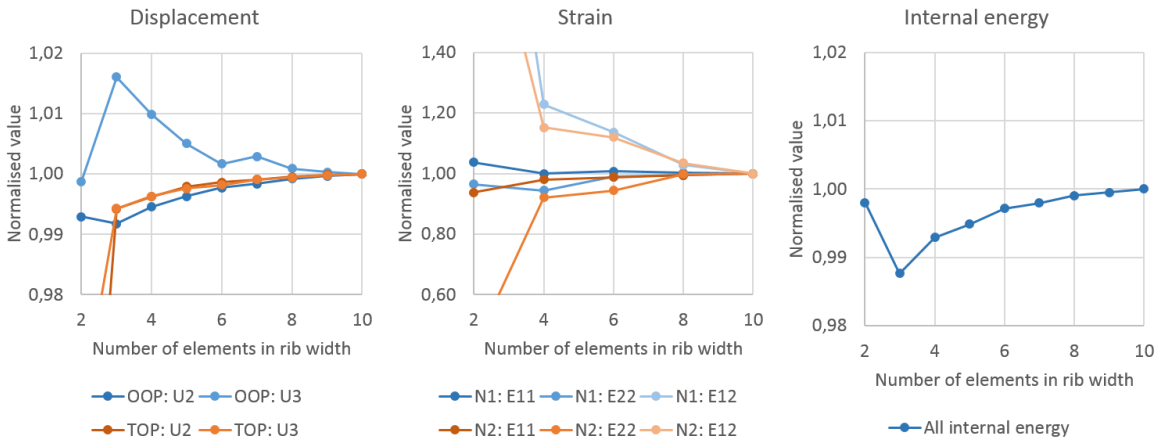

Figure B.2: Graphs showing the convergence of results from the full-thickness patch model as the overall mesh is refined.

Looking at the displacement, it can be seen that it is within 1% of the final value with four elements in the rib width, at which point the total internal energy is within 0.7%. The strains however need eight elements in the rib width before they are close to the final values.

Considering that many designs for space applications are stiffness driven, the use of a coarser

mesh can greatly reduce computation time if strength is not driving the design. Depending on the required accuracy, one can go as low as 4 or even 3 elements in the rib width. Since the overall mesh density influences the element size in all directions, a reduction from 8 to 4 elements in the rib width will result in a reduction of the amount of elements by a factor 8.

Since strength is of interest in the current research, the number of elements in the rib width is set at 8, at this mesh density there is still a 3.5% difference in strains with respect to the finer model but this is considered acceptable.

To determine the value for the aspect ratio of the rib elements, the overall mesh density is kept constant at 8 elements in the rib width, and the aspect ratio is increased. The results are again normalized, and are shown in Figure B.3. Note that in these graphs the finer mesh is towards the left side.

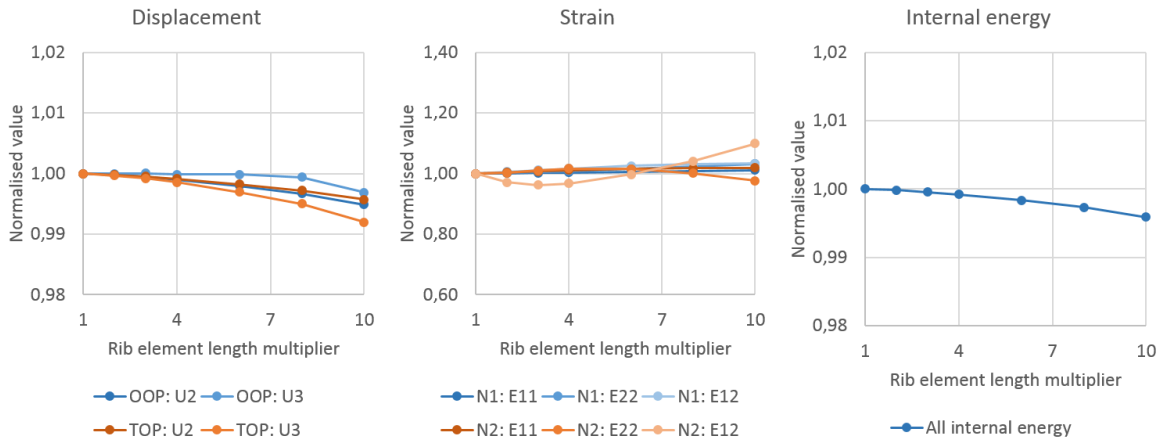

Figure B.3: Graphs showing the divergence of results from the full-thickness patch model as the aspect ratio of the rib elements is increased. The number of elements in the rib width is 8.

The effect of increasing the aspect ratio of the rib elements is rather small, as it can be increased up to 8 without excessive deviations from the results obtained with a fine mesh. However, a conservative value of 3 was selected. This already reduces the amount of elements from 388490 to 230739, a 40% decrease. Further increasing the aspect ratio to 10 would decrease the number of elements to 194835, offering only an additional 9% reduction. Part of the converged mesh is shown in Figure B.4.

The same approach was taken to perform another mesh convergence study on a model with a thin patch, a different bolt location, and another combination of loads. The results were very similar, showing displacements and internal energy within 1% of the results from the finest model at 4 elements in the rib width, and strains requiring 8. Again, the aspect ratio of the rib elements was of little influence on the results.

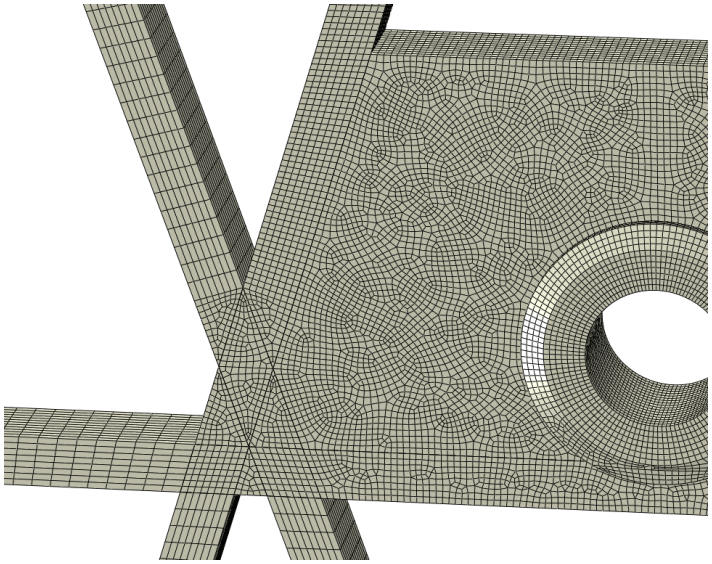

Figure B.4: The converged mesh

B.2 Layup discretization error minimization

A possible source for errors lies in the way Abaqus handles composite layups in laminates modeled using solid elements. These are modeled by applying the specified layup in every element, with the ply thicknesses corrected so the total thickness is unchanged.

To illustrate, consider a composite laminate with a layup $[0/90]_s$, if this were modeled in Abaqus with 4 solid elements through the thickness, this would result in the modeled layup being $([0/90/90/0]_s)_4$, with plies being a quarter of the actual thickness. This approach places 90 degree oriented plies in the outer elements and 0 degree plies in the inner elements, whereas this is not the case in the actual part. Since this approach does not change the ratio in which the separate orientations are present, the A-matrix is unchanged and the zero B-matrix remains zero. However, since the distances of the plies to the neutral plane are modeled differently than they are actually placed, this results in an error in the laminate's D-matrix, which determines the bending behavior of the laminate. In this example the error will be large, since the stiffnesses of the 0 and 90 degree oriented plies differ by an order of magnitude.

Now applying this to the layup of the laminates of the test samples, which consist of equal parts of +45, -45 and 90 degree plies. A $[(45/\text{-}45/90)_n]_s$ layup, with n dependent on the required laminate thickness, could be a possible choice. If a $[45/\text{-}45/90]_s$ layup were specified in Abaqus, this would then result in a model representing a $([45/\text{-}45/90]_s)_m$ layup, where m is the number of elements through the thickness. Due to the modeled layup being dependent on the number of elements through the thickness, the mesh density will influence the error. By calculating the D-matrix of both the actual and Abaqus' layup, using dimensions from the thick patch in the DC1 samples, the error that arises in the elements of the D-matrix can be found. The results depending on the number of elements through the thickness can be seen in Figure B.5.

It can be seen that all elements of the D-matrix show a significant error, especially the D16 and D26 values have a relatively large error, although the absolute value of that error is similar to that of other components.

Instead of adjusting the analysis method, the layup for the parts to be made was slightly changed to $([45/\text{-}45/90]_s)_n$. As can be seen this reduces the error greatly. There is however a requirement on the minimum number of elements through the thickness for the error to be small. Depending on the required accuracy, between 5 and 8 elements through the thickness should be taken as a minimum. Considering that the mesh convergence study shown in section B.1 resulted in a mesh with 12 elements through the thickness, this condition is satisfied.

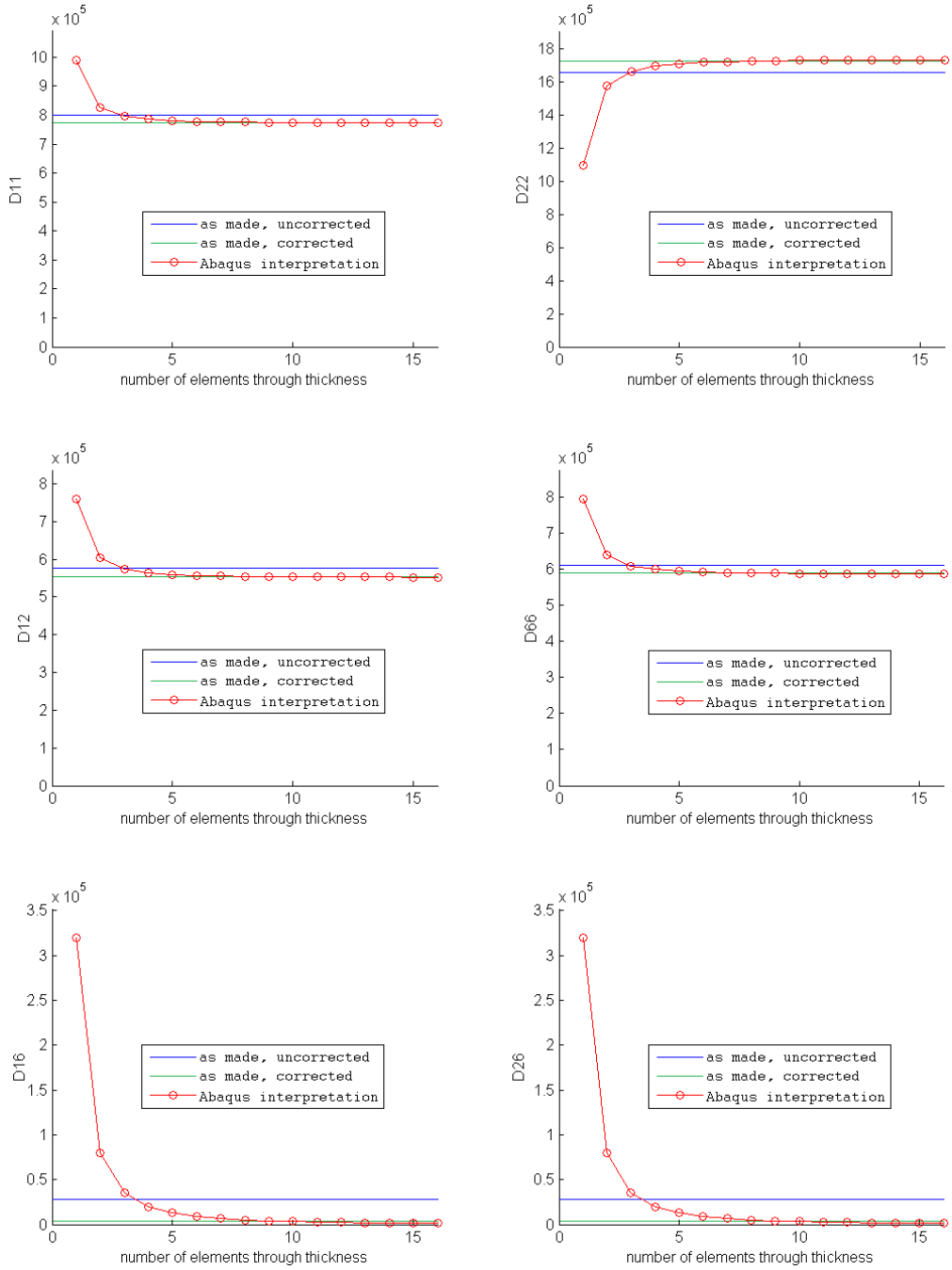

Figure B.5: Errors in the elements of the D-matrix as a result of Abaqus' interpretation of layup in solid elements.

B.3 Node modeling

An encountered difficulty lies in the modeling of the node areas. The height of the nodes is the same as the ribs, but where the ribs cross, the plies of both the ribs overlap. To make room for the plies of the crossing ribs, the plies from the ribs widen at nodes, thus reducing their thickness. Since the change in width is not instantaneous, the plies already start widening near the nodes. This local change in geometry is accompanied by an increasing resin content towards the nodes, and some fibers steering away from the rib direction at small angle in order for the tows to widen. Modeling this geometry would result in a very complex model with material properties varying per element in the rib just outside of the node. Since this is very hard to implement it is instead chosen to model the nodes with constant width ribs. The geometrical layout of this approach is shown in Figure B.6, it also shows the directions in which the fibers are oriented in the node.

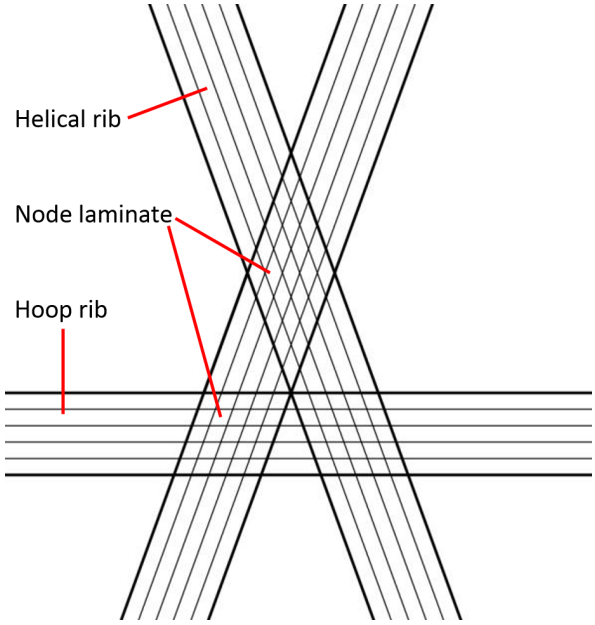

Figure B.6: Orientations of fibers in the nodes.

Three areas where plies overlap can be identified, these are modeled as composite laminates, whereas the ribs are modeled as a homogeneous anisotropic material. The areas with overlapping plies are referred to as 'node laminates' hereafter.

Modeling the node laminates using ply properties of the rib material gives rise to an error, since then only half of the cross-sectional area is given the properties in the direction of each of the intersecting ribs. Practically, this means that in a node half of the material in the direction of a rib is replaced by material with another orientation. Since the stiffness of the composite material is an order of magnitude lower transverse to the fiber direction, this results in a lower than expected stiffness of the node, and thus a higher strain under loading.

This effect can be easily seen when loading a node in the direction of the helical ribs. As can be seen in Figure B.7a, the resulting strain shows to be significantly higher in the node laminates, indicating a lower stiffness in these areas. This is against expectations because all fibers are continuous through the node, and since these have a dominant effect on the stiffness it is not expected to show a large change in stiffness through the node. If anything,

a slight increase in stiffness would be expected as a result of the additional material from the crossing rib.

Now recognizing that only half of the material in the node thickness has to account for the stiffness of an entire rib, a correction to the material properties can be applied. Since the width of the ribs is constant in the model, a factor two correction on the stiffness in the fiber direction is applied, while the properties in the other directions are unchanged since these are dominated by matrix properties. When loading a node with this applied correction it is seen that the strain through the node is a lot more constant, even showing a slightly lower strain where the plies overlap, as expected.

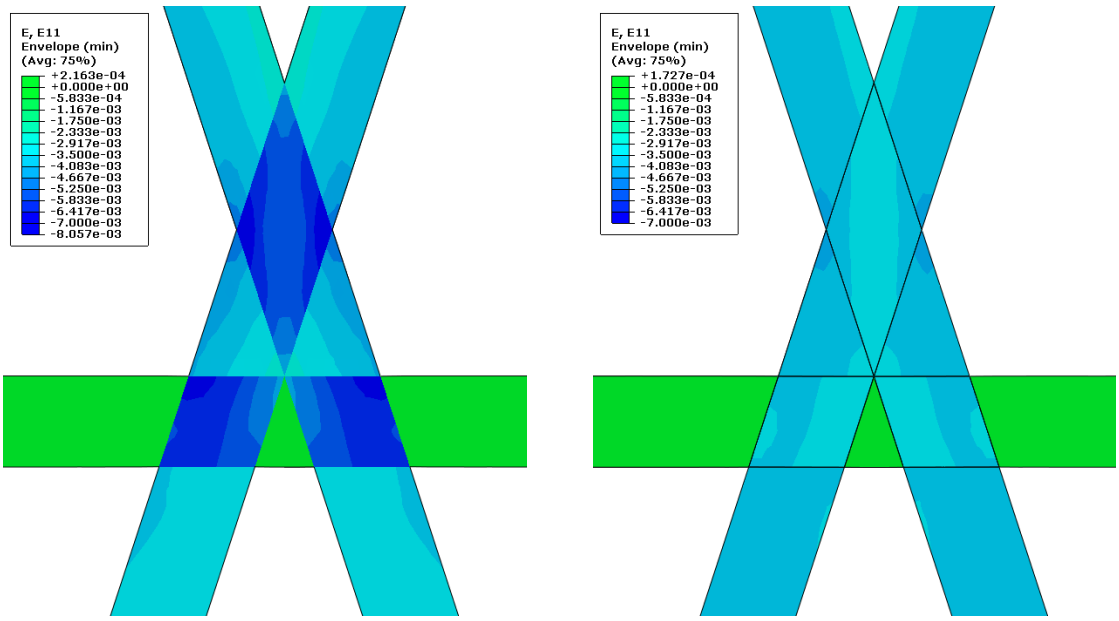

(a) Uncorrected material properties

(b) Double stiffness in the laminates

Figure B.7: Strain in fiber direction in nodes loaded in compression along the helical ribs, with and without corrected properties.

B.4 Bolt load introduction

For the SCT reference case the loads are specified at points on the neutral plane of the structure, and further details about the interfaces are unknown. The lack of this information however has the benefit of requiring a more general solution, which will also make the developed model more widely applicable.

Several different approaches are compared in order to find the most suitable method. In order to provide the most relevant comparison, the loads are a combined in-plane, out-of-plane and bending load, as well as a bolt preload.

At the base of this comparison is a model of a single cell with a relatively large patch, with pinned boundary conditions applied to the edges of this cell. The size of the model is shown in Figure B.8. The mesh of this part is kept the same for all the compared methods, to exclude any possible effect a different mesh may have on the results.

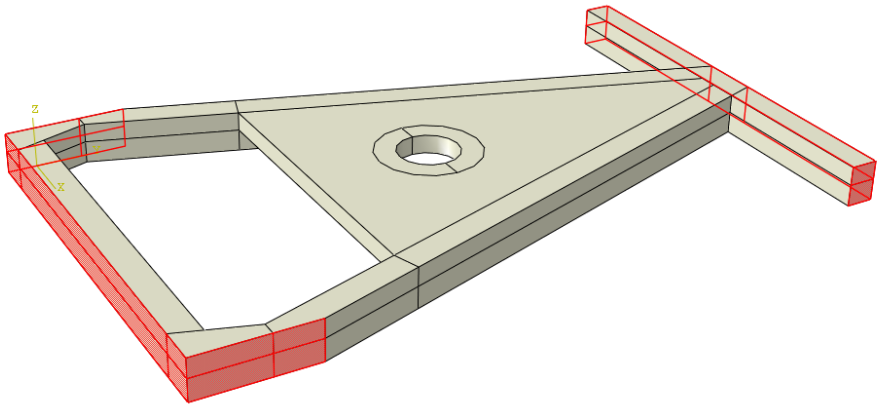

Figure B.8: Size of the model used for comparison, with the pinned boundaries highlighted.

B.4.1 Compared approaches

Six different approaches are compared, which are discussed hereafter.

Solid bolt

The approach that is considered closest to reality is to model a solid bolt, with contact defined between the bolt and the part.[68–70] Since the loads are specified on a point, this point is coupled to the face of the bolt at a distance from the actual interface, in order to allow the bolt to distribute the load into the structure.

The bolt preload is applied by making a section cut in the shaft of the bolt, and applying a 'bolt load' in the first step. This load is a special load that can be applied in Abaqus, it shortens the bolt until the required preload is applied. In the following step, where the other loads are applied, the bolt is fixed at its current length.

Since this model most accurately represents the transfer of loads at the interface, it is used as a reference case for the rest of this comparison.

Spider bolt

An approach that is often taken to simplify bolts is to model the bolt shaft with a beam element, and replacing the bolt head and nut by coupling the ends of the beam to the respective contact surfaces, either with rigid elements, couplings, or beams.[68–70] Due to its appearance this is known as a spider bolt. The resulting model is shown in Figure B.9

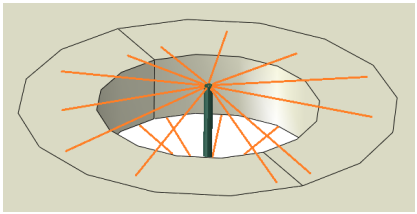

Figure B.9: Spider bolt model showing the bolt shaft and surface couplings.

This method allows the bolt preload to be applied in the same way as it is for the solid bolt. And since the bolt shaft coincides with the points on which the load is defined, the loads can be applied directly to the shaft.

Two of these models were used in the comparison. One used structural coupling, which is a distributing coupling and leaves freedom for the influenced nodes to move relative to each other. The other model uses kinematic coupling, which is a rigid coupling eliminating relative movement between nodes on the affected surface.

Structural surface couplings

Alternative methods exist that do not model the bolt at all, but use only coupling constraints to model the load transfer. [70]

Recognizing how the individual load components act on the different surfaces in the bolted connection, the loads are applied separately to the corresponding surfaces using structural couplings. The in-plane load is coupled to the half of the hole surface in the direction of the load, so it is basically acting on the bearing surface. The out-of-plane load is coupled to the surface that is clamped by the bolt. The moment is coupled to both the hole surface and the clamped surface. These couplings can be seen in Figure B.10. The bolt preload is applied as a pressure load on the area that is clamped by the bolt.

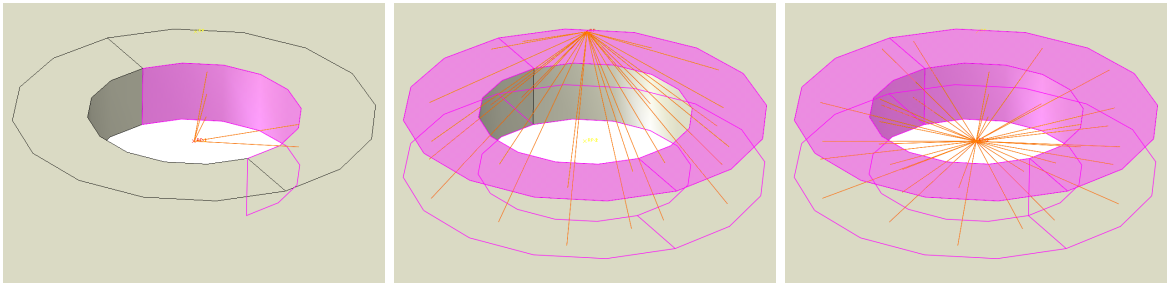

(a) In-plane load (b) Out-of-plane load (c) Moment load

Figure B.10: Coupling of loads to surfaces to simulate a bolt load introduction.

Combined surface couplings

To reduce flexibility in the joint a slightly modified approach is also included in the comparison. The couplings in this approach are the same as in the previously discussed approach, but the moment coupling is changed to a kinematic coupling. The other couplings are unchanged, since more than one kinematic coupling on a surface resulted in numerical problems when solving the model.

Structural surface couplings with additional constraints

This approach uses the same load introduction methods as the structural surface coupling approach mentioned earlier, but with two additional constraints that ensure the surfaces that would usually be in contact with the bolt head or nut remain plane.

B.4.2 Deflection and overall deformation

Differences in the behavior of the load introduction methods are most clearly seen in the overall displacements. These are shown for the compared methods in Figure B.11.

In this image and in further comparisons the numbering is as follows:

1. Solid bolt.
2. Structural surface couplings.
3. Combined structural and kinematic surface coupling.
4. Structural surface couplings with additional constraints.
5. Spider bolt, kinematic coupling.
6. Spider bolt, structural coupling.

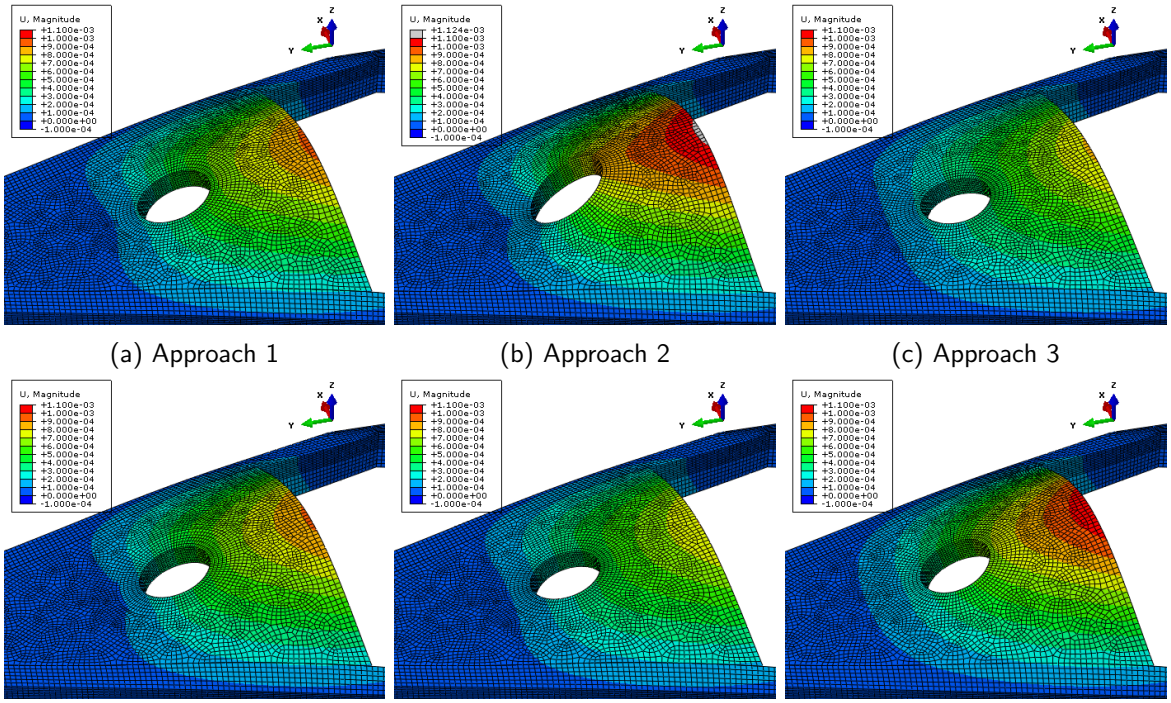

(a) Approach 1 (b) Approach 2 (c) Approach 3

(d) Approach 4 (e) Approach 5 (f) Approach 6

Figure B.11: Comparison of the displacements for several different methods for load introduction at the bolt hole. Displacements are amplified. The solid bolt used in model 1 is removed for clarity.

Keeping in mind that the solid bolt (approach 1) is used as a reference, several things can be observed:

- The approaches 2 and 6, which rely on structural coupling without additional constraints, show displacements that are higher overall. The area around the hole is also deformed in an unrealistic way that would interfere with the bolt if it were present.
- The approaches 3 and 5, which have a kinematic coupling that restricts movement of nodes in the affected areas, have lower displacements overall. This might be attributed to this method modeling some areas more rigidly than they actually are.
- Approach 4, which uses structural coupling for the introduction of loads and additional constraints to enforce a more realistic deformation around the bolt hole, has almost

exactly the same deformation as the model with the solid bolt. The difference in the deformation at the edge of the patch is only 1.2%, and the displacement field is highly similar overall.

B.4.3 Stress in the laminate

Since the differences in overall displacements were high for all but one of the methods, comparison of the stresses is focused only on comparing the solid bolt model and method 4, which uses structural couplings and additional constraints. The other methods were compared as well but again showed large differences, and are thus not presented here.

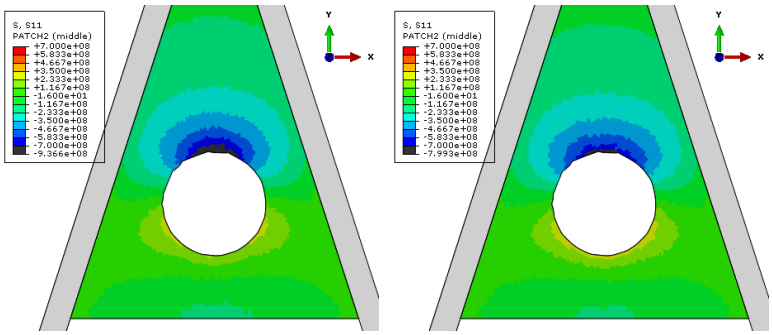

(a) Stress along the fiber, in a 0 degree oriented ply.

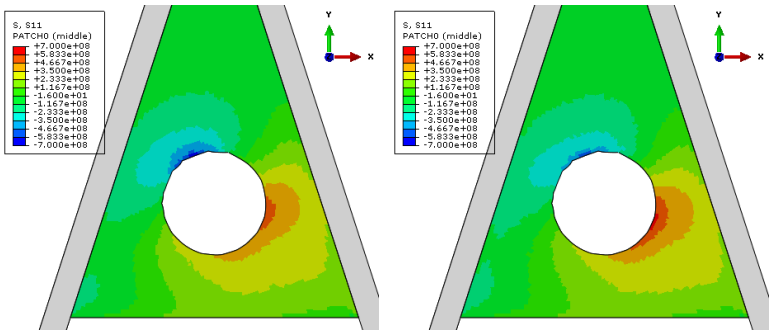

(b) Stress along the fiber, in a 45 degree oriented ply.

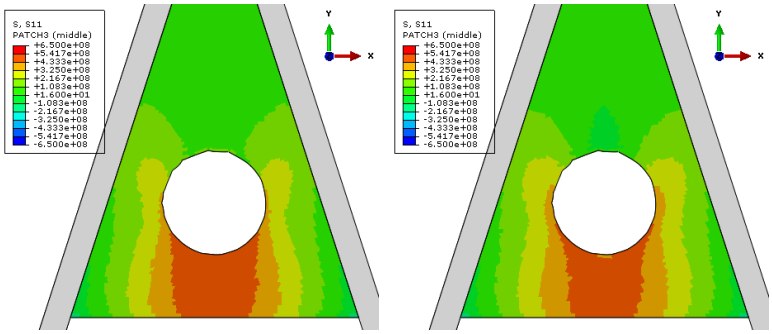

(c) Stress along the fiber, in a 90 degree oriented ply.

Figure B.12: Stress in laminate plies, from the model with a solid bolt (approach 1) on the left, coupling with additional constraints (approach 4) on the right. Areas around the bolt hole are removed, since FE results are not used to predict failure in these regions.

The stress in the fiber direction in the 0, 90, and 45 degree oriented plies is compared. While there are also -45 degree plies in the laminate, the results are practically symmetric with the 45 degree plies. The comparison between the results is shown in Figure B.12. In the shown plots the part of the laminate at the bolt location is removed, since FE results in this area are not used for failure analyses, as was discussed in section 4.2.

Although some differences in magnitude are present, these are only small. The overall distribution is also very similar, so the *coupling with constraints* method is considered a suitable substitute for the solid bolt model.

B.4.4 Computational time

Some significant differences are noticed in computational time and memory required to run the model. Especially the solid bolt model stands out, requiring around 19 minutes to run, using as much as 5.6 GB of memory at its peak. In contrast, all other methods required only 1.5 minute and 2.5 GB of memory. The vastly higher computational time is not only caused by the increased number of elements in the bolt, but also by the numerous iterations necessary for contact initiation and stabilization. That all other methods require practically the same time and memory indicates that their performance is dominated by the structure itself, and the load introduction method is of little influence.

Considering the vast difference in computational time, using one of the faster methods is preferred. Of these, method 4 is by far the best choice.

B.4.5 Limits of applicability of the simplified method

There are some limits imposed by the way the load introduction is modeled though. Since the selected simplified method includes constraints to keep the contact surfaces flat it can not be used for cases where the bolt pretension is not high enough to prevent separation, since in those cases the laminate has some room to deform into a non-flat shape. However, the separation is undesirable in most designs, so this limitation will hardly ever be limiting the use of the simplified method.

Furthermore the equal distribution of the preload over the contact surface implies that the laminate surfaces must be flat and parallel, since the preload would otherwise have an unequal distribution.

B.5 Singular behavior on the interface

In some of the first FE studies on the behavior of the structure the point on the location where the patch, ribs and node meet was found to locally show a very high strain concentration, as shown in Figure B.13.

Not only was there a locally very high strain, but the strain energy density in the element with the highest strain is almost a factor two higher than the neighboring elements in the node laminate. This is undesirable and a reason to refine the mesh in order to reduce the differences in strain energy density between adjacent elements. However, as the mesh was refined locally, the strains did not converge. This is shown in Figure B.14. For this graph the

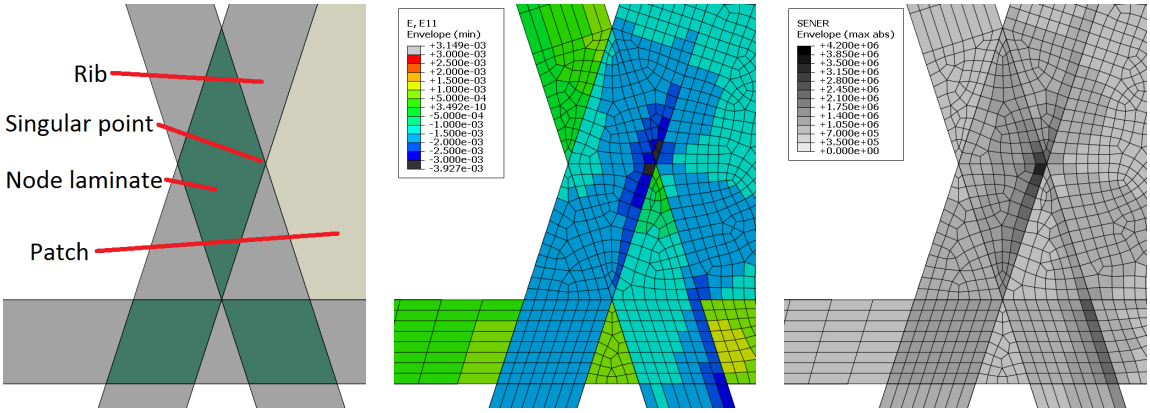

(a) Areas and singular point (b) Strain in the fiber direction (c) Strain energy density

Figure B.13: Location of the singular point, the strain and strain energy density around it.

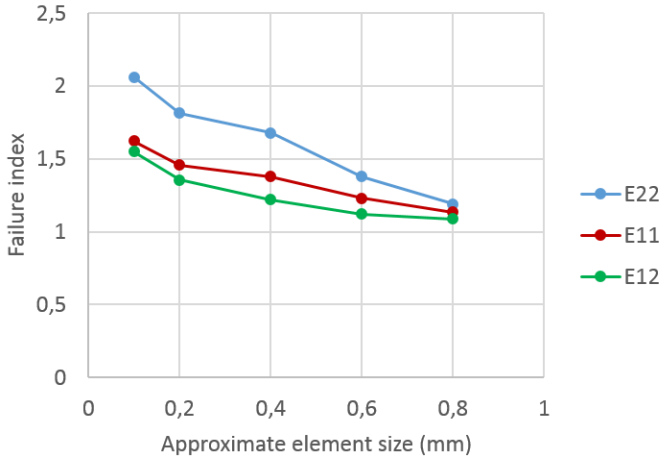

Figure B.14: Failure indexes in the singularity, as the mesh is refined locally.

strains are first divided by the allowable values to get the failure index. Note that the finer mesh is towards the left side of the graph.

It is clear that the strains are not converging to a stable value, instead they show divergent behavior by increasing ever further as the mesh is refined. The relative difference in strain energy density between the most highly strained element and the adjacent elements also did not decrease noticeably. Singular effects like this are not uncommon for FE models, and are often observed in models with sharp corners or material discontinuities. [71,72]

Since the material discontinuities are a direct result of the structural layout, no changes are made there. Geometrically, adding a fillet to remove the sharp corner is also a known method to solve the singular behavior. [72] Since there are multiple sharp corners at the singular point several different local changes are tried in an attempt to resolve the issue. For each of these changes, the mesh convergence was analyzed. The changes in geometry, and the corresponding mesh convergence are shown in Figure B.15.

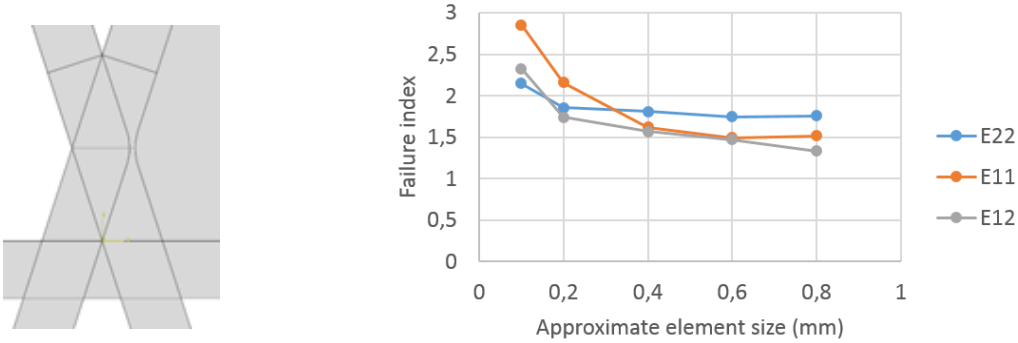

(a) Adding a fillet to the node laminate and the patch.

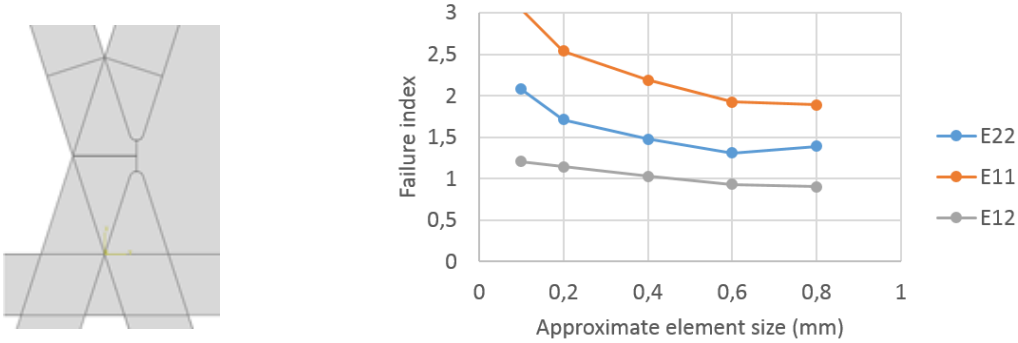

(b) Adding a fillet to both ribs at the singular point.

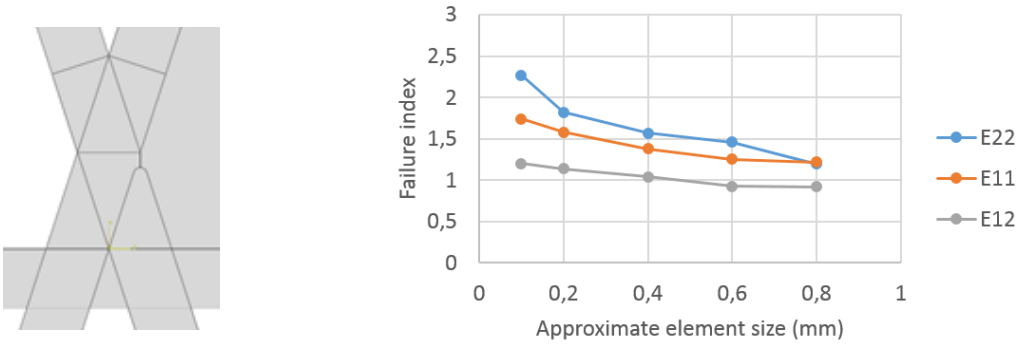

(c) Adding a fillet to only the lower rib at the singular point.

Figure B.15: Changes to local geometry and corresponding failure indexes at the singular point.

As can be seen these changes do not solve the singularity, most cases even show a faster divergence than the original geometry. As a result, it is chosen to keep the original geometry, keeping in mind that the obtained strain and stress results at the singularity can not be used for further analysis.

B.6 Used material properties

Table B.1: Properties of the base composite material, as used in FE analyses. Given values are for a fiber volume fraction of 60%, when a different fiber volume fraction or another correction is applied, the E1 stiffness is changed accordingly.

Hexcel 8552/IM7	
E1	145 GPa
E2	11.5 GPa
E3	11.5 GPa
Nu12	0.32
Nu13	0.32
Nu23	0.45
G12	5.2 GPa
G13	5.2 GPa
G23	3.1 GPa

Table B.2: Properties of the isotropic materials, as used in FE analyses.

Part	Material	Young's modulus	Poisson's ratio
Fixture	1.2510 tool steel	200 GPa	0.33
Bolt	Grade 12.9 steel	200 GPa	0.33
Insert	Aluminum 7075	72 GPa	0.33
Potting	RenCast 2418	5.0 GPa	0.33
Adhesive	3M Scotchweld 9323	2.2 GPa	0.37

Appendix C

Strain gage and displacement data

This appendix gives all the strain gage and displacement data gathered during the tests.

C.1 ORTH

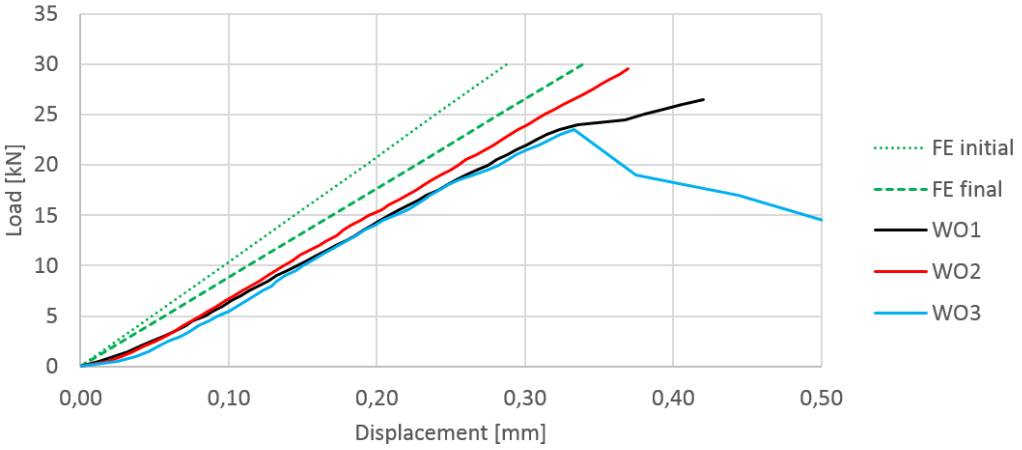

(a) ORTH-WO test samples, without a patch.

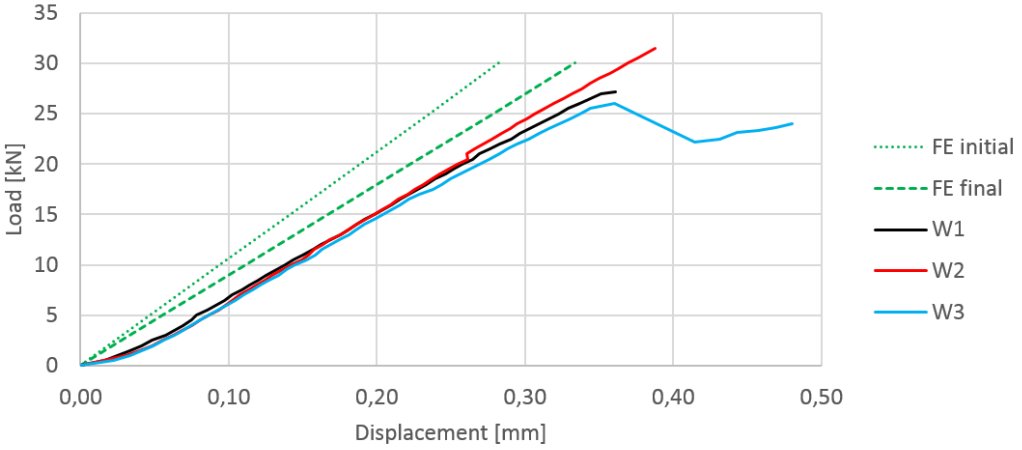

(b) ORTH-W test samples, with a patch.

Figure C.1: Measured displacements of the ORTH tests, with both initial and final FE results.

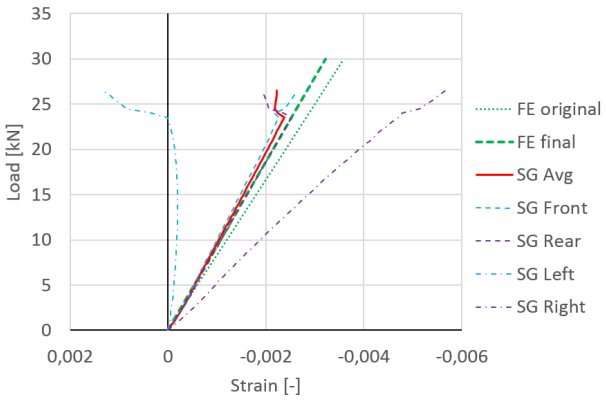

(a) ORTH-WO1 left rib

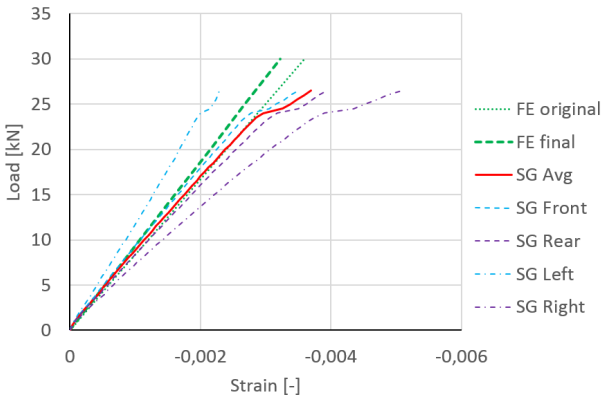

(b) ORTH-WO1 right rib

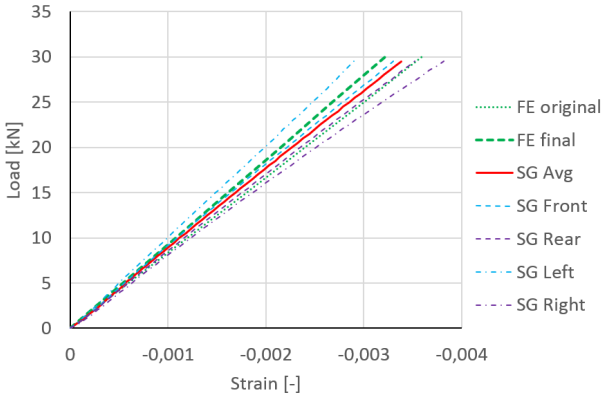

(c) ORTH-WO2 left rib

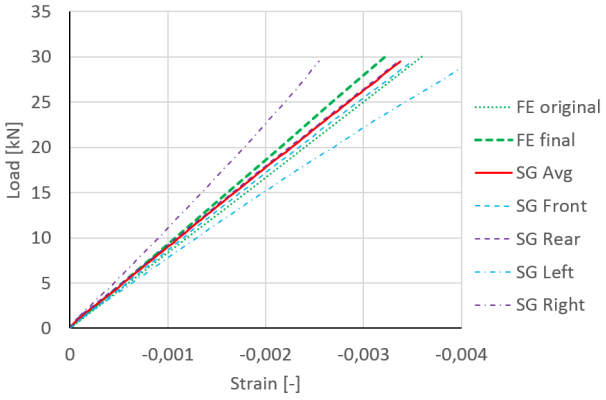

(d) ORTH-WO2 right rib

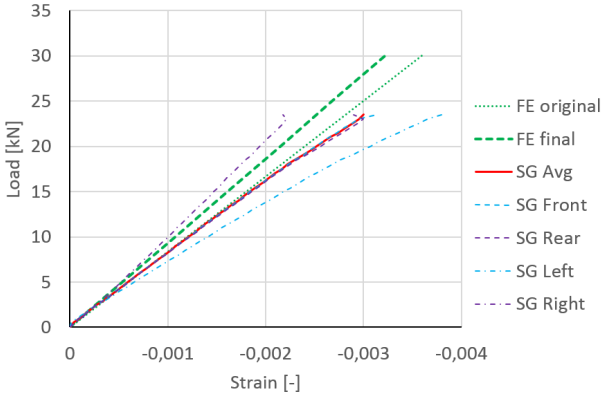

(e) ORTH-WO3 left rib

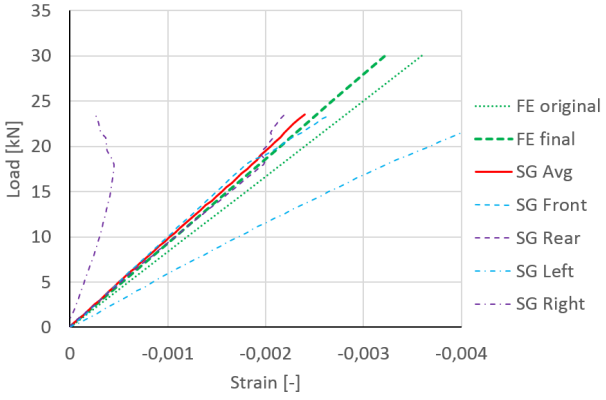

(f) ORTH-WO3 right rib

Figure C.2: Strain gage data of the ORTH-WO samples, with both initial and final FE results.

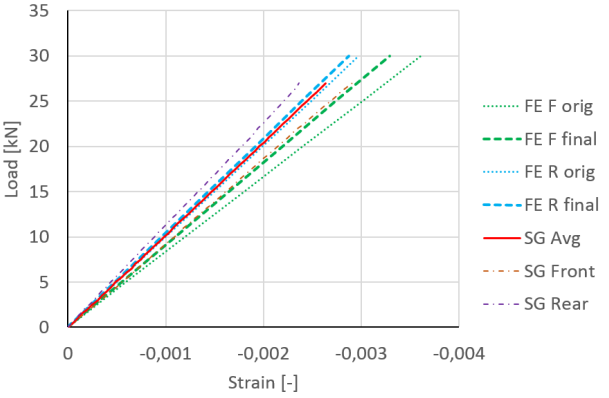

(a) ORTH-W1 left rib

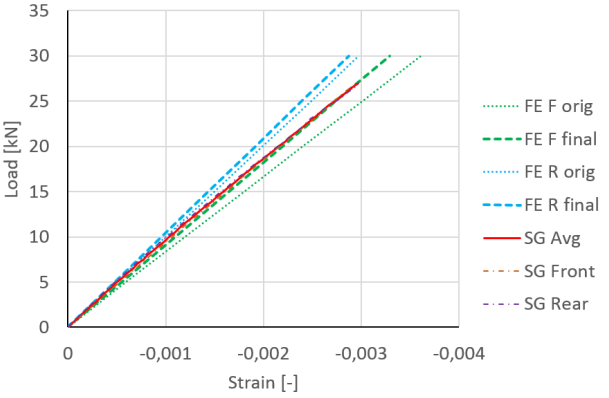

(b) ORTH-W1 right rib

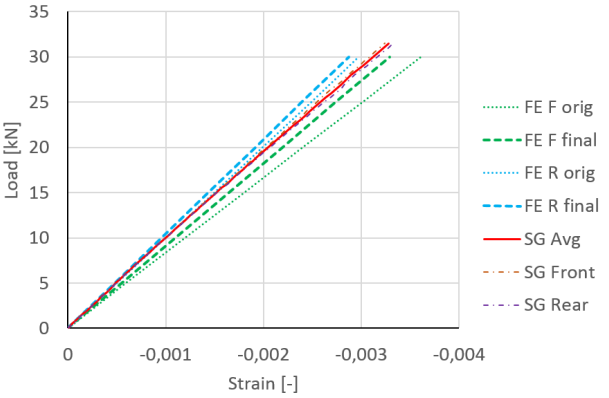

(c) ORTH-W2 left rib

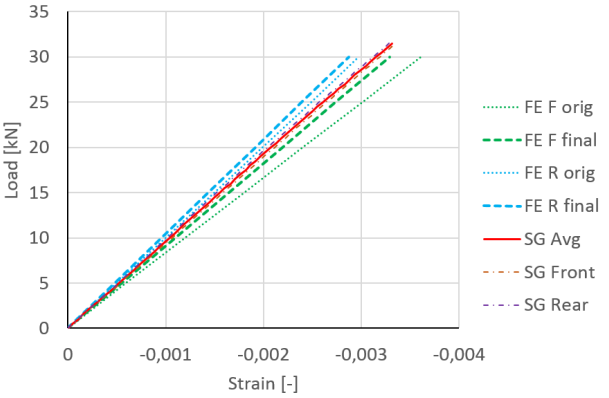

(d) ORTH-W2 right rib

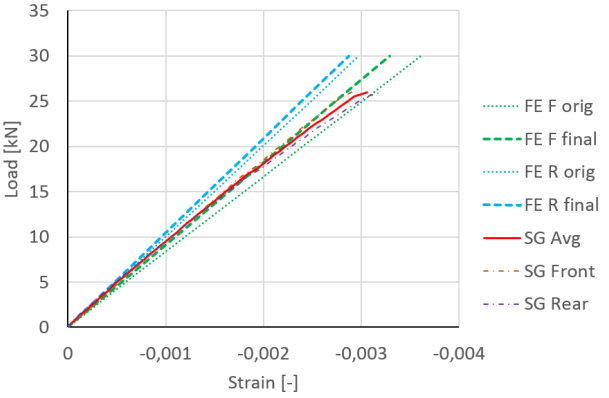

(e) ORTH-W3 left rib

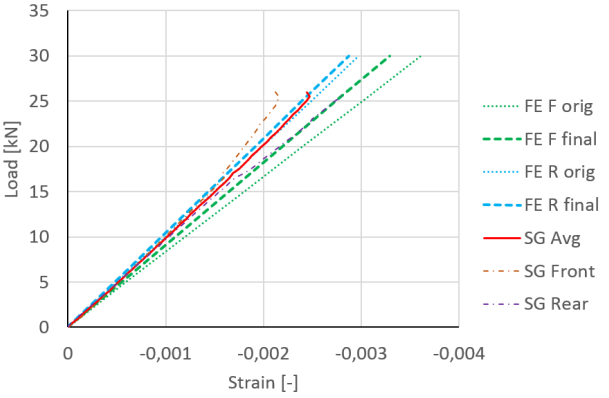

(f) ORTH-W3 right rib

Figure C.3: Strain gage data of the ORTH-W samples, with both initial and final FE results.

C.2 DC1

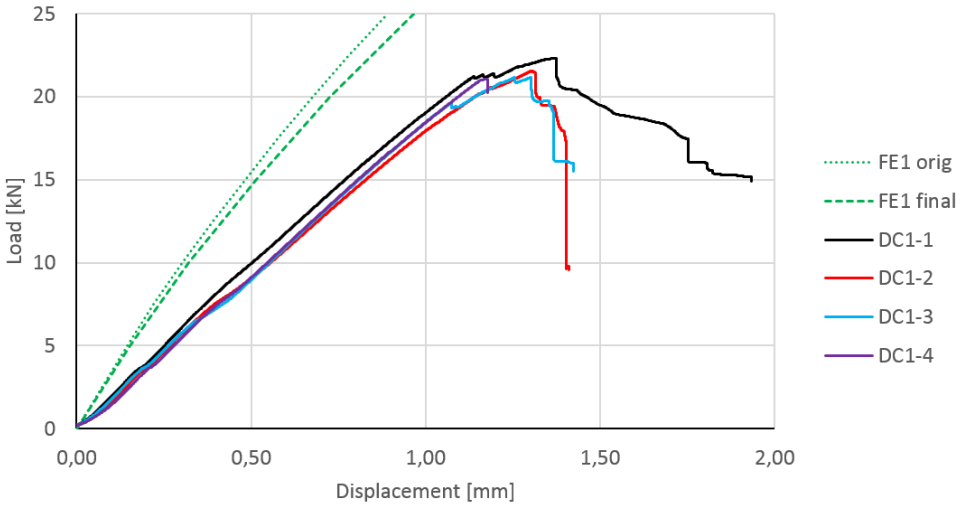

Figure C.4: Overall displacement data of the DC1 samples, with both initial and final FE results.

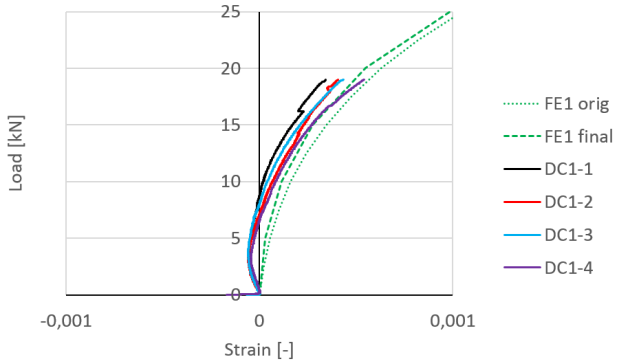

(a) Strain gage 1: Front of rib (DIC side)

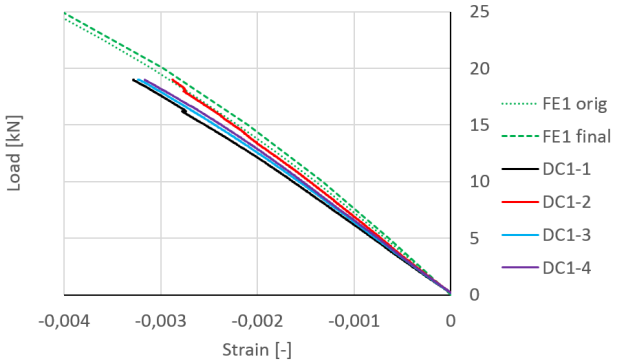

(b) Strain gage 2: Rear of rib

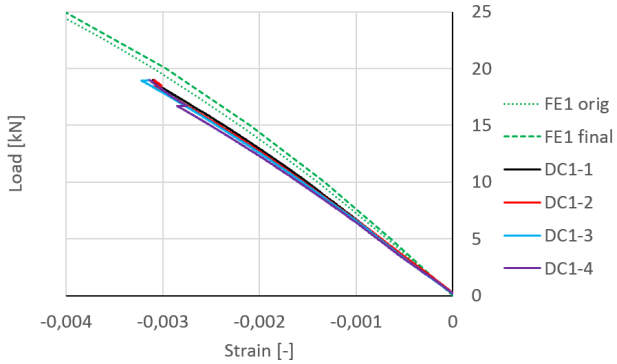

(c) Strain gage 3: Rear of rib

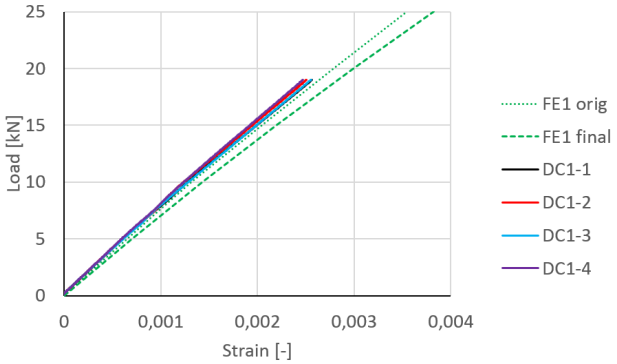

(d) Strain gage 4: Side of hoop rib at attachment

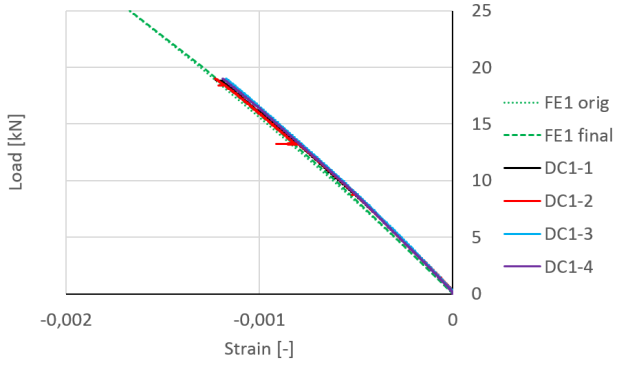

(e) Strain gage 5: Front of fixture

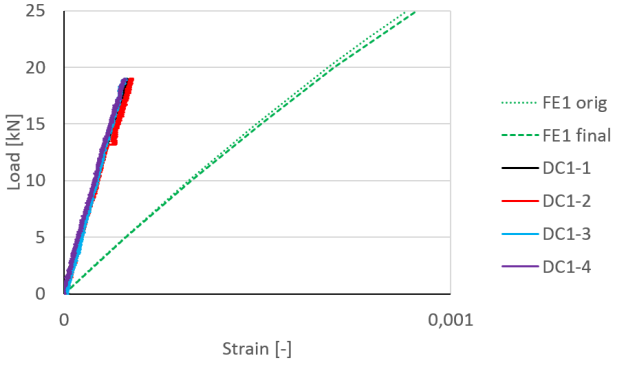

(f) Strain gage 6: Rear of fixture (improperly bonded)

Figure C.5: Strain gage data of the DC1 samples (truncated at 19kN), with both initial and final FE results.

C.3 DC2

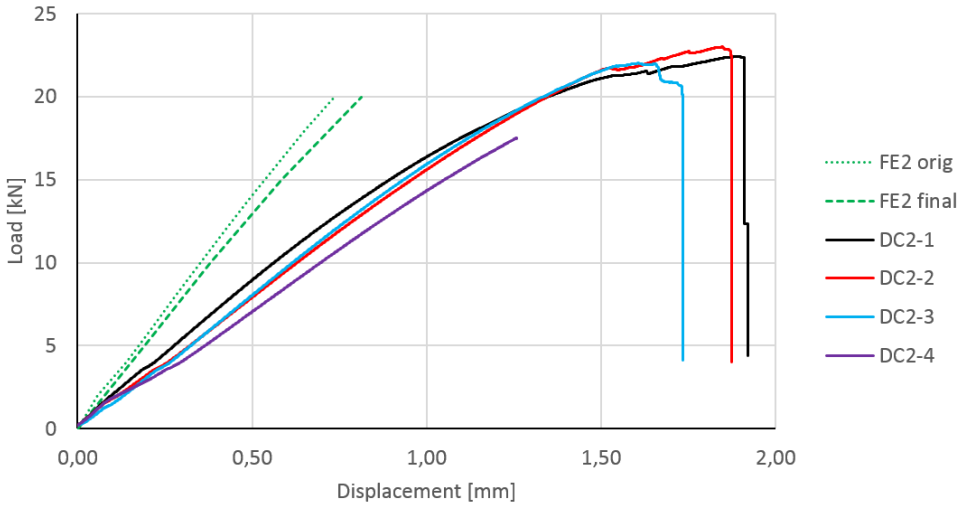

Figure C.6: Overall displacement data of the DC2 samples, with both initial and final FE results.

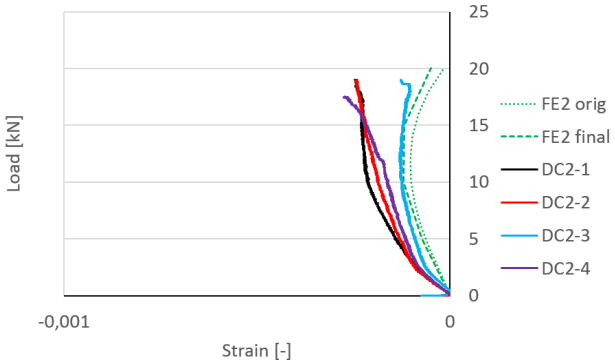

(a) Strain gage 1: Front of rib (DIC side)

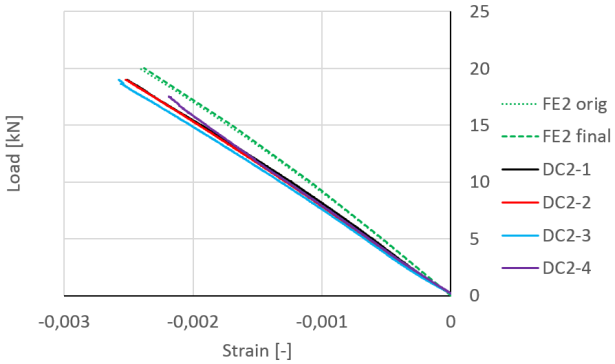

(b) Strain gage 2: Rear of rib

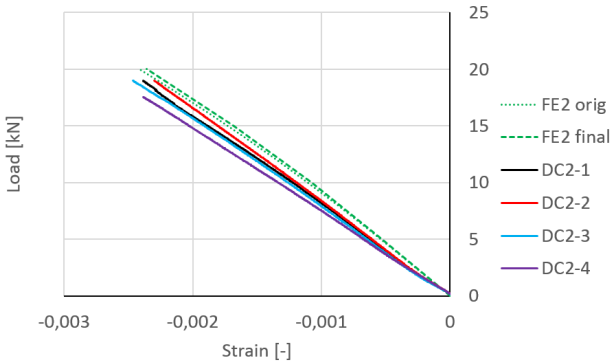

(c) Strain gage 3: Rear of rib

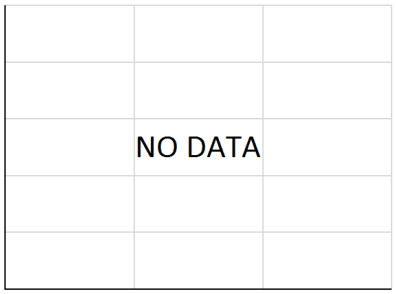

(d) Strain gage 4: Not placed

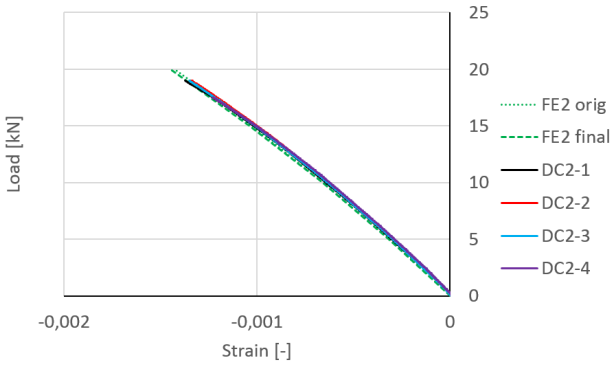

(e) Strain gage 5: Front of fixture

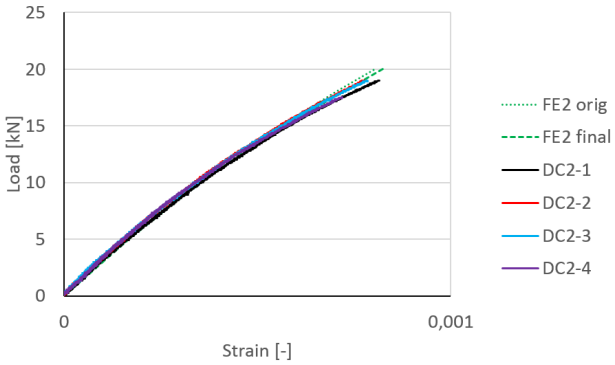

(f) Strain gage 6: Rear of fixture

Figure C.7: Strain gage data of the DC2 samples (truncated at 19kN), with both initial and final FE results.